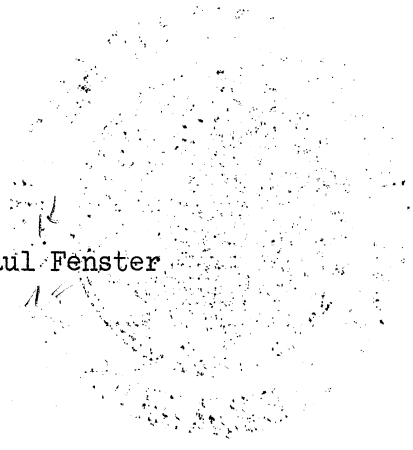


THE UNIVERSITY OF MICHIGAN
INDUSTRY PROGRAM OF THE COLLEGE OF ENGINEERING

THE TRANSIENT THERMAL RESPONSE OF A STEP
PRESSURIZED BOILING LIQUID NITROGEN SYSTEM



Saul Fenster

A dissertation submitted in partial fulfillment
of the requirements for the degree of
Doctor of Philosophy in the
University of Michigan
1958

January, 1959

IP-348

Engu
UMR
1419

Doctoral Committee:

Professor Gordon J. Van Wylen, Chairman
Professor Stuart W. Churchill
Professor John A. Clark
Professor Keith W. Hall
Professor Chia-Shun Yih

ACKNOWLEDGEMENT

The writer wishes to express his gratitude to Professor Gordon J. Van Wylen, Chairman of the Doctoral Committee, for his advice, encouragement, and guidance throughout the course of this investigation.

The writer also expresses his appreciation to Professor John A. Clark, member of the Doctoral Committee, who gave freely of his time and offered many valuable suggestions, and to Doctoral Committee members Professors Stuart W. Churchill, Keith W. Hall, and Chia-Shun Yih for their interest and cooperation.

The financial assistance of the United States Army Ballistic Missile Agency, Redstone Arsenal, Alabama, and the cooperation of Mr. H.G. Paul of that agency is gratefully acknowledged.

The financial assistance of the Shell Oil Company through its Fellowship Program is very much appreciated.

Many thanks go to the Industry Program of the College of Engineering for their cooperation in the preparation of the manuscript.

TABLE OF CONTENTS

	<u>Page</u>
ACKNOWLEDGMENT.....	iii
LIST OF TABLES.....	vi
LIST OF FIGURES.....	vii
NOMENCLATURE.....	xi
 CHAPTER	
I INTRODUCTION.....	1
II EXPERIMENTAL APPARATUS AND PROCEDURE.....	4
III EXPERIMENTAL RESULTS.....	19
IV ANALYSIS AND INTERPRETATION OF EXPERIMENTAL RESULTS	59
A. Steady State Boiling of a Saturated Liquid.....	59
B. Pressurization Process.....	59
C. Period from Start of Pressurization to Steady State Boiling.....	61
D. Wall and Liquid Temperature Transients Following Pressurization.....	63
E. Time Variation of the Heat Transfer Coefficient.....	72
F. Longitudinal Liquid Temperature Gradients...	85
G. Turbulent Boundary Layer Considerations.....	106
H. Time for First Net Boiloff.....	109
I. Dimensionless Temperature vs. Dimensionless Time.....	110
J. Summary.....	111
V RECOMMENDATIONS FOR FURTHER WORK AND CONCLUDING REMARKS.....	112

TABLE OF CONTENTS CONT'D

	<u>Page</u>
APPENDIX - PART I.....	114
APPENDIX - PART II.....	143
BIBLIOGRAPHY.....	146

LIST OF TABLES

<u>Table</u>		<u>Page</u>
I	Temperature vs. Time Data	117 - 127
II	Heat Transfer Coefficient vs. Time	128 - 137
III	Data Used for Calculating τ^* and Tabulated Values of τ^*	138
IV	Tabulated Values of τ_b and τ_b/τ^*	139
V	Comparison of Minimum Heat Transfer Coef- ficients with Values Computed Using Correlation for Vertical Surfaces in Turbulent Flow	140
VI	$\Delta h/\Delta h_0$ for Low Heat Flux Runs	141
VII	Turbulent Boundary Layer Results for Run R6-400-35, $\tau = 35$ Sec.	142

LIST OF FIGURES

<u>Figure</u>		<u>Page</u>
1	Basic Test Cylinder Dimensions and Thermocouple Locations.....	5
2	Primary Power Circuit	6
3	Guard Heater Circuit	7
4	Test Assembly	8
5	Experimental Layout	9
6	Part of the Experimental Setup Showing Test Assembly, Electrical Control Table, Vacuum Pump, Pressure Regulator, Pressure Gauges, and Speedomax and AZAR Units...	12
7	Part of the Experimental Setup Showing Sanborn Recorder, Nitrogen Charging Bottle, Dewar Flask, McLeod Gauge, and Pressure Gauges.....	12
8	Part of the Experimental Setup Showing Gas Meter, Vacuum Pump, Heat Exchanger, and part of Pressure Regulator.....	13
9	Pressurization Cylinder	13
10	View of Electrical Control Table Showing Primary Power Variacs, Guard Power Variacs, Galvanometers, and Primary Power Switching Arrangement	14
11	Wall and Liquid Temperatures vs. Time, Run R5-300-20 ..	22
12	Heat Transfer Coefficient vs. Time, Run R5-300-20.....	23
13	Wall and Liquid Temperatures vs. Time, Run R5-700-20 ..	24
14	Heat Transfer Coefficient vs. Time, Run R5-700-20	25
15	Wall and Liquid Temperatures vs. Time, Run R6-400-35 ..	26
16	Heat Transfer Coefficient vs. Time, Run R6-400-35	27
17	Wall and Liquid Temperatures vs. Time, Run R6-500-35 ..	28
18	Heat Transfer Coefficient vs. Time, Run R6-500-35	29
19	Wall and Liquid Temperatures vs. Time, Run R6-600-35 ..	30
20	Heat Transfer Coefficient vs. Time, Run R6-600-35	31

LIST OF FIGURES CONT'D

<u>Figure</u>		<u>Page</u>
21	Wall and Liquid Temperatures vs. Time, Run R7-300-35 ...	32
22	Heat Transfer Coefficient vs. Time, Run R7-300-35	33
23	Wall and Liquid Temperatures vs. Time, Run R7-500-35 ...	34
24	Heat Transfer Coefficient vs. Time, Run R7-500-35	35
25	Wall and Liquid Temperatures vs. Time, Run R7-700-35 ...	36
26	Heat Transfer Coefficient vs. Time, Run R7-700-35	37
27	Wall and Liquid Temperatures vs. Time, Run R8-300-20 ...	38
28	Heat Transfer Coefficient vs. Time, Run R8-300-20	39
29	Wall and Liquid Temperatures vs. Time, Run R8-500-20 ...	40
30	Heat Transfer Coefficient vs. Time, Run R8-500-20	41
31	Wall and Liquid Temperatures vs. Time, Run R8-600-20 ...	42
32	Heat Transfer Coefficient vs. Time, Run R8-600-20	43
33	Wall and Liquid Temperatures vs. Time, Run R8-700-20 ...	44
34	Heat Transfer Coefficient vs. Time, Run R8-700-20	45
35	Dimensionless Liquid Temperature vs. Dimensionless Time, x = 2 inches	46
36	Dimensionless Liquid Temperature vs. Dimensionless Time, x = 6 inches	47
37	Dimensionless Liquid Temperature vs. Dimensionless Time, x = 10 inches	48
38	Dimensionless Liquid Temperature vs. Dimensionless Time ..	49
39	Heat Flux vs. Temperature Difference for Boiling Liquid Nitrogen, 35 psig.....	50
40	Heat Flux vs. Temperature Difference for Boiling Liquid Nitrogen, 20 psig.....	50
41	Heat Flux vs. Temperature Difference for Boiling Liquid Nitrogen, Atmospheric Pressure.....	50

LIST OF FIGURES CONT'D

<u>Figure</u>		<u>Page</u>
42	Heat Flux vs. Temperature Difference for Boiling Liquid Nitrogen	51
43	Boiling Heat Transfer Coefficient vs. Heat Flux, Atmospheric Pressure	52
44	Boiling Heat Transfer Coefficient vs. Heat Flux, 20 psig	53
45	Boiling Heat Transfer Coefficient vs. Heat Flux, 35 psig.	54
46	Heat Flux vs. τ_b and τ^* , 20 psig	55
47	Heat Flux vs. τ_b and τ^* , 35 psig	56
48	Heat Flux vs. τ_b and τ^*	57
49	Heat Flux vs. Dimensionless Time for First Net Boiloff ..	58
50	Comparison of Actual and Idealized Heat Transfer Coefficients	63
51	Sketch Defining Geometrical Quantities Used in Idealized Analysis	64
52	Wall and Liquid Transients - Idealized Analysis	69
53	Comparison of Idealized Theory with Run R8-700-20	70
54	Comparison of Idealized Wall and Liquid Transients with Data	71
55	Curves Showing Definition of Δh and Δh_0	78
56	Viscous Attenuation of the Heat Transfer Coefficient	82
57	Viscous Attenuation of the Heat Transfer Coefficient	83
58	Liquid Velocity and Temperature Profiles	88
59	Sketch Depicting Quantities Used in Shell Temperature Analysis	89
60	Liquid Temperature vs. Longitudinal Location (Idealization). $q/A = 1500 \text{ BTU/hr.ft}^2$	91

LIST OF FIGURES CONT'D

<u>Figure</u>		<u>Page</u>
61	Liquid Temperature vs. Time (Idealization). $q/A = 1500 \text{ BTU/hr.ft}^2$	92
62	Liquid Temperature vs. Longitudinal Location (Idealization). $q/A = 3000 \text{ BTU/hr.ft}^2$	93
63	Liquid Temperature vs. Time (Idealization). $q/A = 3000 \text{ BTU/hr.ft}^2$	94
64	Liquid Temperature vs. Longitudinal Location, Run R6-400-35	95
65	Liquid Temperature vs. Longitudinal Location, Run R6-500-35	96
66	Liquid Temperature vs. Longitudinal Location, Run R6-600-35	97
67	Convection Pattern in Liquid	99
68	Core Velocity vs. Time, Run R6-500-35	101
69	Core Velocities vs. Longitudinal Location, Run R6-400-35..	102
70	Core Velocities vs. Time, Run R6-400-35	103
71	Curve Illustrating Core Velocity Determination Technique	105
72	Curve Illustrating Core Velocity Determination Technique	105
73	Curve Illustrating Core Velocity Determination Technique	105
74	Longitudinal Location vs. Displacement Boundary Layer Thickness, Run R6-400-35	108

NOMENCLATURE

A_c	Core area
A_s	Shell area
A_{δ^*}	Area corresponding to δ^*
B	See Equation (7), p. 65
B_λ	See Equation (49), p. 144
c_1	See Equation (14), p. 66
c_2	See Equation (15), p. 66
c_3	See Equation (37), p. 90
C_1	See Equation (30), p. 84
C_2	See Equation (27), p. 73
c_{pL}	Specific heat of liquid
c_{pw}	Specific heat of wall material
D	See Equation (8), p. 65
d	Mean test cylinder diameter
E	See Equation (9), p. 65
e	Base of natural logarithms
F	See Equation (50), p. 144
G	See Equation (52), p. 144
g	Gravitational acceleration
Gr	Grashof number, $\beta_L \Delta T g \rho_L^2 x^3 / \mu_f^2$
h	Heat Transfer coefficient
h_{bo}	Boiling heat transfer coefficient at time zero
h_{FC}	Free convection heat transfer coefficient
h_{FCo}	Free convection heat transfer coefficient at time zero

NOMENCLATURE (CONT'D)

h_s	Step heat transfer coefficient
Δh	$h - h_{FC}$
Δh_o	$h_{bo} - h_{FCo}$
k_L	Thermal conductivity of liquid
L	Liquid level
$dm/d\tau)_{cv}$	Time rate of change of vapor mass in control volume
n	Nucleate boiling exponent
Nu	Nusselt number, hL/k_L
p_1	Initial test cylinder pressure
p_2	Final test cylinder pressure
$dp/d\tau)_{cv}$	Time rate of change of control volume pressure
Pr	Prandtl number, $c_{pL}\mu_f/k_L$
q	Heat rate
q/A	Heat flux
$(q/A)_o$	See Equation (46), p. 144
Re	Reynolds number, see Equation (26), p. 73
Re_x	Length Reynolds number, $u_s x / \nu_f$
$Re_{x,max.}$	Maximum length Reynolds number
s	Shell thickness
$t_1 \text{ sat.}$	Saturation temperature of liquid at initial pressure
$t_2 \text{ sat.}$	Saturation temperature of liquid at final pressure
t_{wx}	Wall temperature at longitudinal location x
t_w	Wall temperature
t_{wo}	Wall temperature at time zero

NOMENCLATURE (CONT'D)

t_{Lx}	Liquid core temperature at longitudinal location x
t_L	Liquid temperature
t_{Ls}	See Equation (36), p. 89
ΔT	$t_w - t_L$
ΔT_0	$t_w - t_L$ at time zero
u	Velocity, see Equation (26), p. 73
u_c	Core velocity
u_s	Shell velocity
$u_{s,max}$	Maximum velocity in boundary layer
w_b	Mass boiloff rate
w_c	Condensation rate
w_i	Mass rate of vapor entering test cylinder
w_L	Mass of liquid under test
w_o	Mass rate of vapor leaving test cylinder
x	Coordinate, measured upward from test cylinder bottom
y	Coordinate, measured radially inward from inside diameter of test cylinder wall
α	See Equation (12), p. 66
β	See Equation (13), p. 66
β_L	Volumetric coefficient of expansion of liquid
δ	Boundary layer thickness
δ^*	Displacement boundary layer thickness
Δ	Test cylinder wall thickness
θ	$t_{Lx} - t_1 \text{ sat.}$
θ^*	$t_2 \text{ sat.} - t_1 \text{ sat.}$

NOMENCLATURE (CONT'D)

θ_w	$t_w - t_{wo}$
λ	See Equation (46) p. 144
μ_f	Absolute viscosity of liquid
ν_f	Kinematic viscosity of liquid
ρ_L	Liquid density
ρ_w	Density of wall material
τ	Time
τ_b	Time for first net boiloff
τ^*	See Equation (3), p. 20

CHAPTER I

INTRODUCTION

This investigation is concerned with the effects upon certain properties and parameters due to a "step" or rapid pressurization of a liquid nitrogen system undergoing steady state nucleate boiling at atmospheric or near-atmospheric pressure under conditions of constant wall heat flux.

It is of particular interest to make such a study at this time because such phenomena play a role in liquid fuel missile performance. The liquid oxygen containers of missiles are pressurized just prior to firing in order to produce a subcooled liquid, hence insuring against cavitation in the pump forcing liquid oxygen into the rocket engines.

Consideration of the missile problem governed to some degree the design of the test cylinder and the selection of the test fluid. The latter was chosen to be a cryogenic substance. Liquid nitrogen rather than liquid oxygen was selected because it is relatively safe to work with and is readily available.

Pressurization of a boiling liquid causes cessation of boiling, after which follow, if heat input is maintained, a transient single-phase free convection process, transient two-phase free convection, and finally re-established steady boiling at the new pressure. The transient free convection processes cited are of a special kind because they are greatly influenced by the boiling which occurred in the cylinder prior to pressurization.

Analytical investigations made into transient free convection deal with fluids initially at rest and at the same temperature as the vertical contacting wall.

For example, using laminar boundary layer theory Illingworth (10), and Siegel (25) studied the transient free convection which results when a vertical flat plate undergoes a step temperature increase or suddenly begins to produce a uniform heat flux.

Theoretical analyses of steady state free convection from vertical surfaces with laminar boundary layers have been made by Sparrow and Gregg (27) for the constant heat flux wall, Ostrach (22) for a constant temperature wall, and Sparrow and Gregg (28) for a non-isothermal wall. These deal with a boundary layer which has zero thickness at the bottom edge of the plate.

McAdams (20) summarizes the results of several workers dealing with dimensionless correlations for heat transfer from vertical plates and outside of vertical cylinders by steady state natural convection in the laminar and turbulent regimes.

That the heat transfer coefficient is reduced for the case of closed ended vertical tubes, relative to that for vertical plates, has been shown by several investigators. The experimental aspects of their work have in common provision for abstraction of the heat being transferred through the cylinder walls so that a steady or quasi-steady state results.

Hartnett and Welsh (9) in this way have examined constant flux heat transfer through the walls of a vertical tube. It is deduced from their work that the average heat transfer coefficient is approxi-

mately half of what is predicted for the vertical plate using the Jakob ⁽¹³⁾ correlation. Furthermore, the coefficient of heat transfer was found to increase as the distance from the bottom of the cylinder increased.

Martin and Cohen ⁽¹⁹⁾, and Martin ⁽¹⁸⁾ deal with heat transfer to various liquids contained in vertical tubes with constant temperature walls. They found that the heat transfer rate was greatest at the top of the tube and suggest that while there is a general condition of turbulence, laminar flow may be taking place at the bottom of the tube.

Eckert and Diaguila ⁽⁴⁾ found that the Nusselt number may be as much as 35 percent lower than the value predicted for turbulent free convection from a flat vertical plate. They too dealt with a constant temperature tube.

Lighthill ⁽¹⁶⁾, in a theoretical analysis of free convection in tubes, discusses the existence of three laminar and three turbulent regimes, and predicts that a stagnant portion may exist at the bottom of the tube in both the laminar and turbulent cases.

Siegel and Norris ⁽²⁶⁾ have reported on their experimental work dealing with turbulent free convection in a partially enclosed space between two heated vertical plates at substantially uniform wall flux. They found that when the space between the vertical plates was closed at the sides and bottom, the Nusselt number was lower for a given Grashof number than predicted by the Jakob ⁽¹³⁾ correlation.

Some of the literature connected with other phases of the problem under study will be cited in the body of the thesis where the necessity for their application will be more apparent.

CHAPTER II

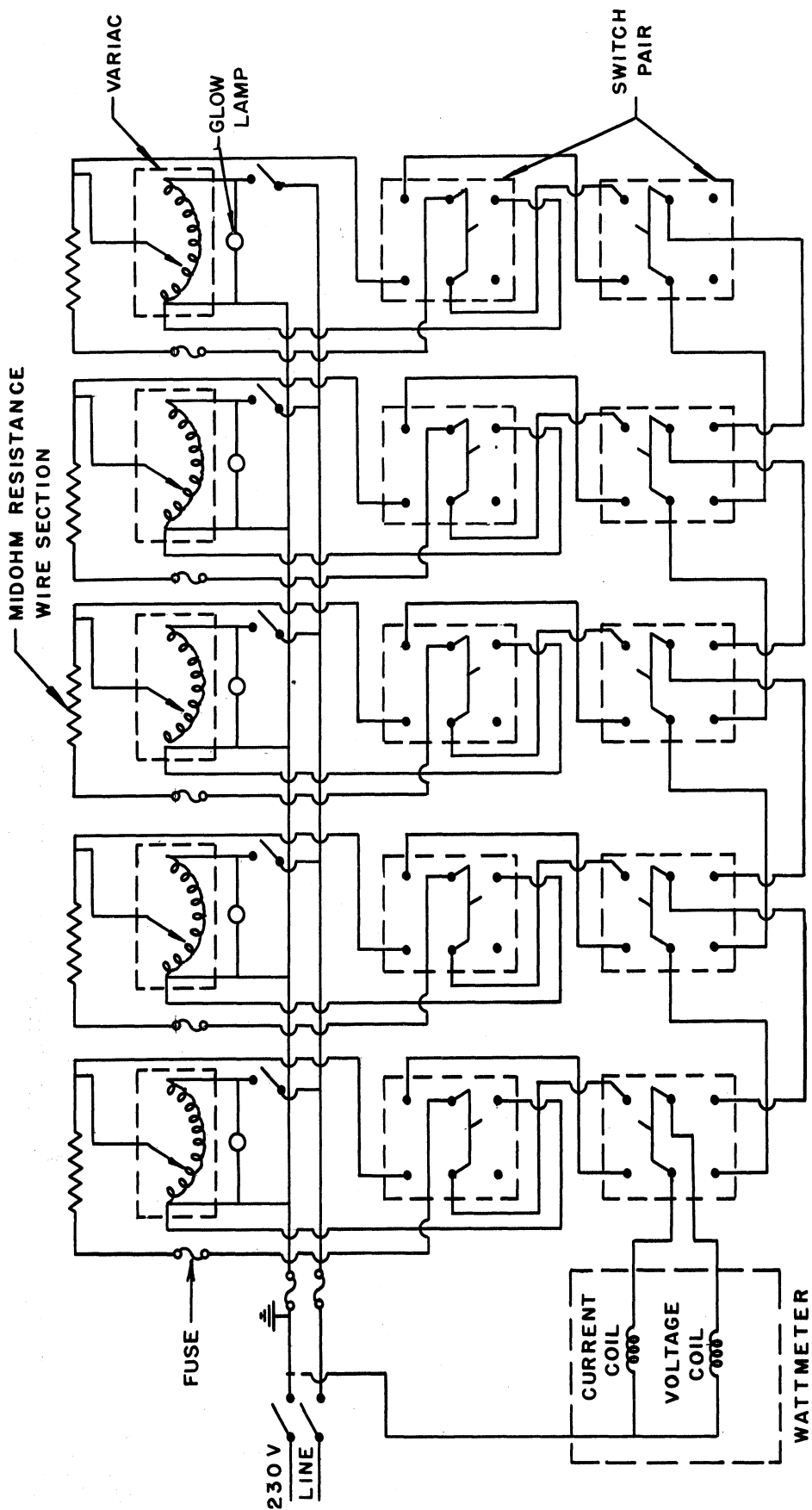
EXPERIMENTAL APPARATUS AND PROCEDURE

The experimental work described herein was carried out in the Heat Transfer and Thermodynamics Laboratory associated with the Department of Mechanical Engineering.

While this research was not intended to exactly duplicate dimensions and conditions existing with regard to liquid oxygen containers of missiles, certain design decisions were made bearing in mind possible missile application.

It was decided to use, for the primary test container, a thin walled aluminum cylinder with a length to diameter ratio equal to two. Its basic dimensions are shown in Figure 1. The top and bottom plates are each one half inch thick. This thickness is great enough to permit pressurization to 50 psig without requiring internal or external reinforcing ribs which would tend to disturb and augment heat input to the primary test cylinder.

The experimental setup was designed to provide constant wall heat flux. For this purpose, electrical power was provided by five sections of circumferentially wound heater wire called Midohm, manufactured by the Driver-Harris Company. It is a nickel-copper alloy resistance wire covered with two thicknesses of Fiberglass insulation. The electrical power input to the heaters was measured by a single Weston wattmeter accurate to within 1% of true power. By a suitable switching arrangement, shown in Figures 2 and 10, the same wattmeter was used to measure power through each heat segment individually. Electrical power



KNIFE SWITCHES NORMALLY IN DOWN POSITION
FOR POWER READING, INDIVIDUAL SWITCH PAIR IN UP POSITION

Figure 2. Primary Power Circuit.

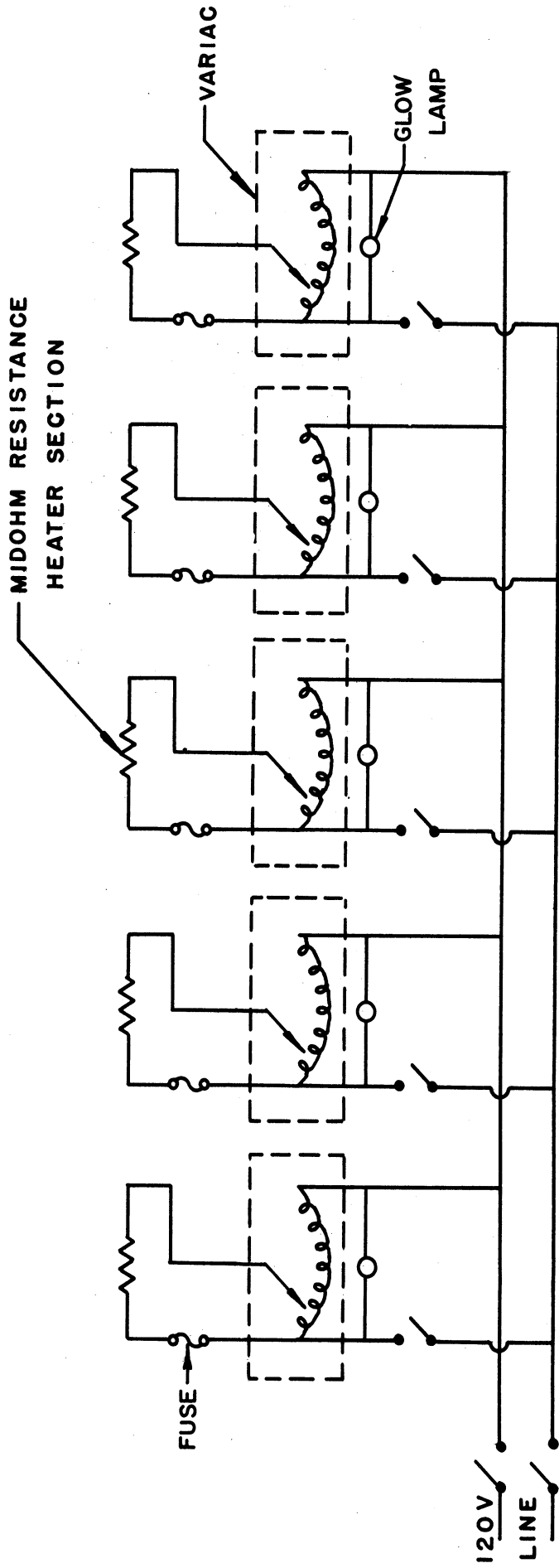


Figure 3. Guard Heater Circuit.

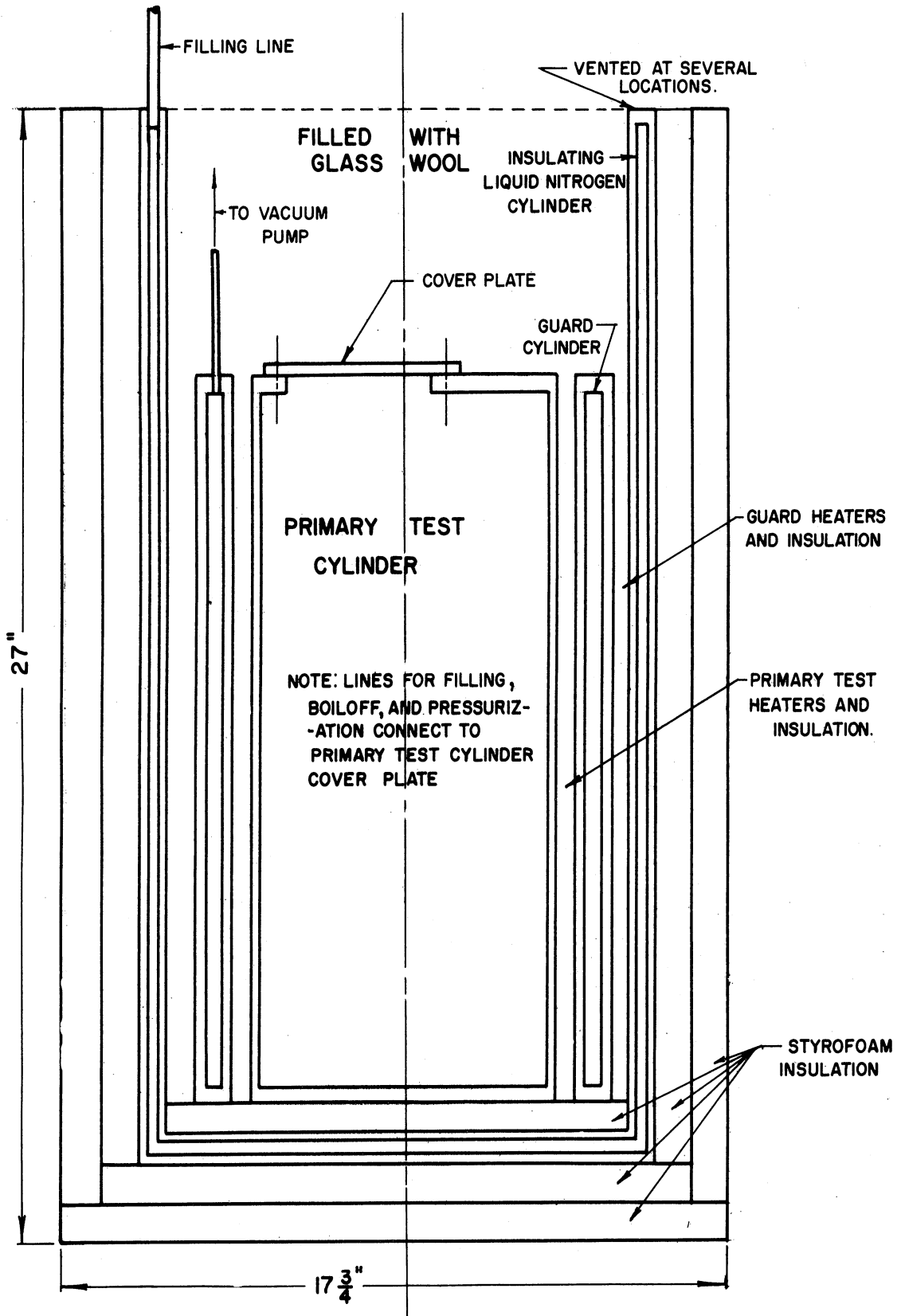


Figure 4. Test Assembly.

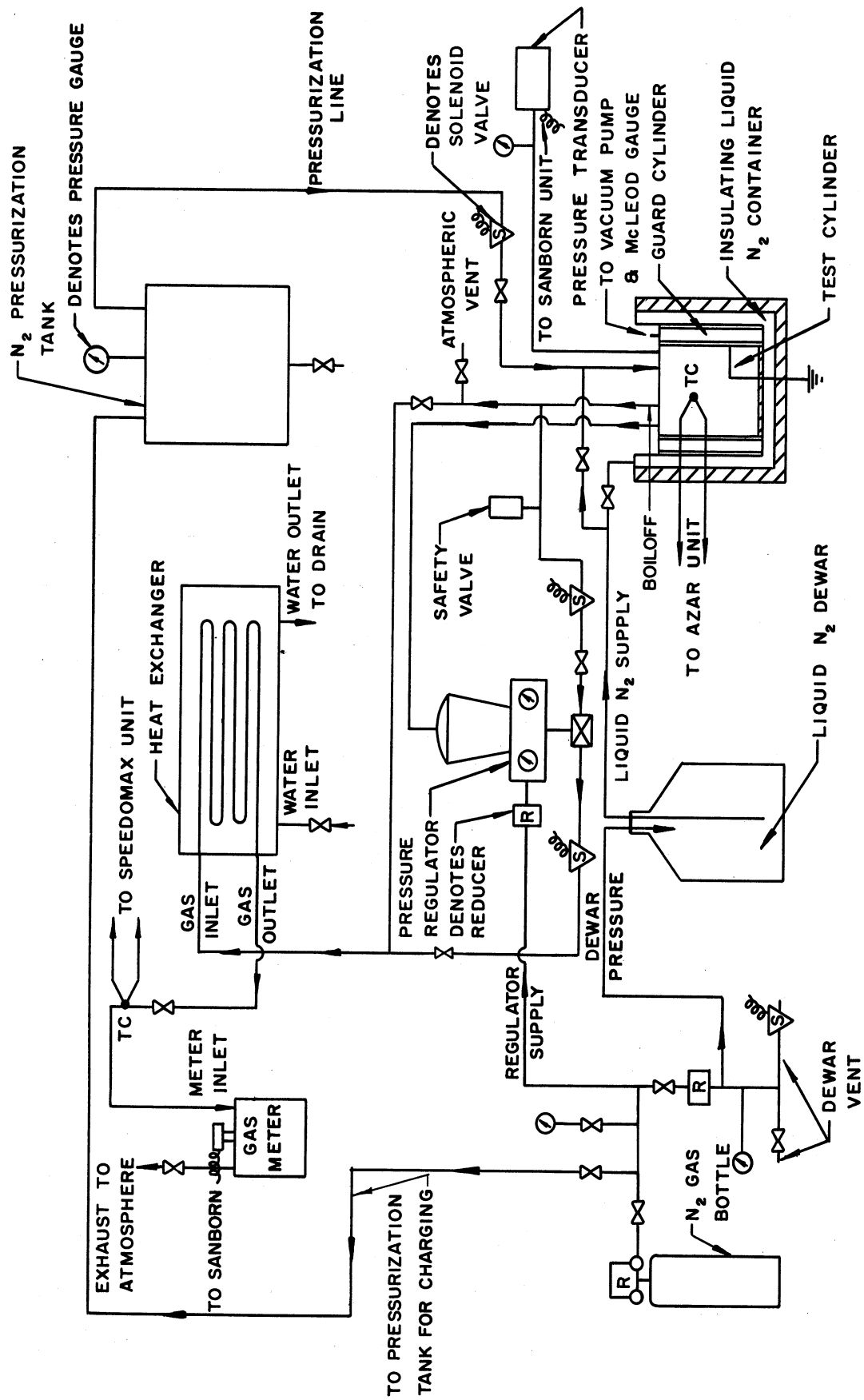


Figure 5. Experimental Layout.

was controlled by Variac auto transformers, one transformer for each section of primary heater wire.

Around the primary test cylinder fits a double-walled cylindrical container shown in Figure 4, which was evacuated by a Cenco Megavac vacuum pump in order to reduce heat losses. The vacuum was measured by a McLeod gauge, which normally read about 30 microns pressure during a run.

Five guard heater segments are wound around the outer diameter of this evacuated cylinder, each corresponding to a section of the primary test heaters. Midohm wire was used for the guard heaters, and the power controlled by five Variacs. At five vertical locations corresponding to the midpoint of the heater sections, difference thermocouples are located between the inner and outer diameters of the evacuated guard cylinder. The current due to any temperature difference between the thermocouples thus located was read on five G-M galvanometers. The guard heater Variacs were used then to regulate guard heater power in order to cause the galvanometers to read approximately zero throughout the entire experiment. In this way, there was good assurance that the primary power being measured was in fact the power going through the walls of the primary test cylinder. That this is true was verified by the fact that heat flux, measured electrically was in good agreement with flux calculated from liquid nitrogen boiloff rates. The guard heater control circuit is shown in Figure 3.

The primary test cylinder and the evacuated guard cylinder are placed inside of a large double-walled cylindrical liquid nitrogen container with a double-walled bottom. This container cooled the outer

guard cylinder wall so that the sought after zero temperature difference could be achieved. It also served to provide a nearly constant, low temperature wall to further reduce heat losses. The potential for heat flow from the liquid contained in the primary cylinder through its unheated bottom was thus never greater than the difference in temperature between the liquid nitrogen in the outermost container and the liquid nitrogen in the primary test cylinder. The outermost container was filled before the primary cylinder and occasionally refilled during the course of a run. It is vented at several locations in order to permit easy filling, and to minimize pressure buildup during the course of a run, which would cause the temperature of the liquid nitrogen to rise resulting in poorer guard heater control. The entire test assembly is shown in Figures 4 and 6. Except for the Styrofoam insulation, the test assembly is made entirely of 5052 aluminum (2½% magnesium, 0.25% chromium). The thicknesses of Styrofoam shown in Figure 4 are separated by aluminum foil in order to reduce radiation effects and to minimize any water vapor penetration of the insulation.

Liquid nitrogen was obtained from a Joy Liquid Nitrogen Generator. Its purity was high enough to permit the use of the physical properties of pure nitrogen (References 6, 7, 11, 12, 21, 29).

Temperatures were measured at five longitudinal locations in the test cylinder wall, and ten locations in the liquid nitrogen under test. These thermocouple locations are shown in Figure 1. The thermocouples are constructed of 30 gauge copper and constantan wire. The wall thermocouples were secured by drilling fine holes into the wall at an angle so that the insertion length of the couples could be nearly

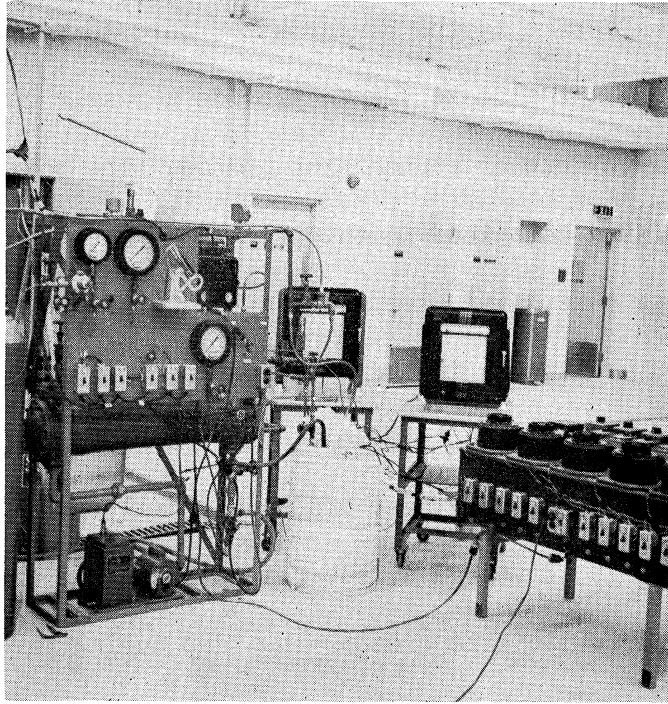


Figure 6. Part of the Experimental Setup Showing Test Assembly, Electrical Control Table, Vacuum Pump, Pressure Regulator, Pressure Gauges, and Speedomax and AZAR Units.

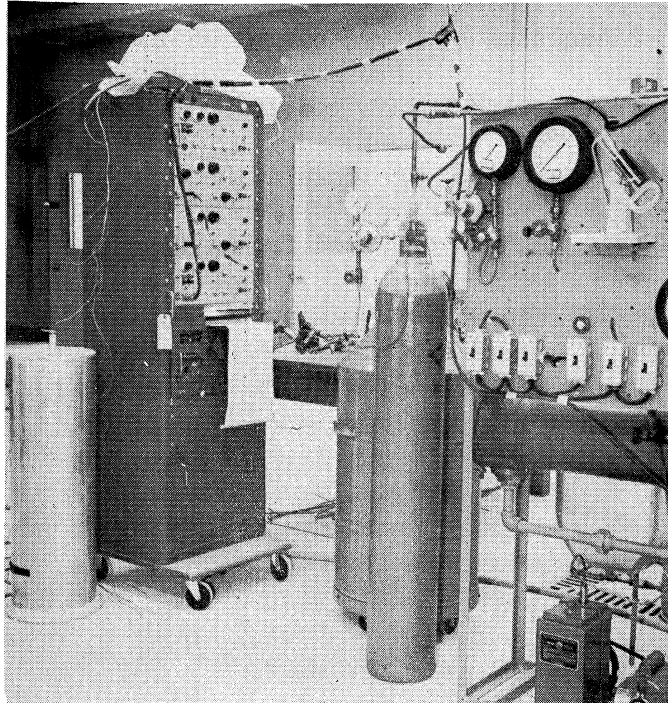


Figure 7. Part of the Experimental Setup Showing Sanborn Recorder, Nitrogen Charging Bottle, Dewar Flask, McLeod Gauge, and Pressure Gauges.

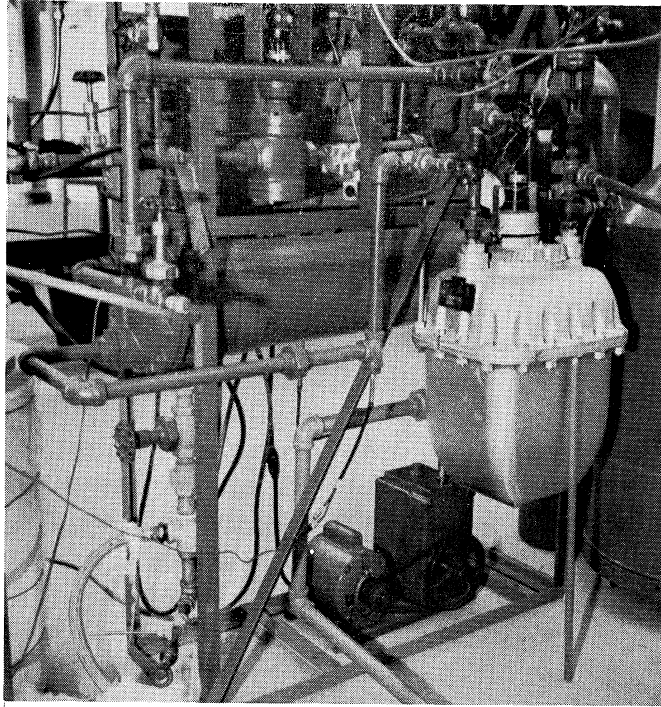


Figure 8. Part of the Experimental Setup Showing Gas Meter, Vacuum Pump, Heat Exchanger, and Part of Pressure Regulator.

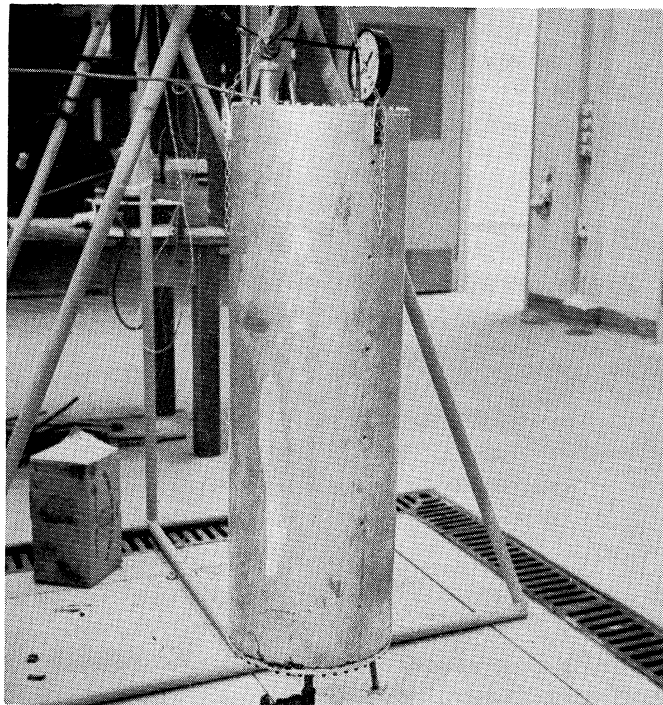


Figure 9. Pressurization Cylinder.

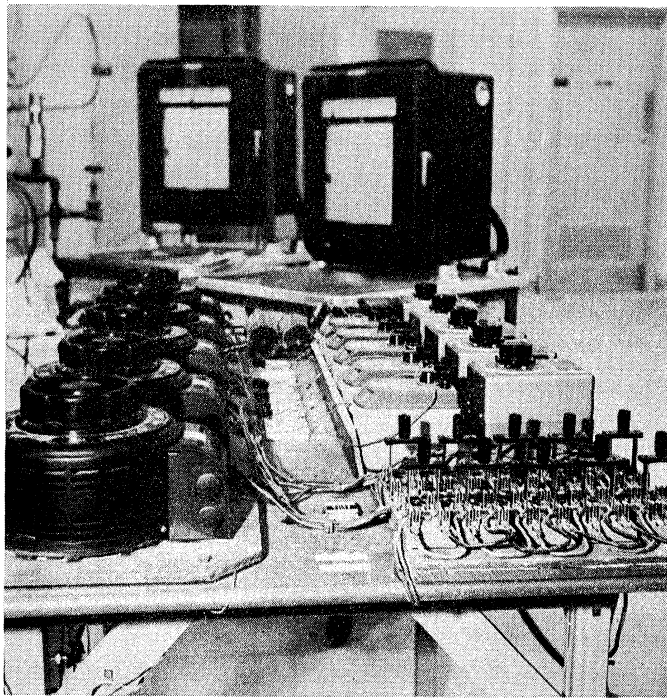


Figure 10. View of Electrical Control Table Showing Primary Power Variacs, Guard Power Variacs, Galvanometers, and Primary Power Switching Arrangement.

as great as the thickness of the cylinder wall. After insertion, the wall was peened over. The wall temperature so measured was taken to be the temperature of the surface contacting the liquid nitrogen because the temperature drop across the entire wall at maximum heat flux was calculated to be only about half a degree. The thermocouples measuring liquid temperatures are held at their respective positions by securing them to a stainless steel gridwork.

Wall and liquid temperatures, accurate to $\pm 0.5^{\circ}\text{F}$, were measured and recorded by a twenty point adjustable zero adjustable range recording potentiometer, the Leeds and Northrup AZAR unit shown in Figures 6 and 10. Liquid nitrogen at atmospheric pressure was used for the cold reference junction.

Test cylinder pressure was measured by a bourdon tube type pressure gauge, accurate to within ± 0.2 psi, and also measured and recorded by a Consolidated strain-gauge type pickup used in conjunction with the carrier preamplifier of a Sanborn 150 recorder, shown in Figure 7. The pressure pickup was calibrated against the bourdon gauge.

A Rockwell bellows type gas meter, accurate to within 2% of reading, was used to measure boiloff from the primary test cylinder. A Helipot continuous rotation potentiometer was attached to the pointer shaft of the gas meter, and a direct current voltage obtained from a dry cell impressed across two of the three terminals of the Helipot. Thus the output voltage is proportional to pointer shaft rotation. This voltage was measured and recorded by the Sanborn 150 recorder, using the AC-DC preamplifier.

Commercially obtainable nitrogen gas bottles were used to fill the pressurization cylinder shown in Figure 9. The gas charge in the latter was used for pressurizing the liquid nitrogen under test.

Pressure regulation of the primary test cylinder was accomplished by a Fisher Wizard pressure regulator.

Since the Rockwell meter was not designed for gases as low in temperature as the nitrogen boiloff, the cold nitrogen gas coming from the primary cylinder was fed through a tubular heat exchanger using city water at close to ambient temperature to heat the gas. The heat exchanger may be seen in Figure 8. The temperature of the gas entering the meter was measured and recorded by a Leeds and Northrup Speedomax unit, shown in Figures 6 and 10. During a run, the temperature of this gas remained substantially constant between 60 and 70°F depending upon the water temperature and gas and water flow rates. The entire experimental layout is shown in Figure 5.

A carbon resistor located in the test cylinder seventeen inches from the bottom, was placed in series with a milliammeter and a dry cell in order to provide a simple means of liquid level indication when the cylinder was being filled. Since the rate of heat transfer from the resistor is greater to the liquid nitrogen than to the gaseous mixture occupying the cylinder before it is filled, and above the liquid surface while it is being filled, the rate of heat dissipation increased when the rising liquid surface came into contact with the carbon resistor. This increased heat loss caused the temperature of the resistor to drop and its resistance thus increased, resulting in diminished current reading on the milliammeter. This reading was quickly checked

by noting the temperatures of appropriate liquid thermocouples being recorded on the AZAR unit. While the indication of the resistor was not instantaneous, the error introduced was small because the filling rate was intentionally kept low. Immediately upon reaching the prescribed level, the Dewar flask being emptied of liquid nitrogen was vented by solenoid valve, then further relieved by a hand valve.

The important points of the experimental procedure are as follows:

(a) The vacuum pump was started and all electronic instruments turned on at least one hour prior to the start of filling.

(b) The outermost liquid nitrogen container was filled.

(c) Filling of the test cylinder was then begun.

(d) Power was turned on in the primary heaters.

(The filling was begun before power was turned on in order to provide some cooling for the heater wires, which could burn out if there were no heat abstraction by liquid nitrogen or cold nitrogen vapor).

(e) The test cylinder was filled to seventeen inches.

(f) Fine adjustment of heater power was made.

(g) Guard heaters were turned on and first voltage adjustment made.

(h) The liquid nitrogen was permitted to boil down to such level as necessary to insure steady boiling. This was done by watching for wall temperature repetition on the AZAR unit.

(i) Pressurization was effected by opening the solenoid valve located between the pressurization cylinder and the test cylinder, as shown in Figure 5.

(j) The pressure in the test cylinder was maintained at a value slightly less than the set value for the pressure regulator, in order to prevent the latter from opening prematurely. If pressurization were discontinued too soon, the test pressure would have dropped due to condensation of the pressurizing gas. Any pressure buildup which would follow would be attributable, not to external pressurization, but to self-pressurization.

The pressurization was discontinued when there was no longer any tendency for the cylinder pressure to drop. This means that the rate of boiloff was essentially equal to the condensation rate. After this point, the regulator opened, and the Sanborn recorded what is, for this experiment, defined as first net boiloff.

CHAPTER III

EXPERIMENTAL RESULTS

On the following pages the basic experimental results sought after in this investigation are presented. In the chapter following, explanation and analysis of these results are given.

These provide raw answers to the preliminary questions which prompted this research:

1. How are wall and liquid transients affected by the level of heat flux and pressurization.
2. What longitudinal and radial liquid gradients exist as can be determined from the thermocouple coverage.
3. What is the nature of the heat transfer coefficient transient following pressurization, and how is it affected by flux and pressure.
4. How is time for first net boiloff influenced by the system variables.
5. What is the relationship between time for first net boil-off and the time required for the liquid to reach saturation if no boiling is assumed to occur.

Odd numbered Figures 11 through 33 show the wall and liquid temperature transients for various levels of heat flux, and pressurization to 20 and 35 psig. Time zero on these graphs, as well as all others in this investigation in which "time" is the abscissa, represents the point at which pressurization is begun. As indicated, each run begins with steady boiling at atmospheric or near atmospheric pressure, and ends with steady boiling at the new pressure. Tabulated

data for these graphs are given in Table I of the Appendix. Since the liquid temperatures at the centerline, and those midway between the centerline and the wall are substantially the same at a given time and distance above the cylinder bottom, only one liquid temperature is reported for a prescribed thermocouple location.

By defining dimensionless temperature and time ratios these data may be reduced to a single curve for each longitudinal location. As the ordinate in such a representation θ/θ^* is used. θ is the instantaneous temperature of the liquid above the initial saturation temperature:

$$\theta \equiv t_{Lx} - t_{1 \text{ sat.}} \quad (1)$$

θ^* is defined as the difference between the final and initial saturation temperatures:

$$\theta^* \equiv t_{2 \text{ sat.}} - t_{1 \text{ sat.}} \quad (2)$$

As the abscissa, a dimensionless time, τ/τ^* , is used. τ is the time after pressurization is begun. τ^* represents the time required for the mass of liquid nitrogen under test to be heated from its initial to its final saturation temperature at the prescribed heat flux, assuming no boiling occurs anywhere in the system:

$$\tau^* \equiv \frac{w_L c_{pL} (t_{2 \text{ sat.}} - t_{1 \text{ sat.}})}{(q/A) \cdot A} = \frac{w_L c_{pL} \theta^*}{q} \quad (3)$$

Curves of θ/θ^* vs. τ/τ^* are given in Figures 35 - 38 and points tabulated in Table I of the Appendix.

The instantaneous value of the local inside coefficient of heat transfer is calculated from the defining equation:

$$h \equiv \frac{(q/A)}{t_{WX} - t_{LX}} \quad (4)$$

The results of these calculations are seen in even numbered Figures 12 through 34, and in Table II of the Appendix.

In Figures 39 - 42 the heat flux is plotted against the average values of the temperature difference between the wall and saturated liquid for steady state boiling at 0, 20 and 35 psig.

Corresponding to these curves, Figures 43 - 45 show the heat transfer coefficient for boiling liquid nitrogen vs. heat flux.

The time for first net boiloff, τ_b , as defined in Chapters II and IV is shown as a function of heat flux in Figures 46 - 48. Table III of the Appendix is a tabulation of values for these curves.

Figure 49 is a plot of heat flux vs. a dimensionless time for first boiloff, τ_b/τ^* .

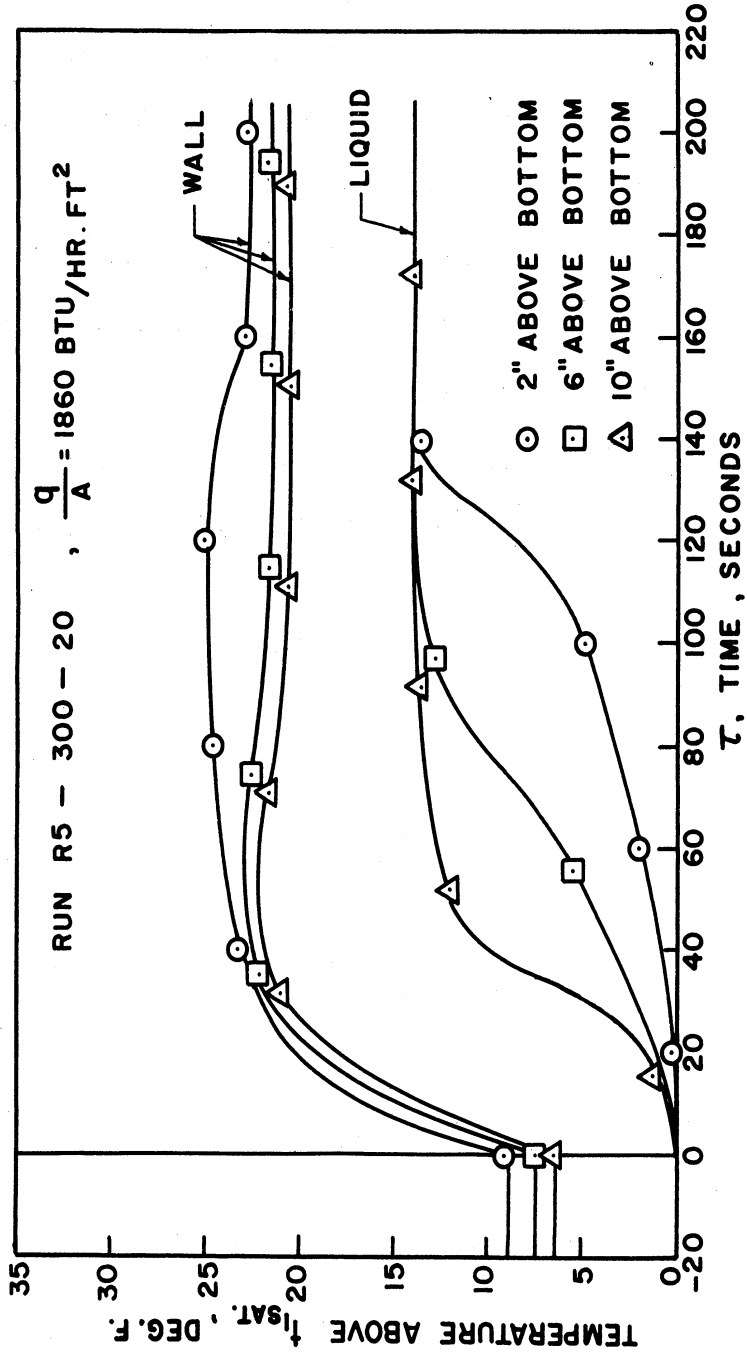


Figure 11. Wall and Liquid Temperatures vs. Time, Run R5-300-20.

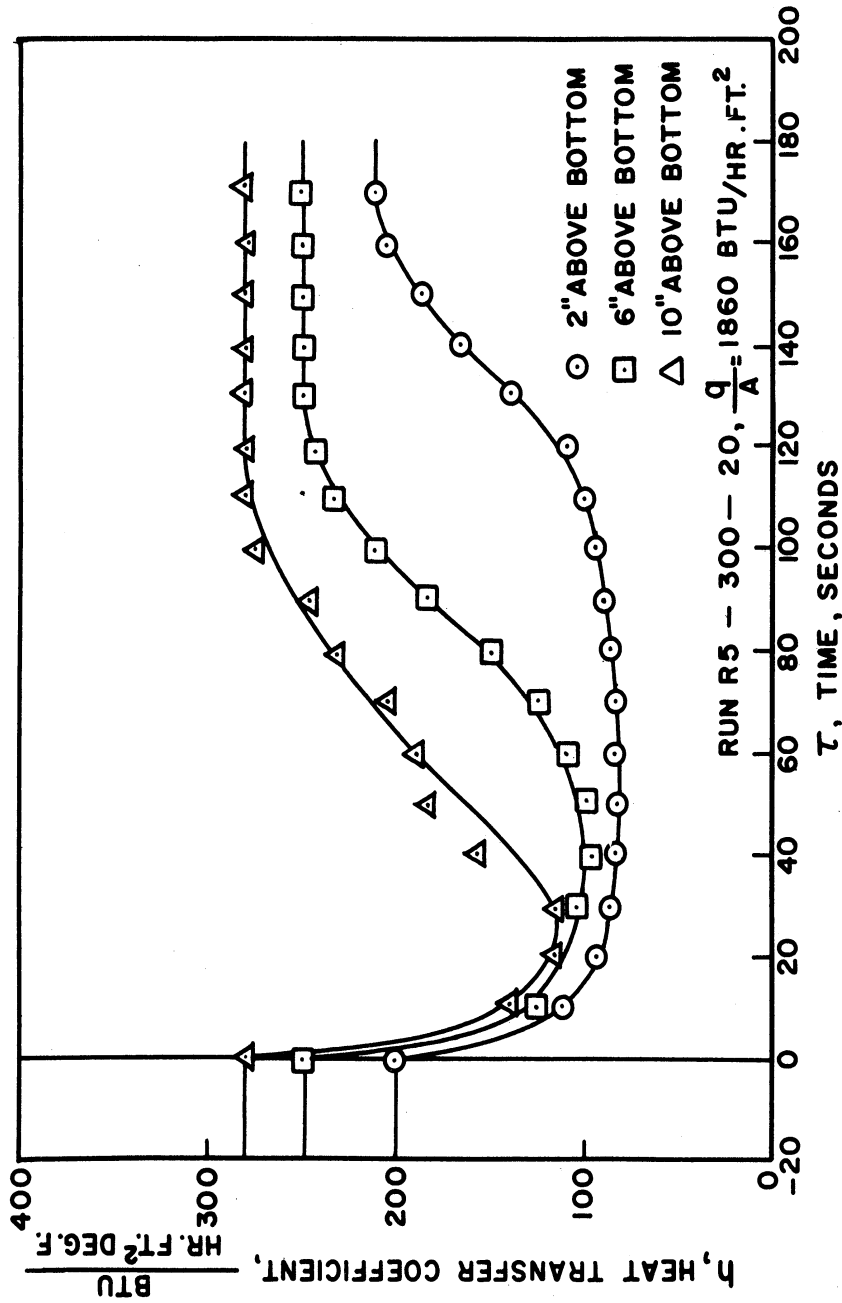


Figure 12. Heat Transfer Coefficient vs. Time, Run R5-300-20.

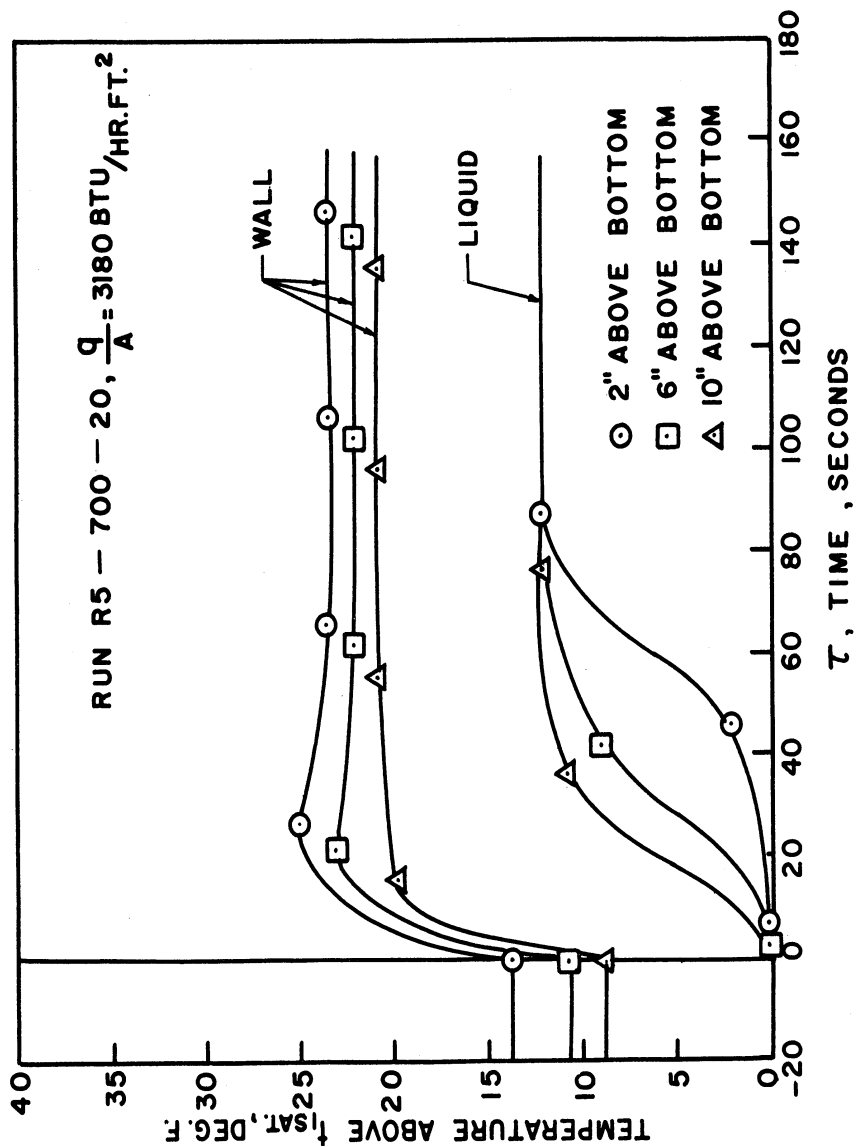


Figure 13. Wall and Liquid Temperatures vs. Time, Run R5-700-20.

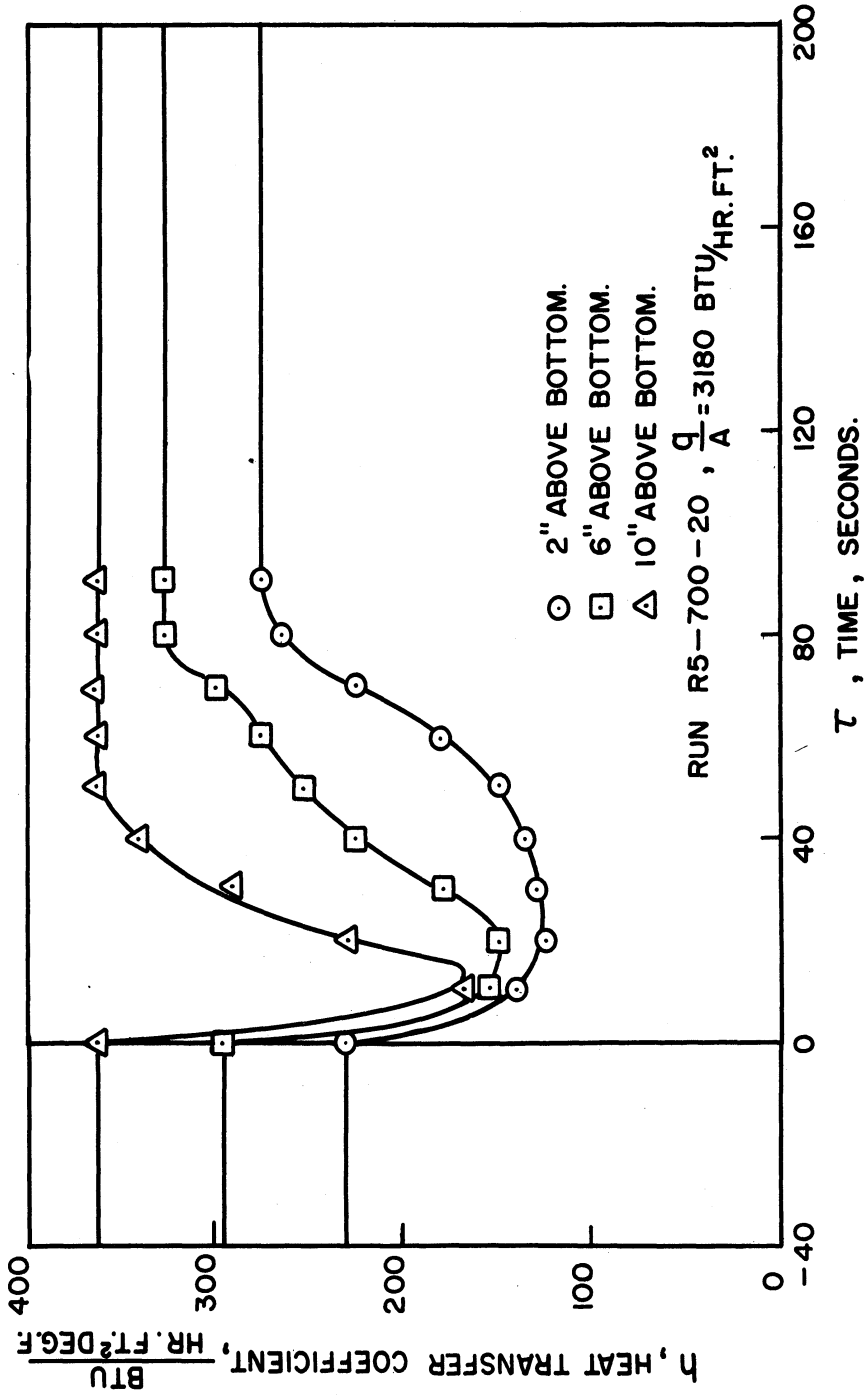


Figure 14. Heat Transfer Coefficient vs. Time, Run R5-700-20.

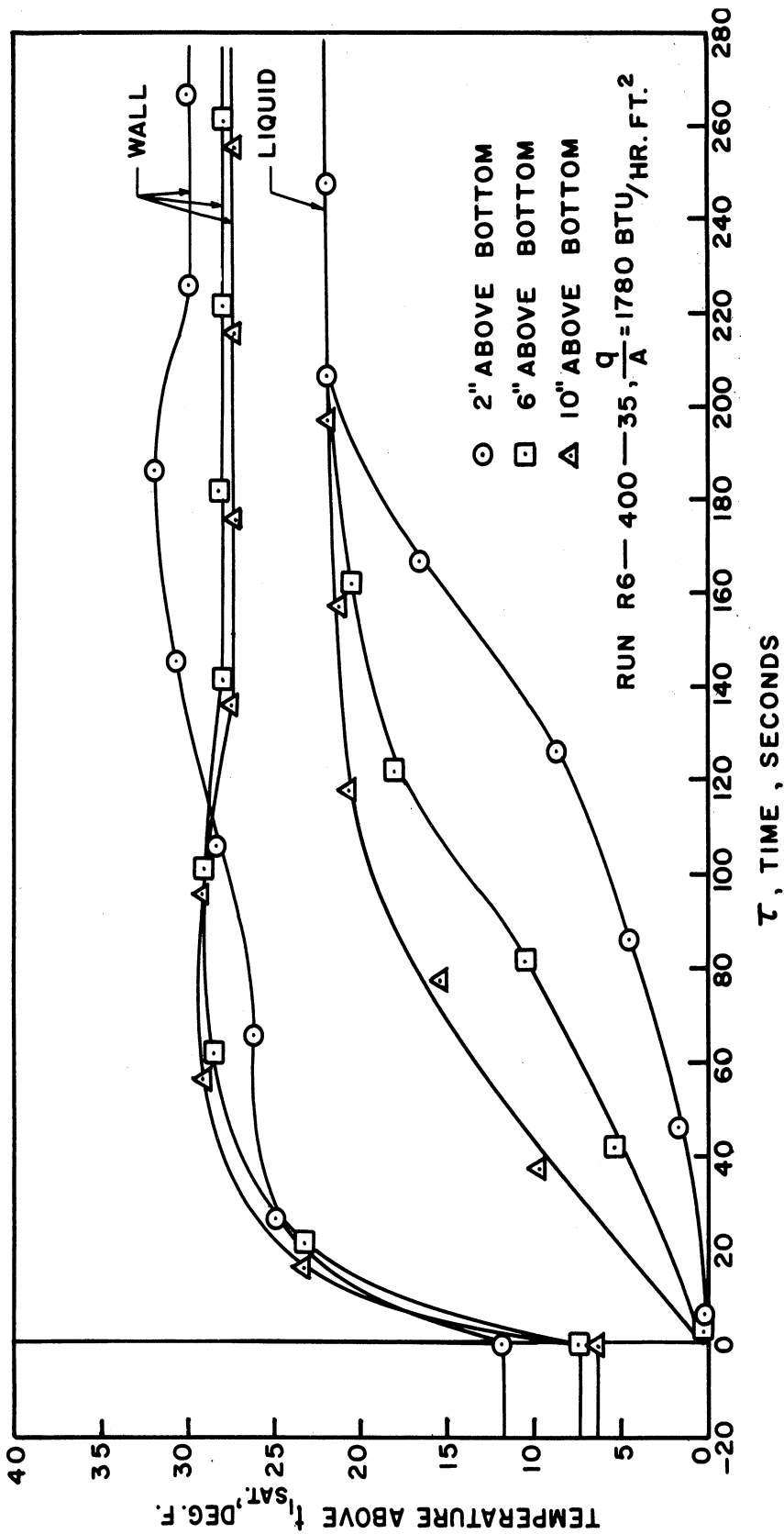


Figure 15. Wall and Liquid Temperatures vs. Time, Run R6-400-35.

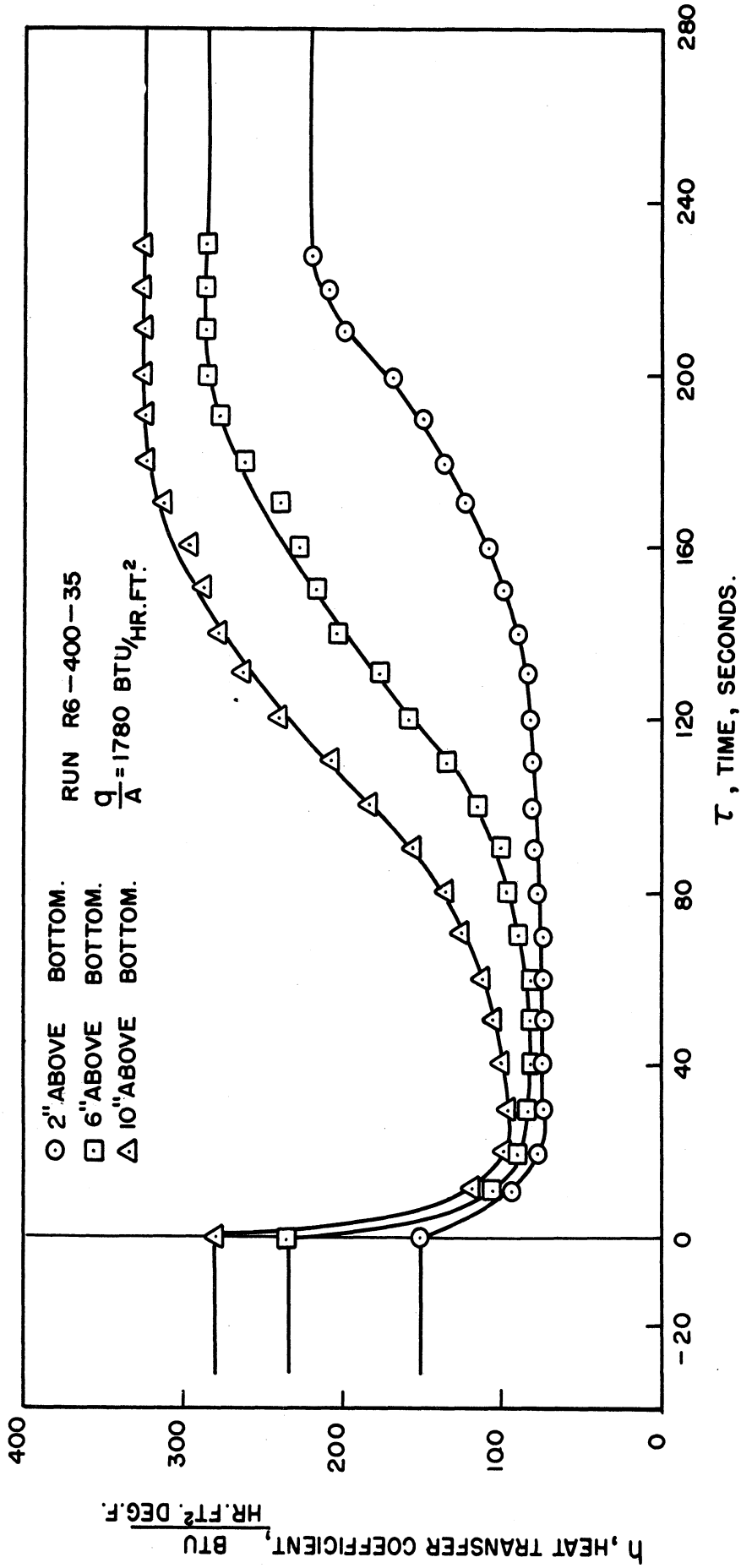


Figure 16. Heat Transfer Coefficient vs. Time, Run R6-400-35.

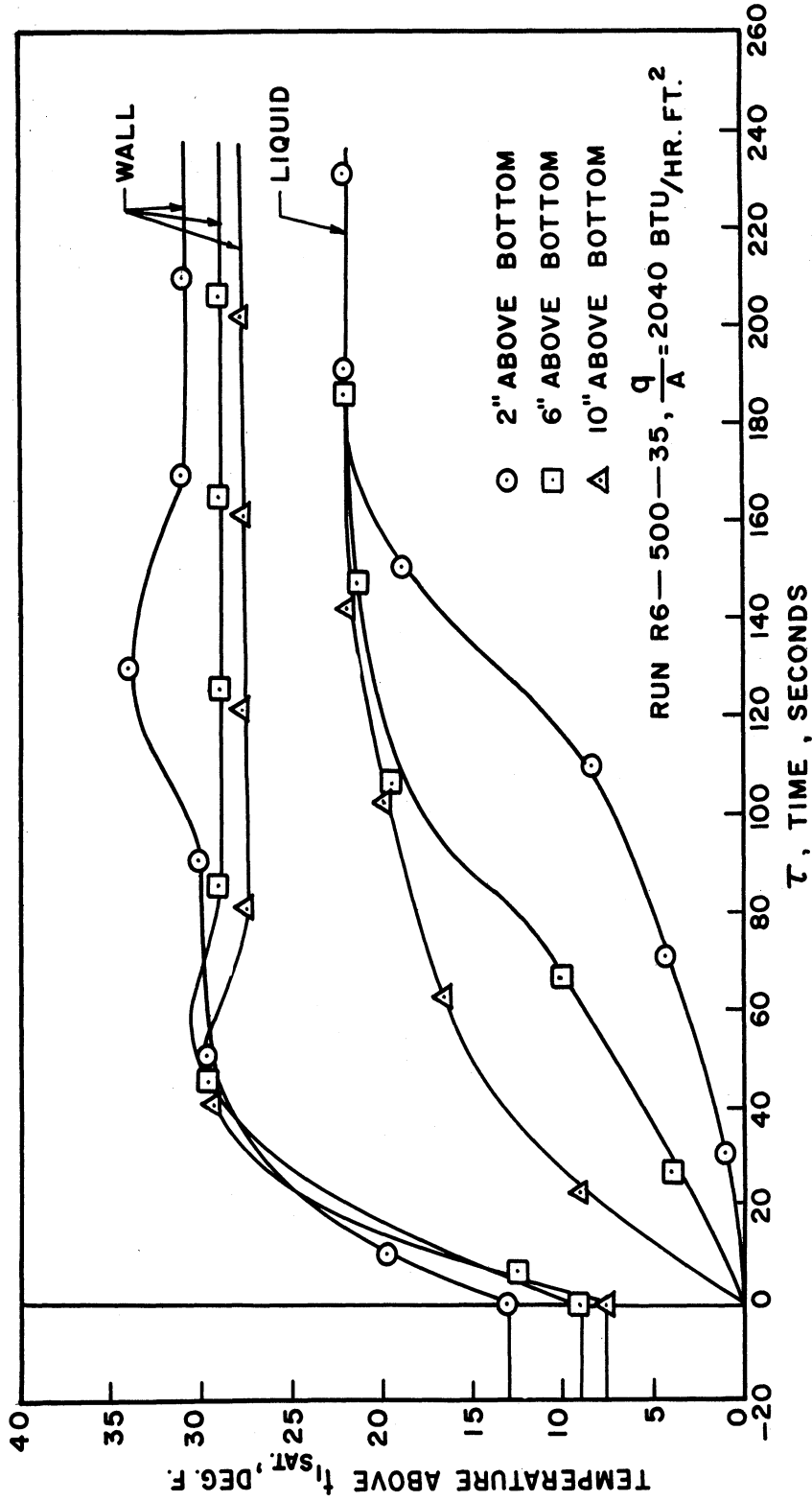


Figure 17. Wall and Liquid Temperatures vs. Time, Run R6-500-35.

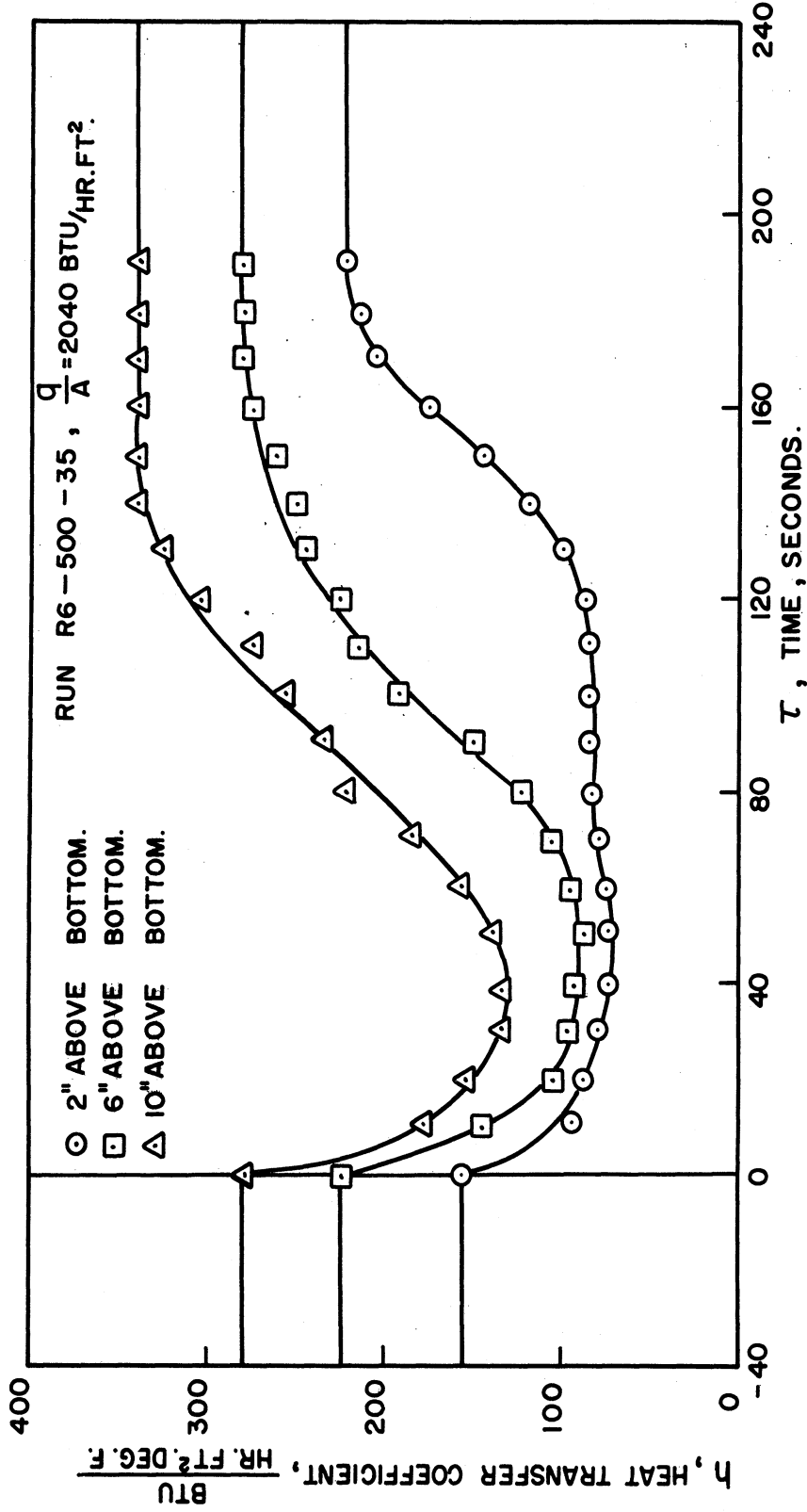


Figure 18. Heat Transfer Coefficient vs. Time, Run R6-500-35.

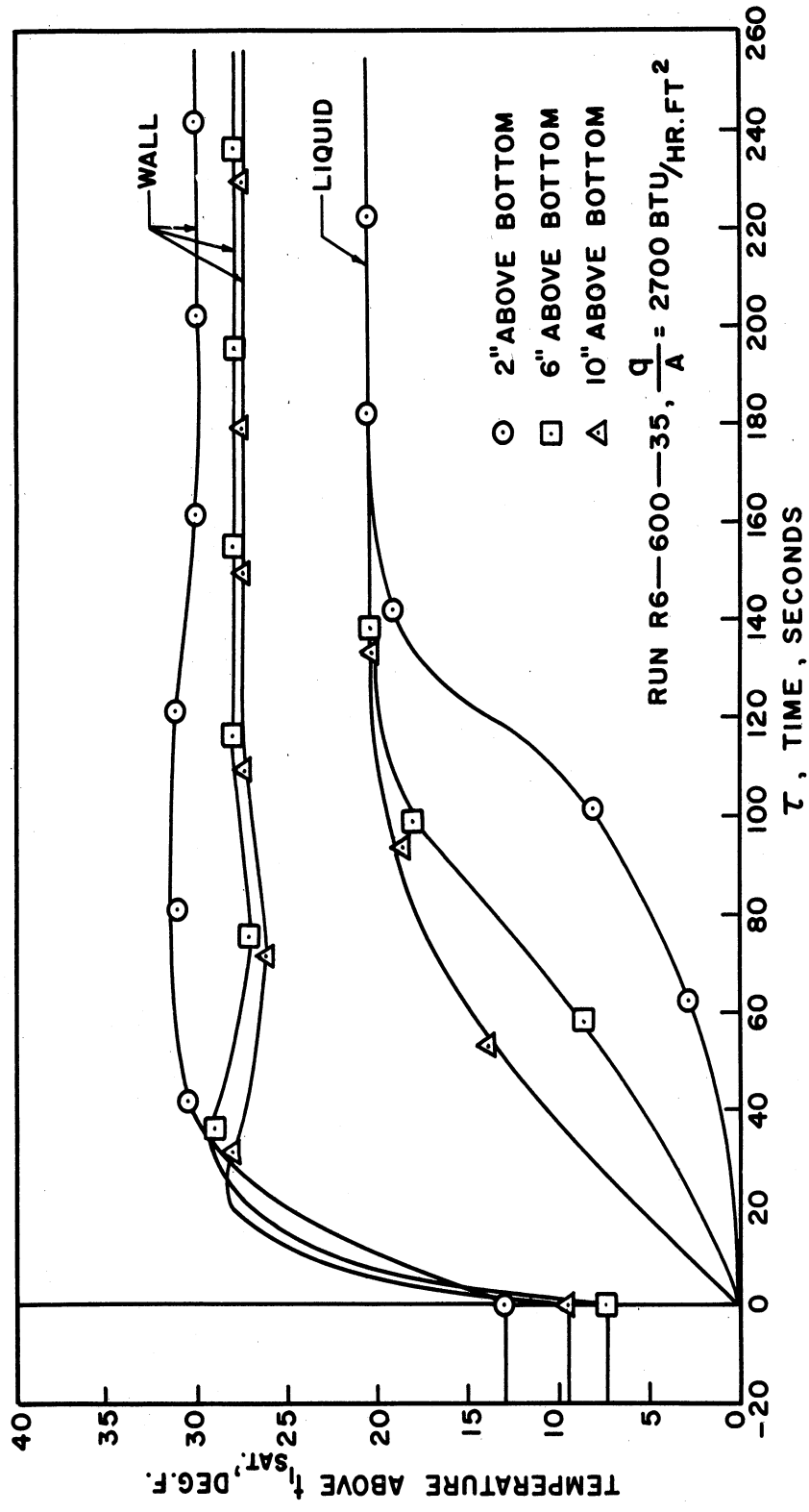


Figure 19. Wall and Liquid Temperatures vs. Time, Run R6-600-35.

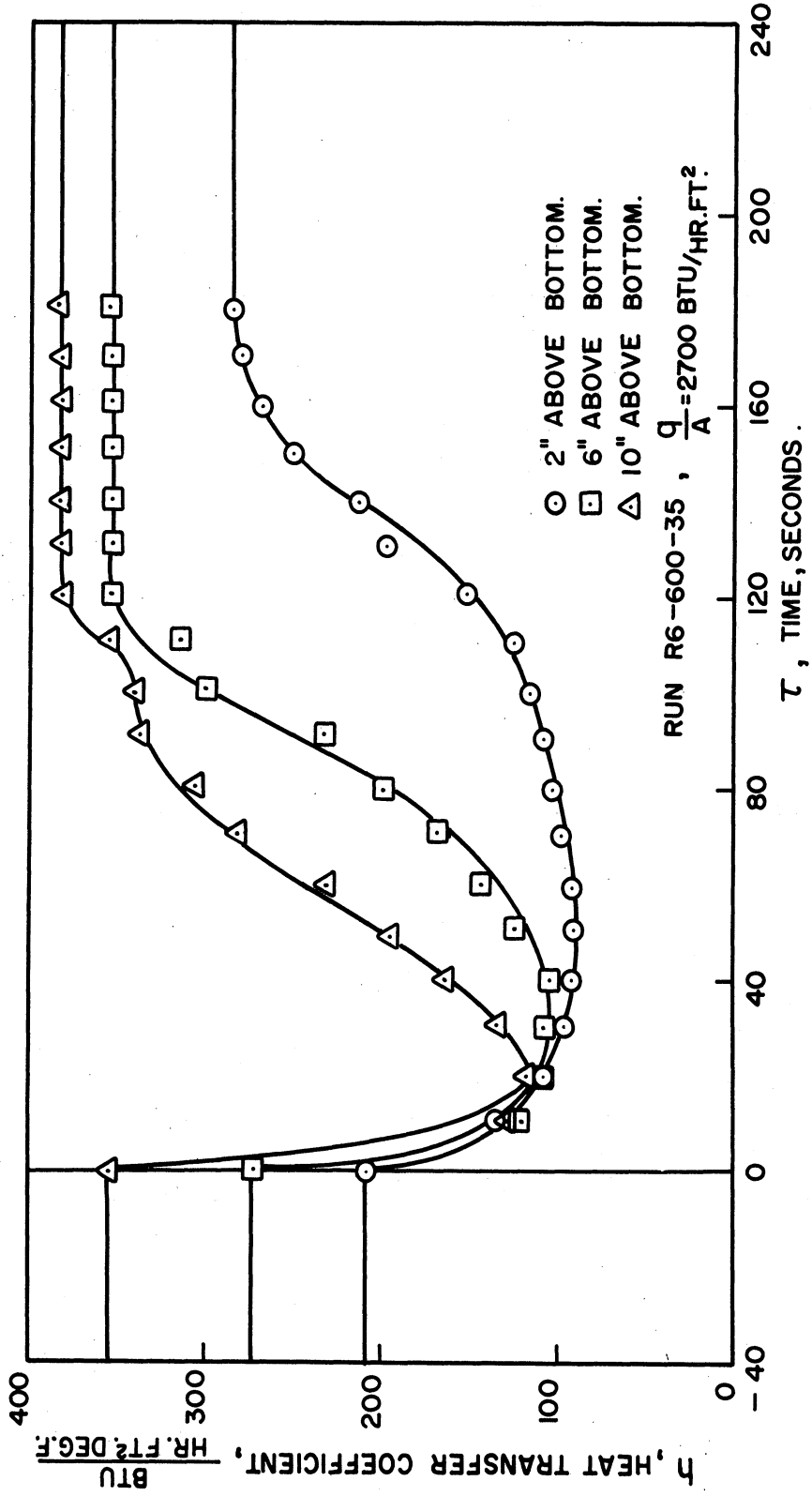


Figure 20. Heat Transfer Coefficient vs. Time, Run R6-600-35.

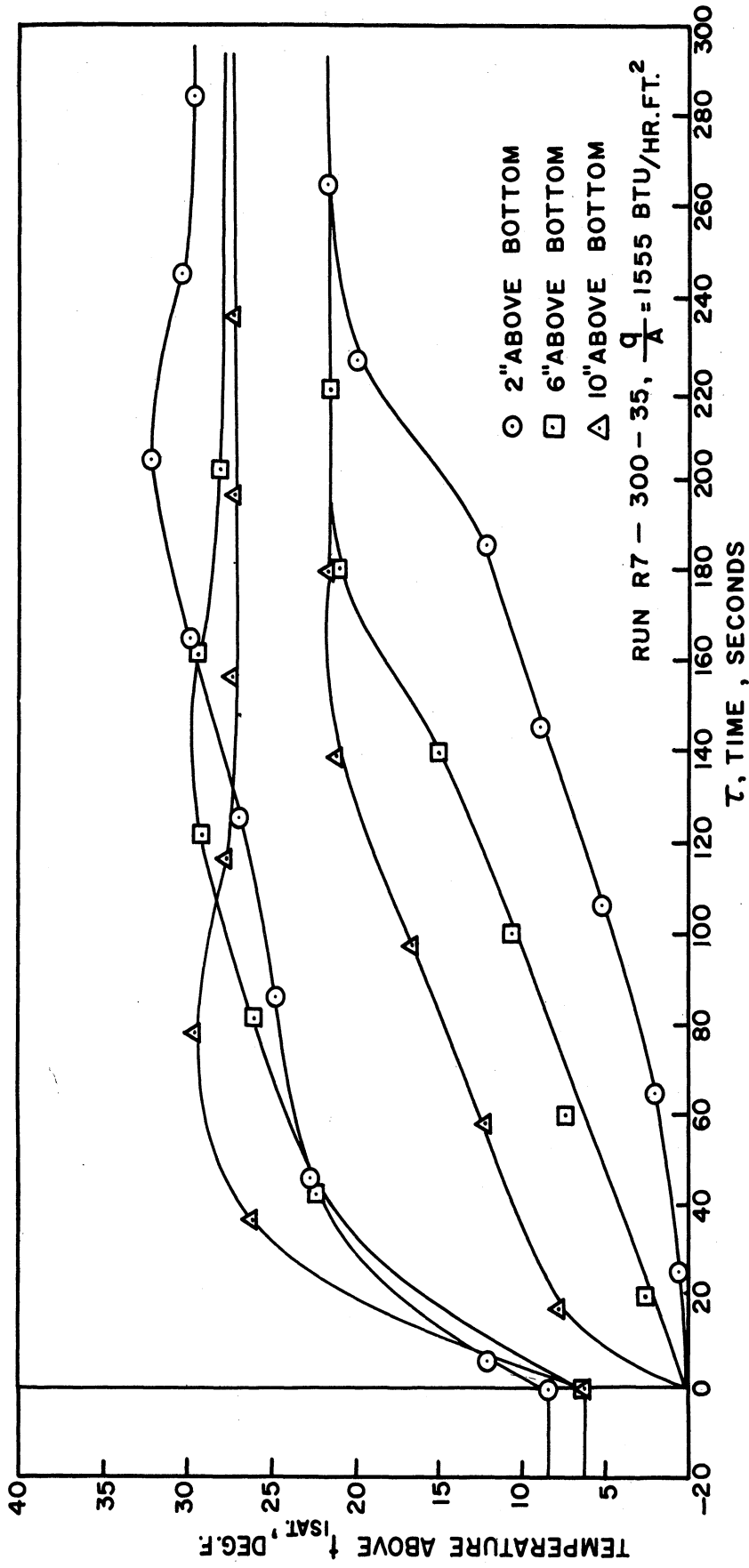


Figure 21. Wall and Liquid Temperatures vs. Time, Run R7-300-35.

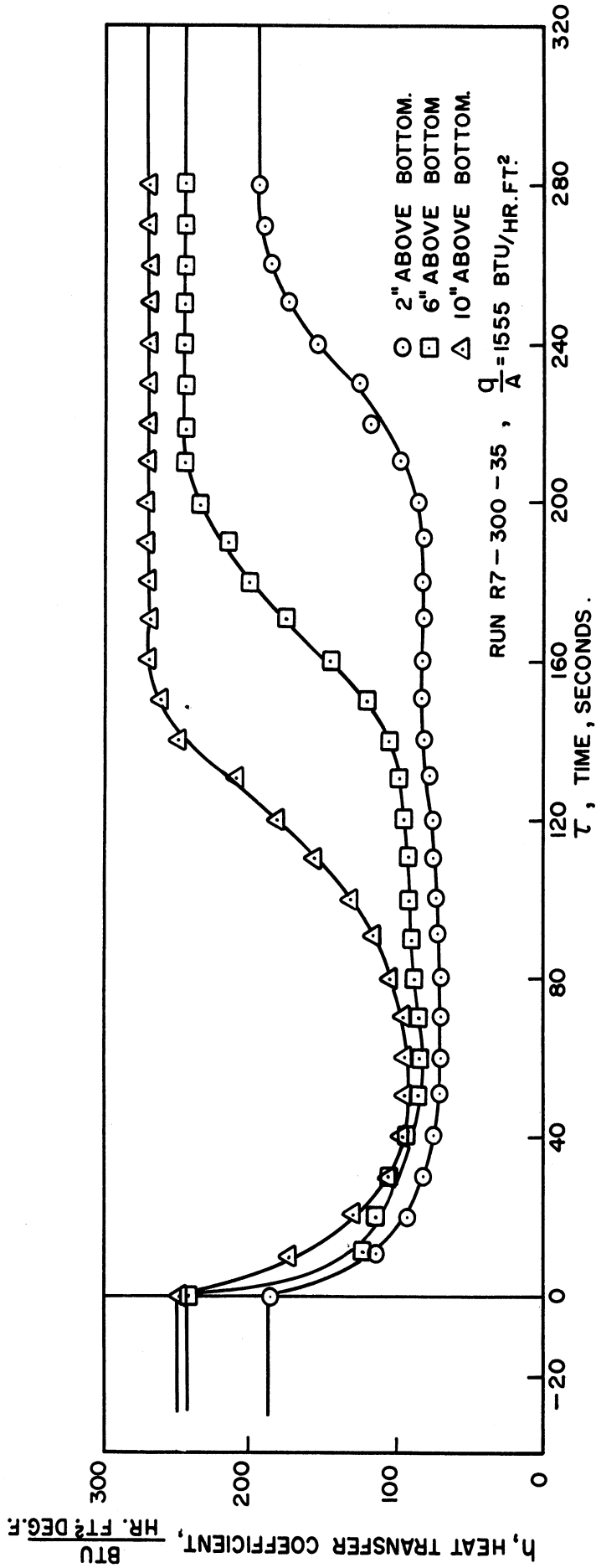


Figure 22. Heat Transfer Coefficient vs. Time, Run R7-300-35.

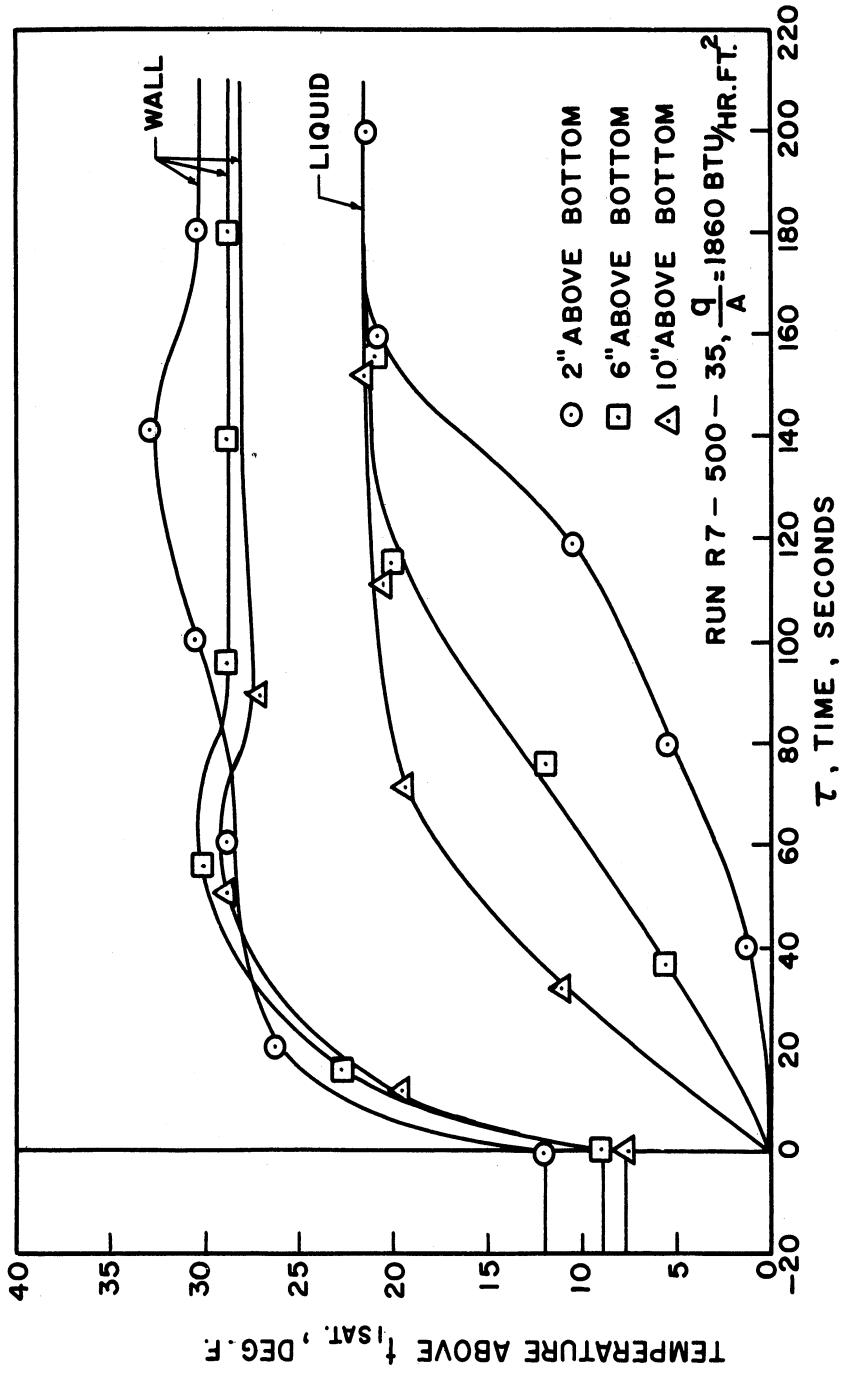


Figure 23. Wall and Liquid Temperatures vs. Time, Run R7-500-35.

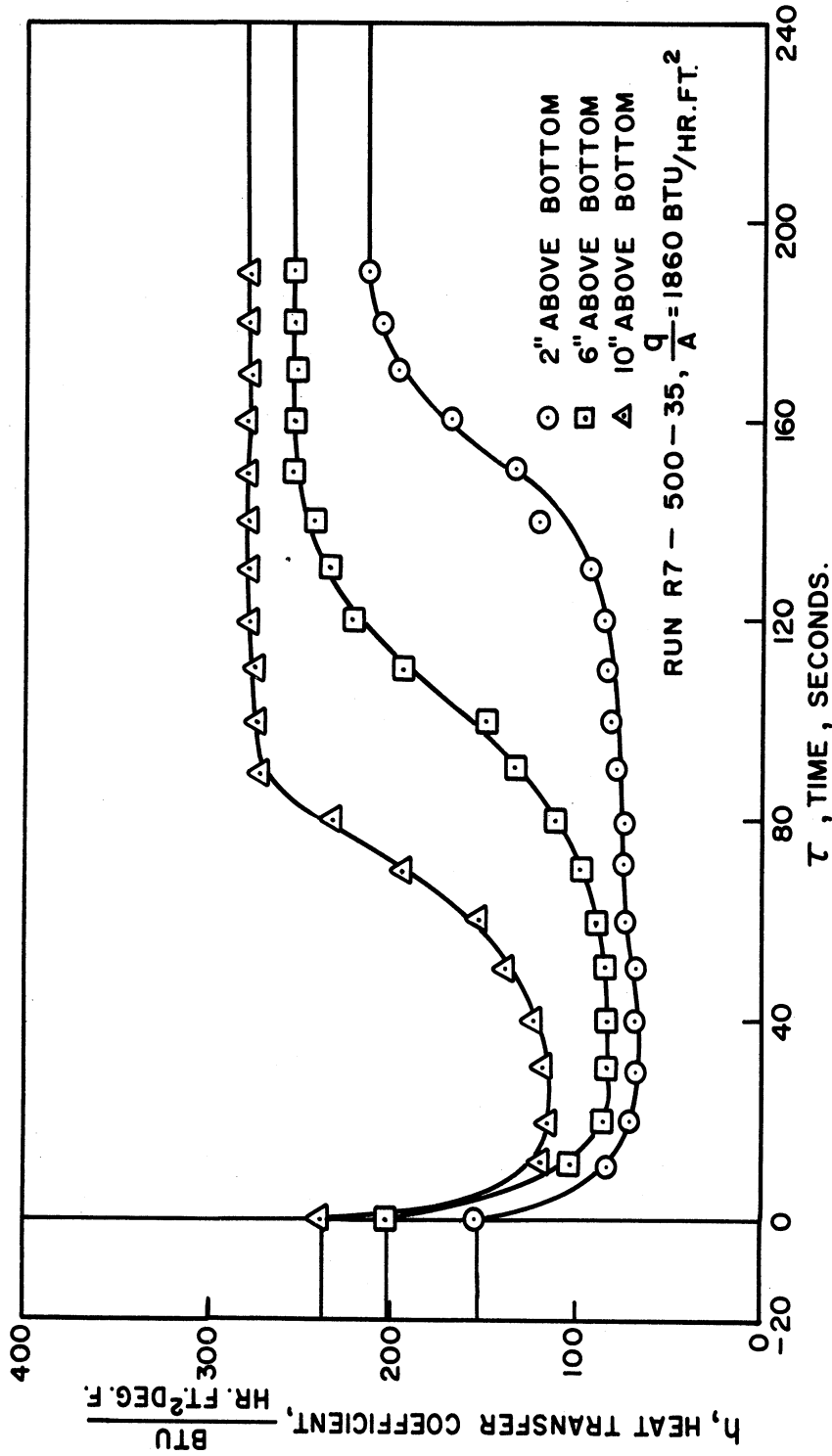


Figure 24. Heat Transfer Coefficient vs. Time, Run R7-500-35.

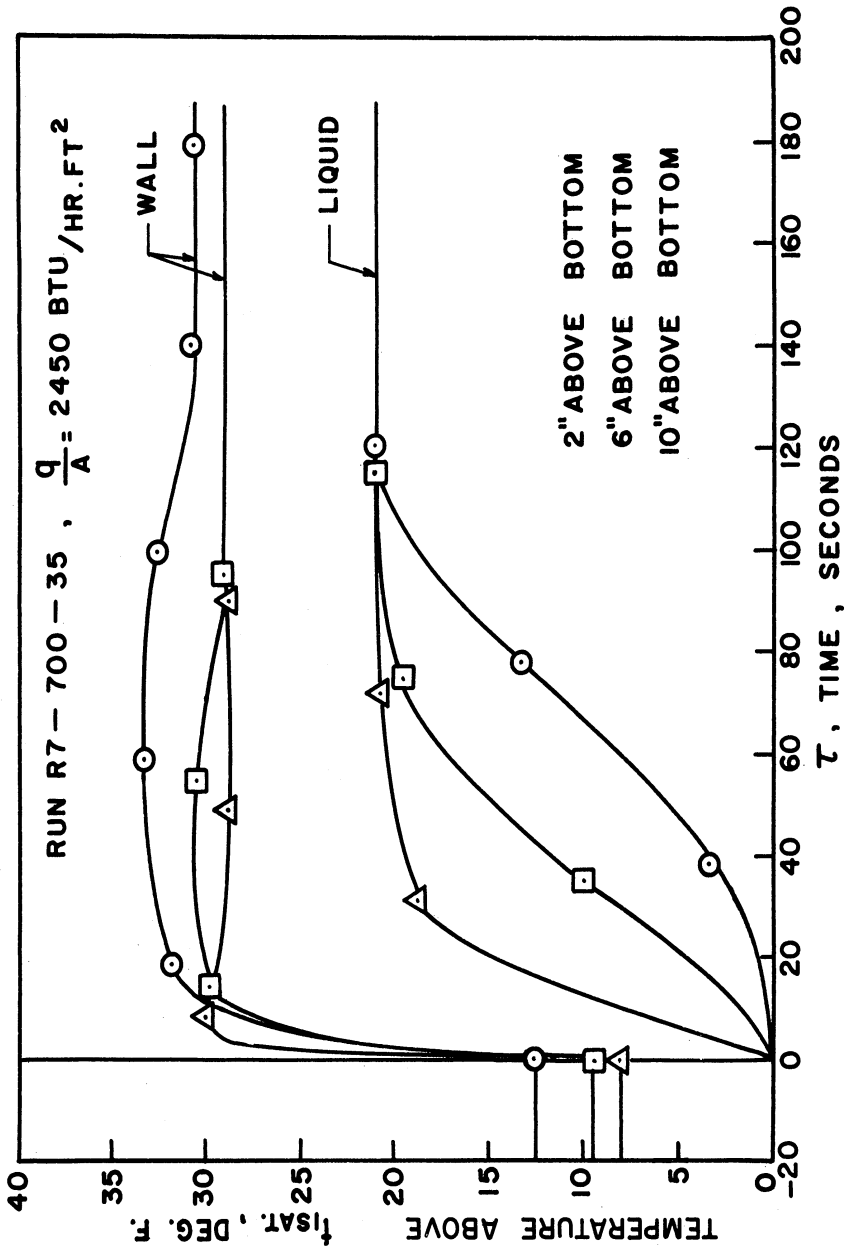


Figure 25. Wall and Liquid Temperatures vs. Time, Run R7-700-35.

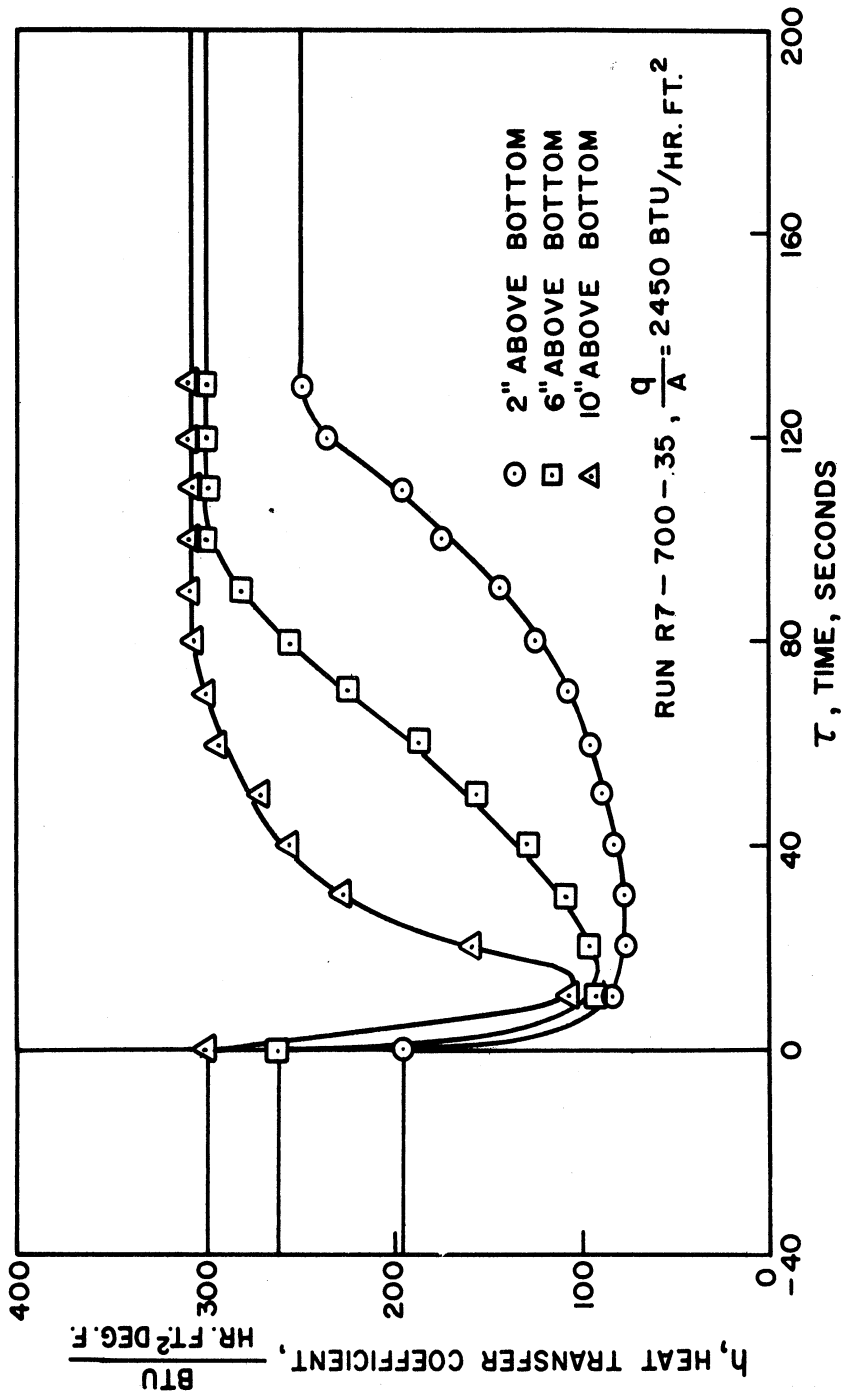


Figure 26. Heat Transfer Coefficient vs. Time, Run R7-700-35.

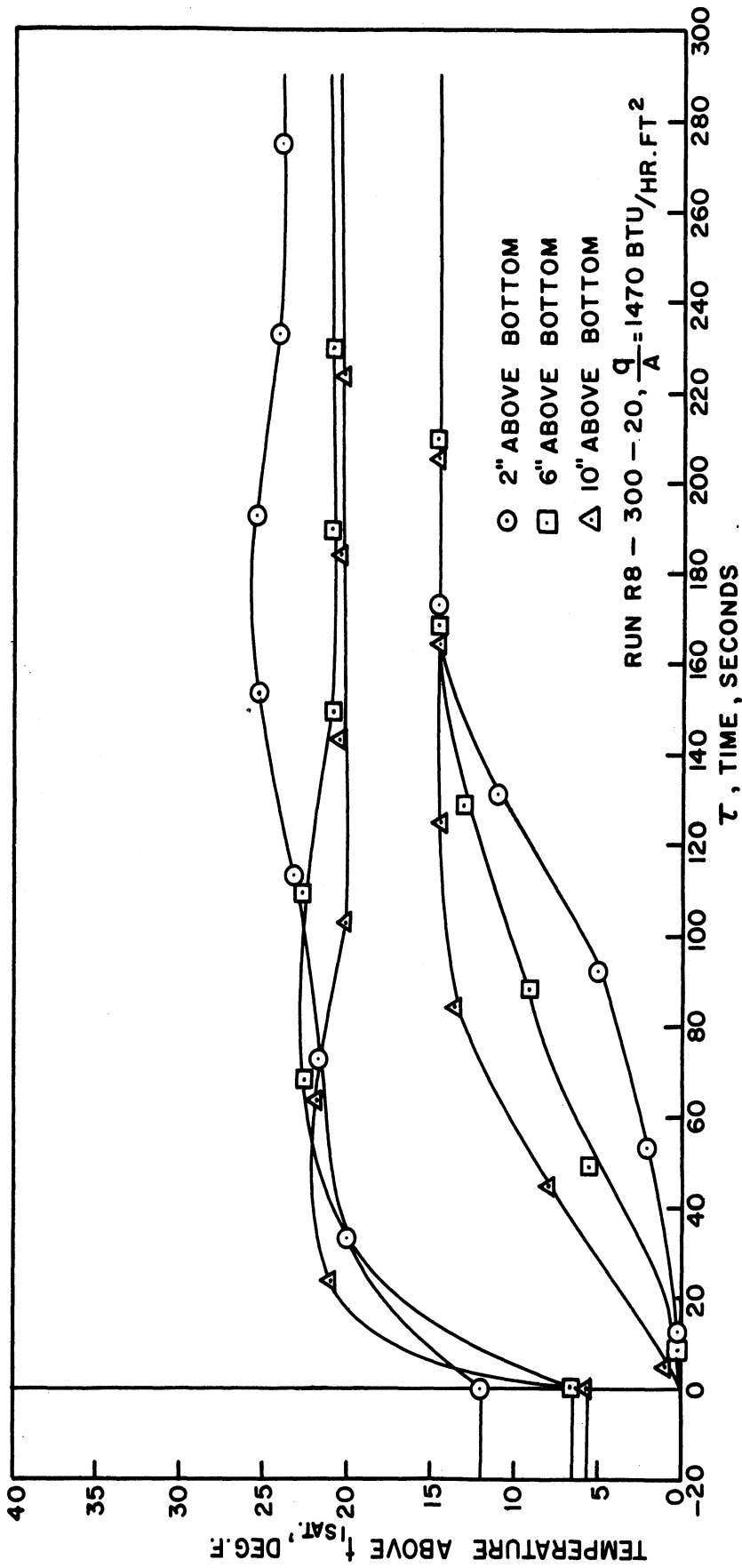


Figure 27. Wall and Liquid Temperatures vs. Time, Run R8-300-20.

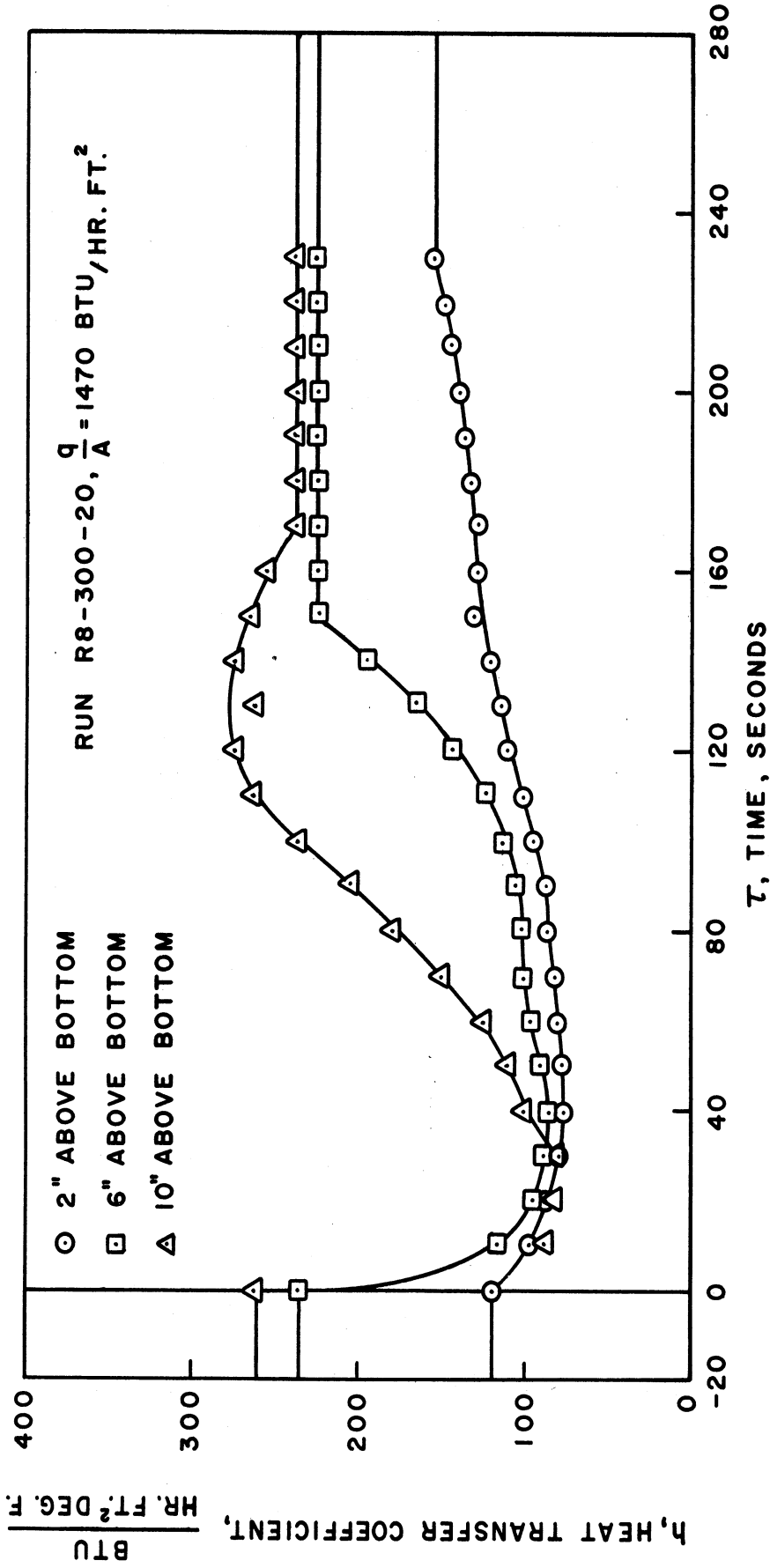


Figure 28. Heat Transfer Coefficient vs. Time, Run R8-300-20.

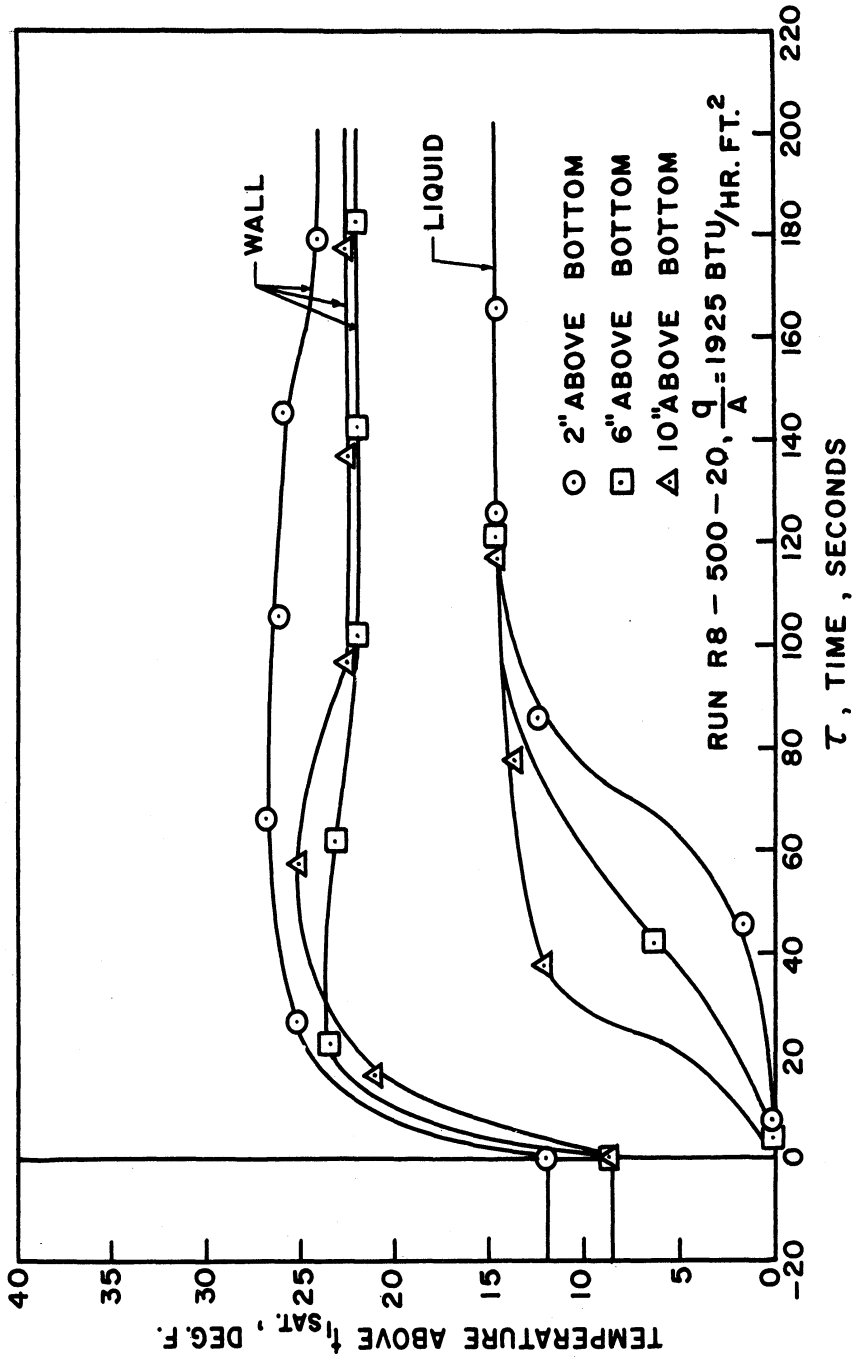


Figure 29. Wall and Liquid Temperatures vs. Time, Run R8-500-20.

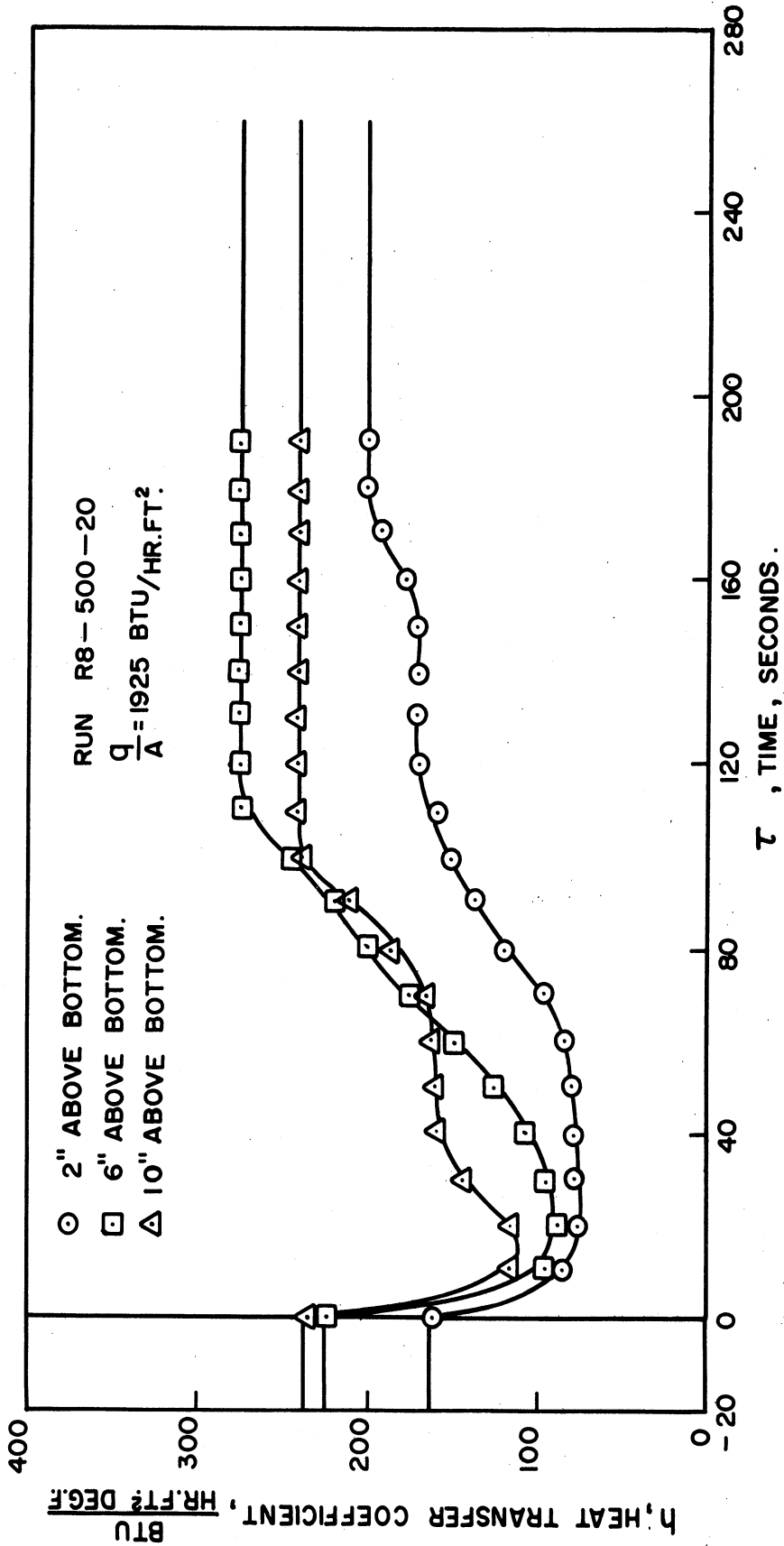


Figure 30. Heat Transfer Coefficient vs. Time, Run R8-500-20.

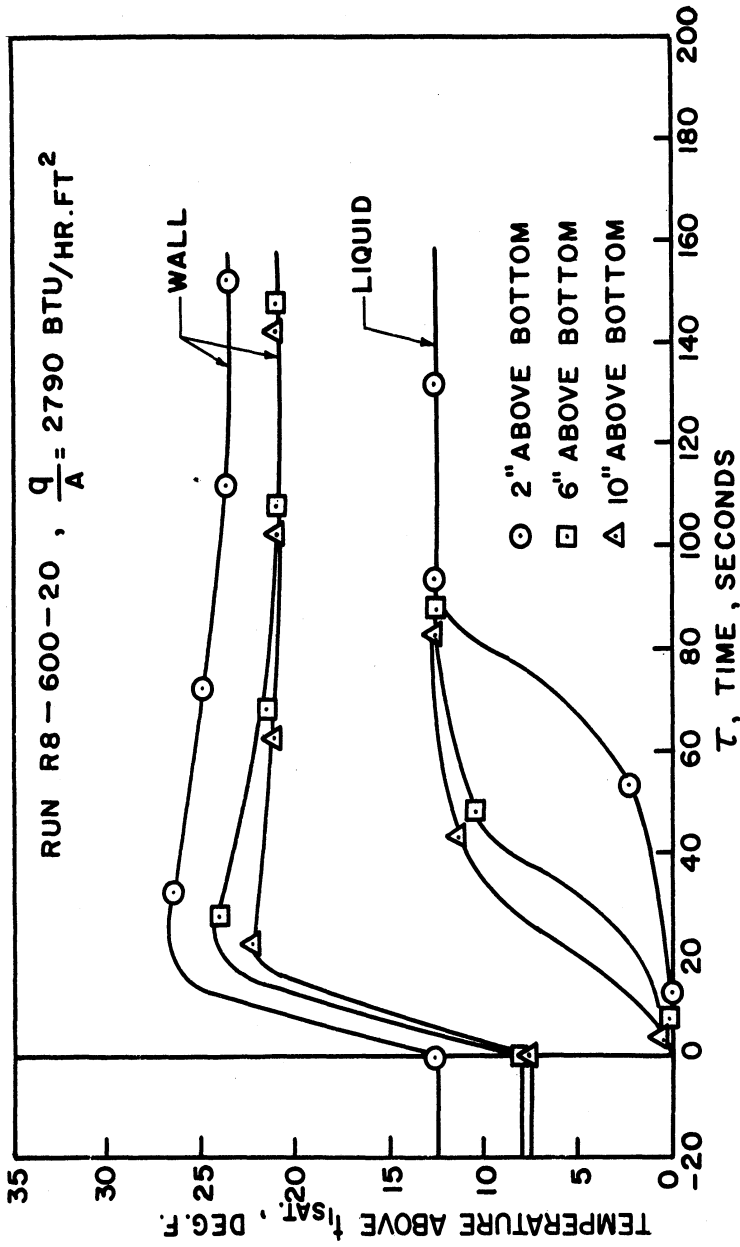


Figure 31. Wall and Liquid Temperatures vs. Time, Run R8-600-20.

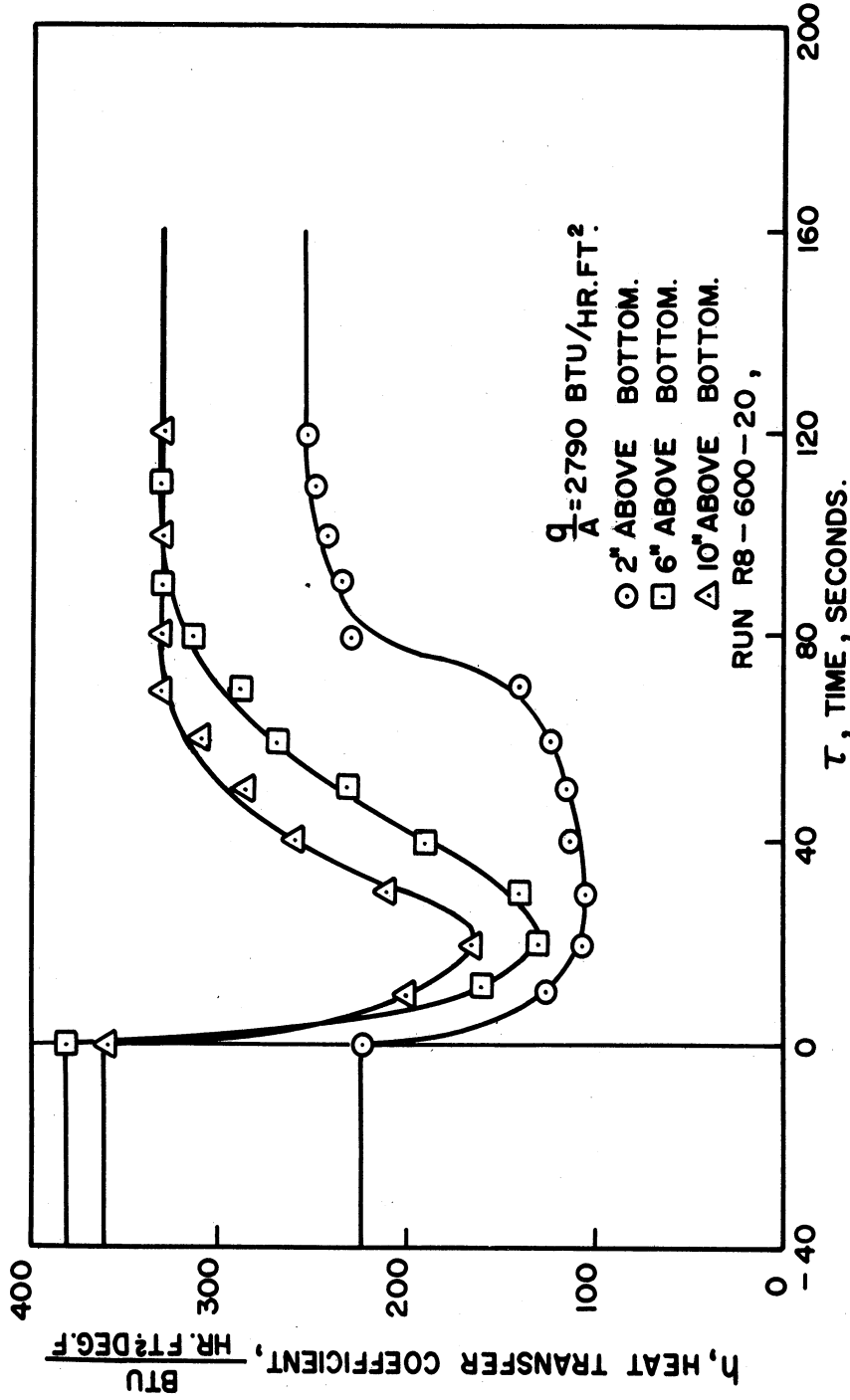


Figure 32. Heat Transfer Coefficient vs. Time, Run R8-600-20.

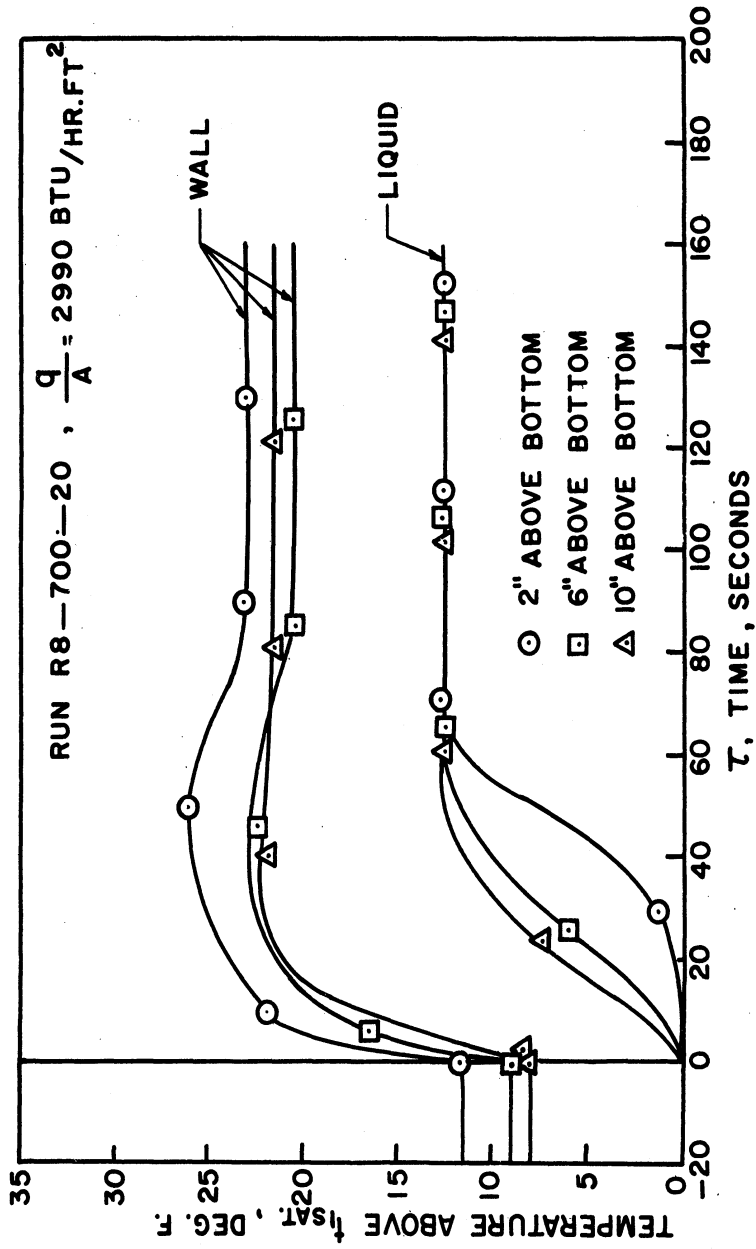


Figure 33. Wall and Liquid Temperatures vs. Time, Run R8-700-20.

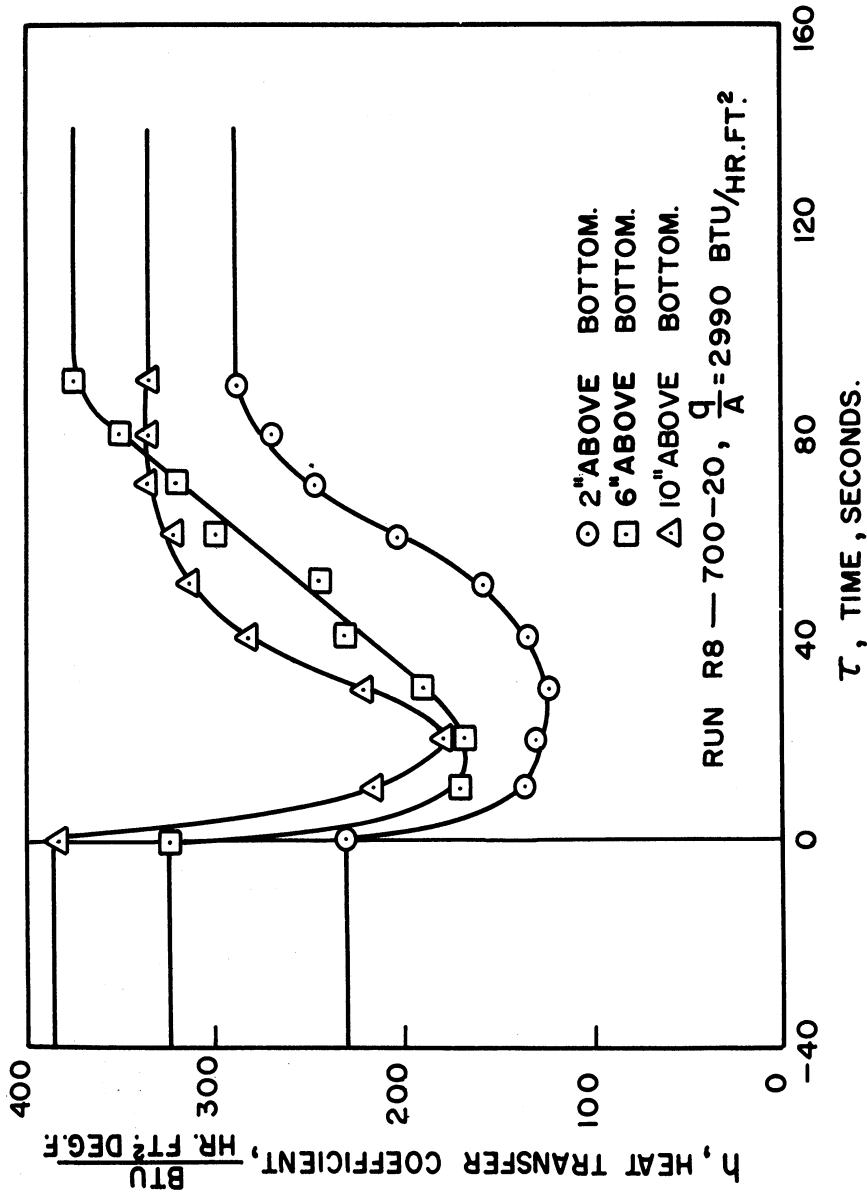


Figure 34. Heat Transfer Coefficient vs. Time, Run R8-700-20.

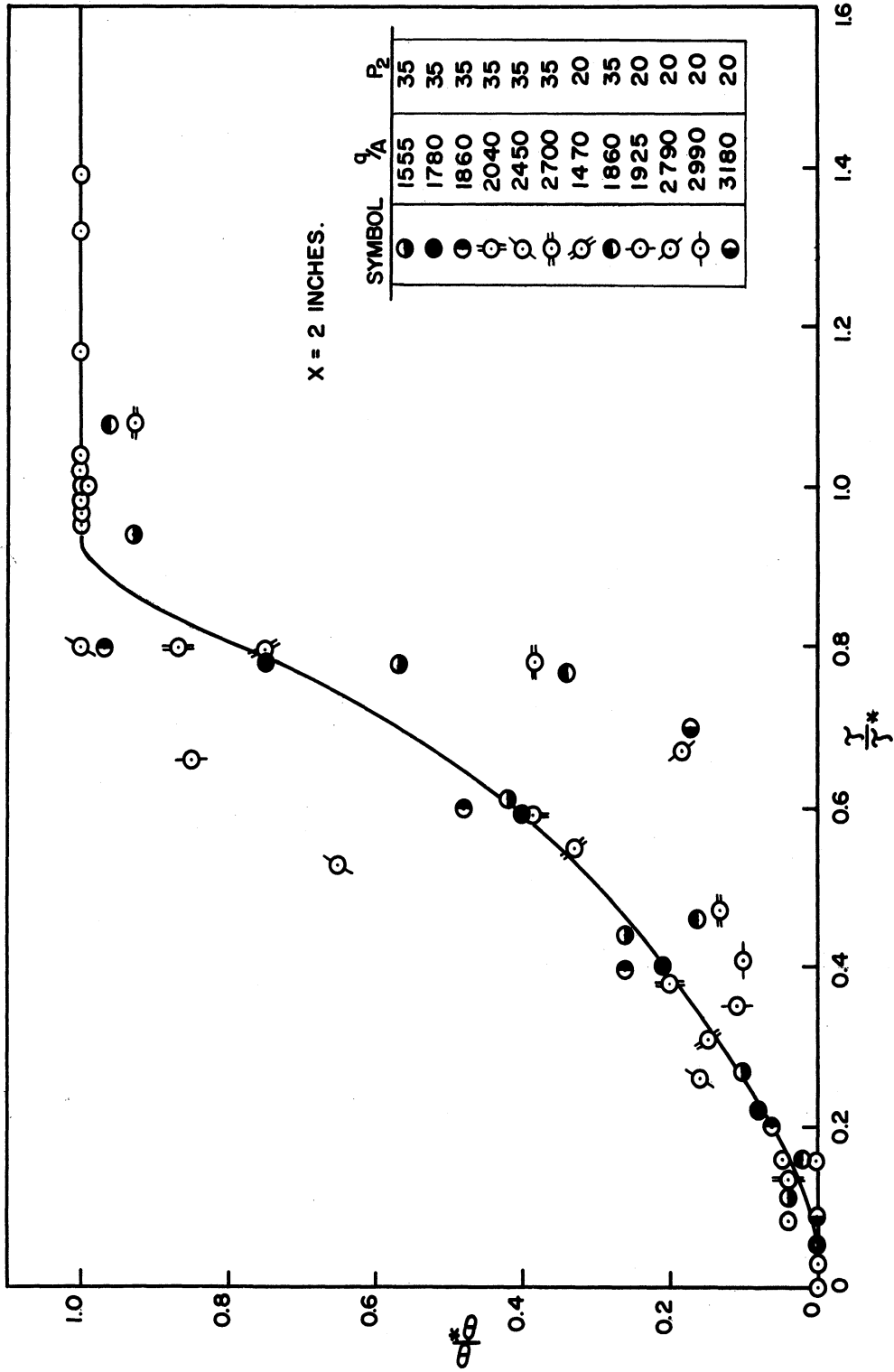


Figure 35. Dimensionless Liquid Temperature vs. Dimensionless Time, x = 2 inches.

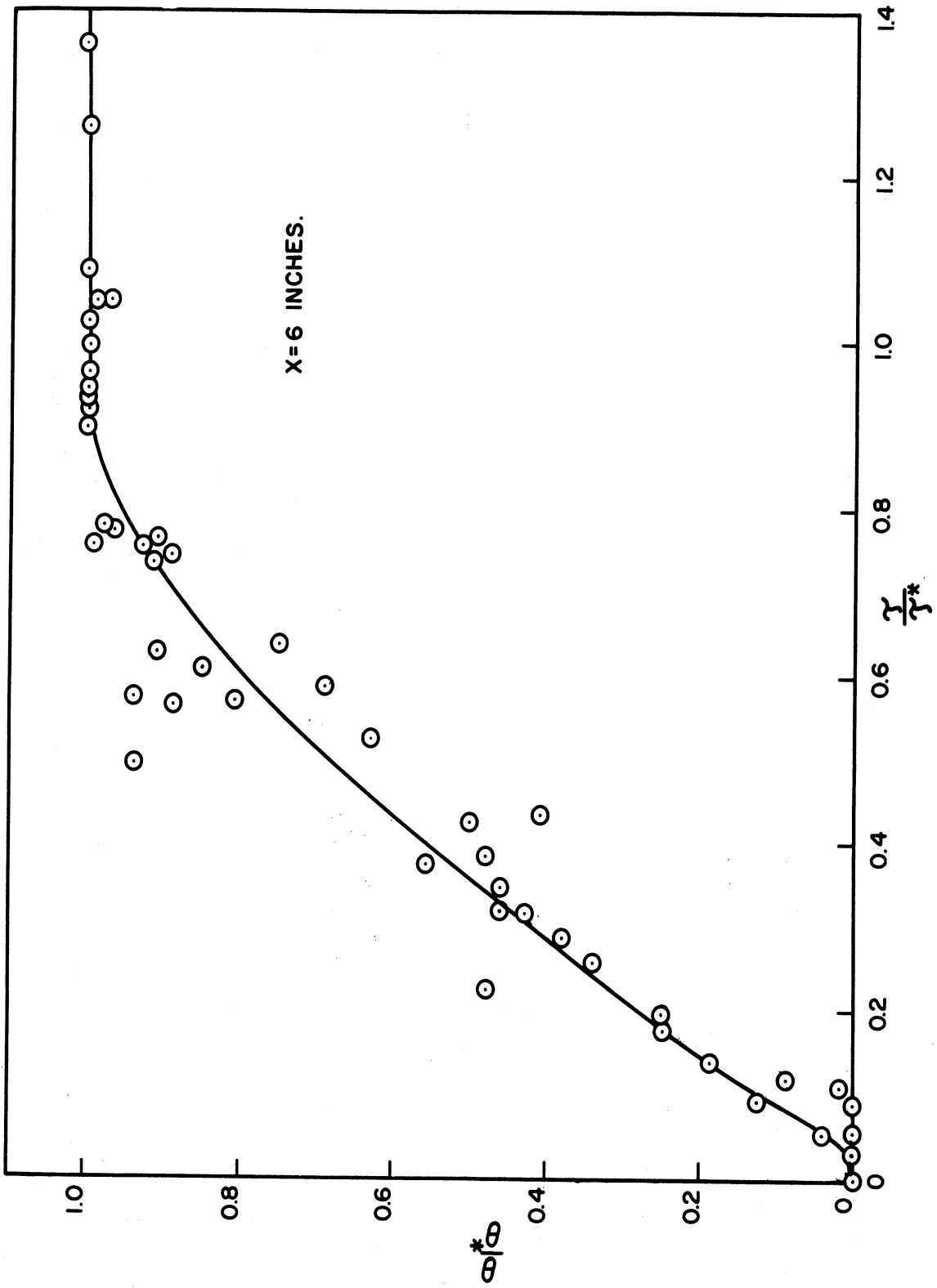


Figure 36. Dimensionless Liquid Temperature vs. Dimensionless Time, $x = 6$ inches.

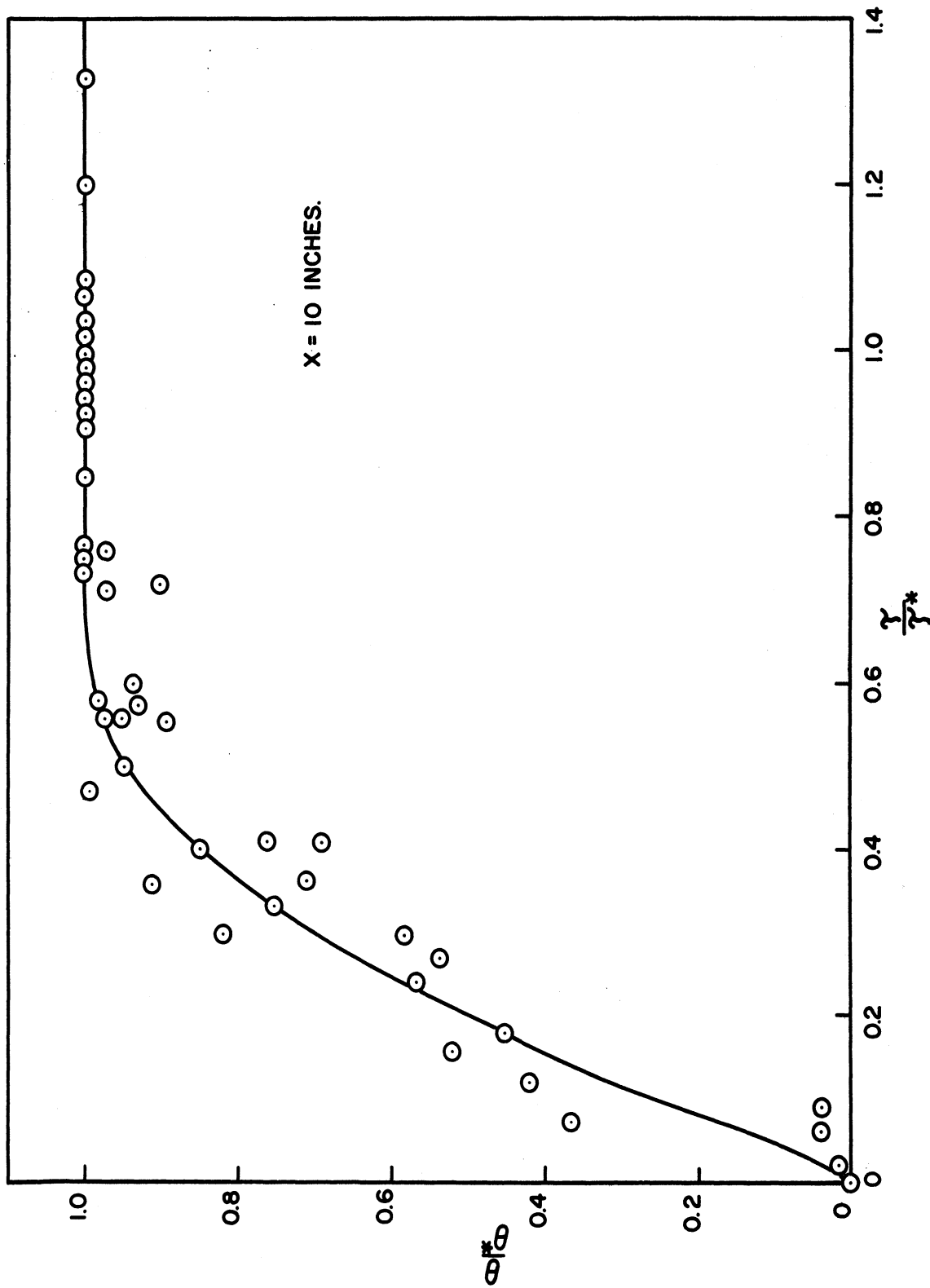


Figure 37. Dimensionless Liquid Temperature vs. Dimensionless Time, $x = 10$ inches.

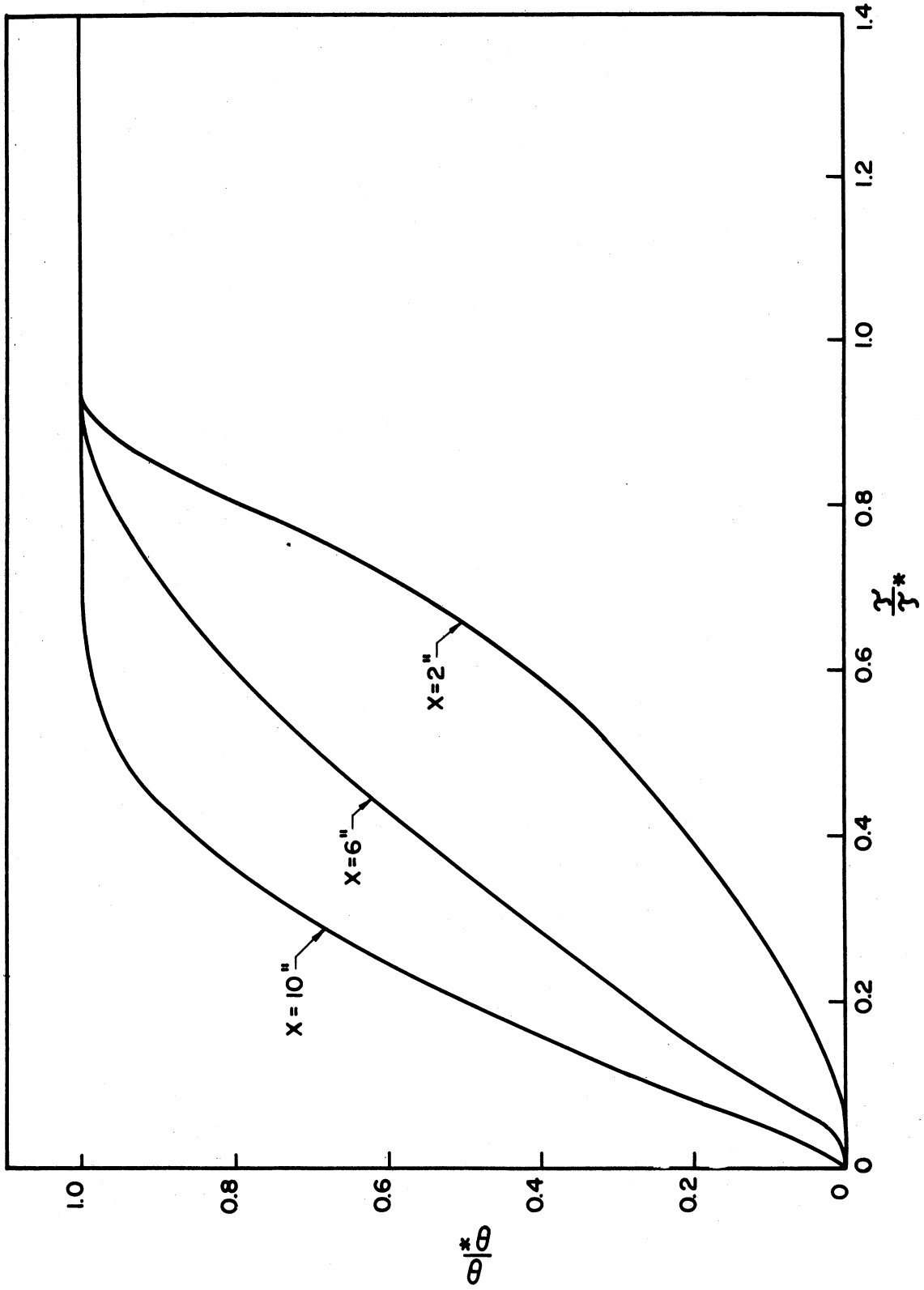


Figure 38. Dimensionless Liquid Temperature vs. Dimensionless Time.

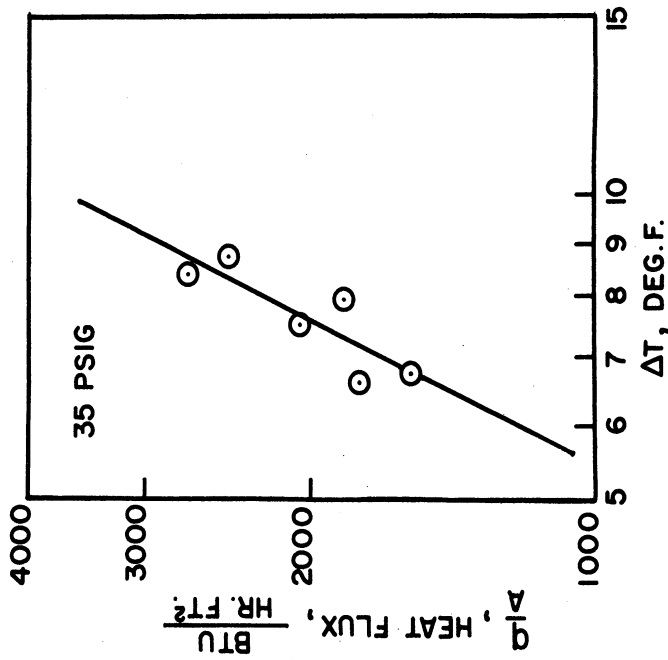


Figure 39

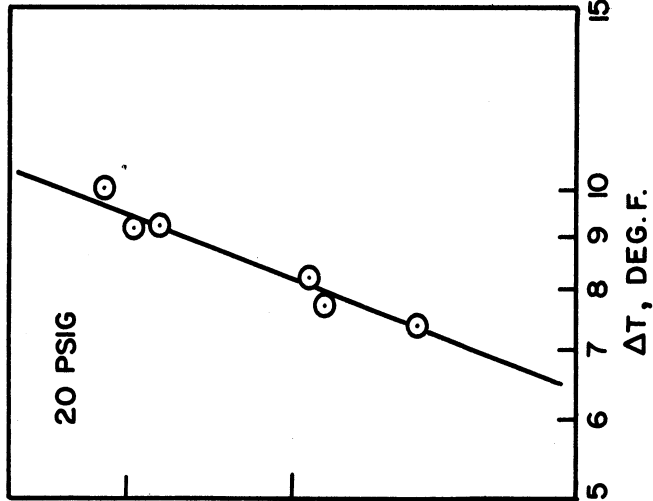


Figure 40

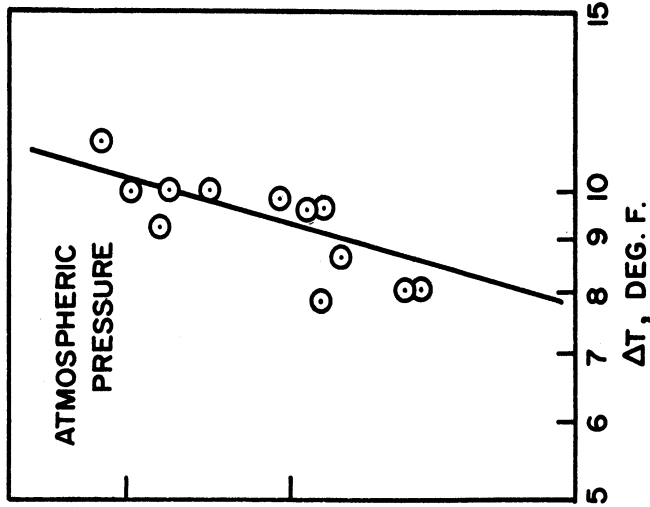


Figure 41

Heat Flux vs. Temperature Difference For Boiling Liquid Nitrogen.

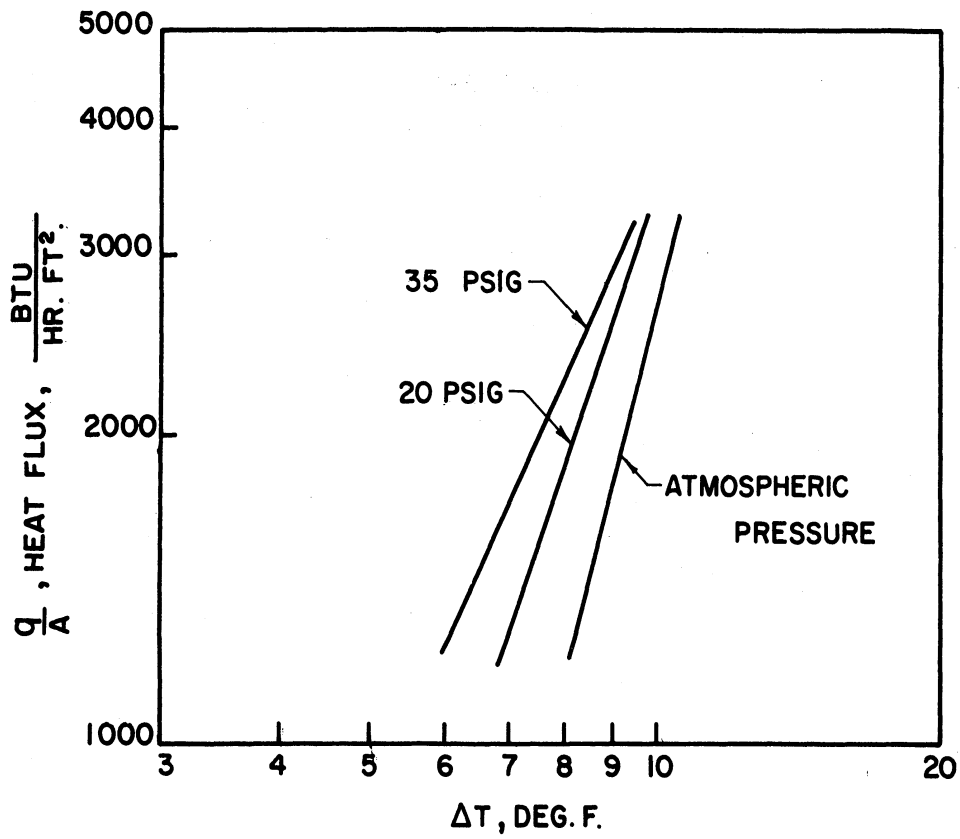


Figure 42. Heat Flux vs. Temperature Difference For Boiling Liquid Nitrogen.

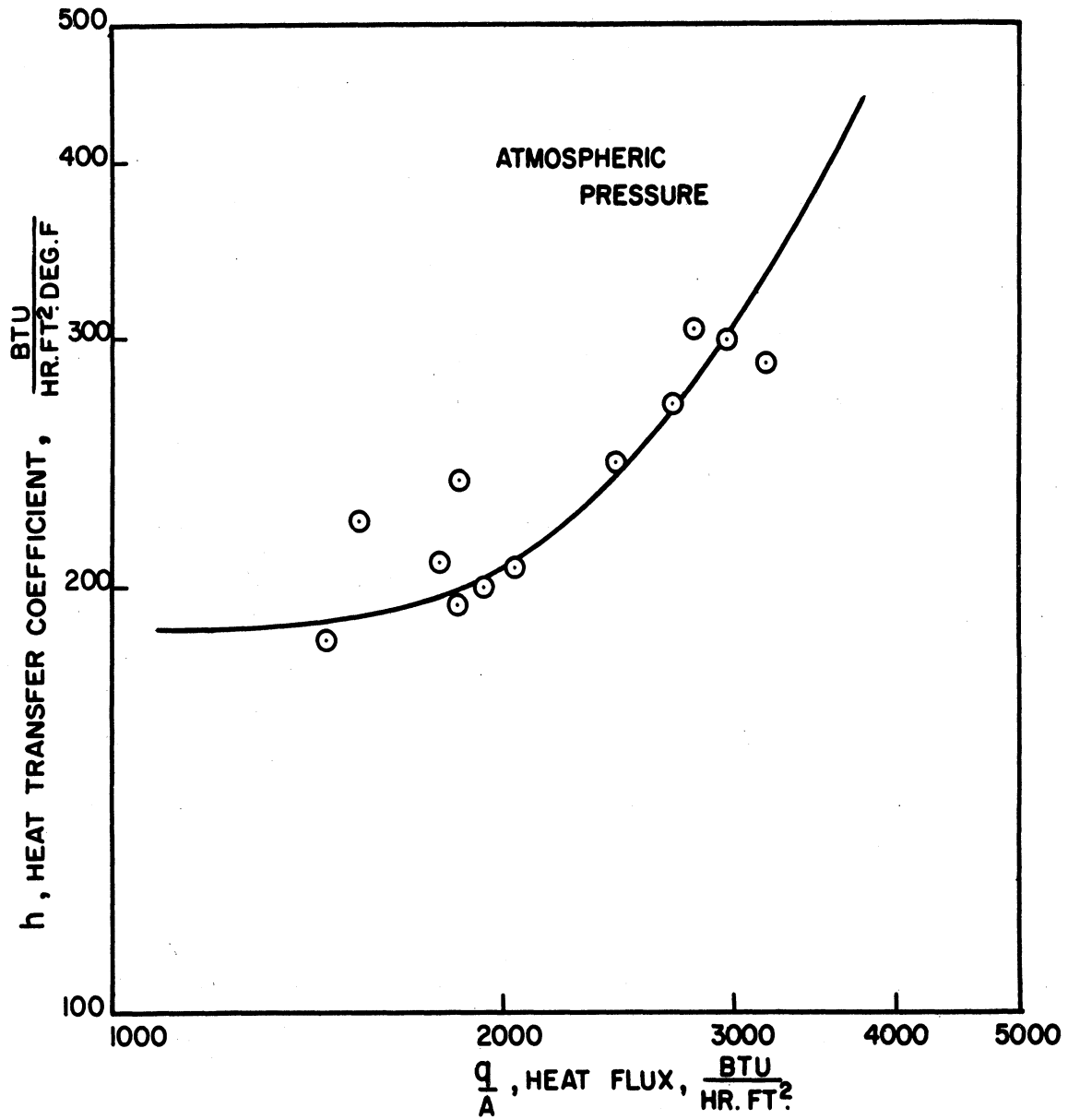


Figure 43. Boiling Heat Transfer Coefficient vs. Heat Flux, Atmospheric Pressure.

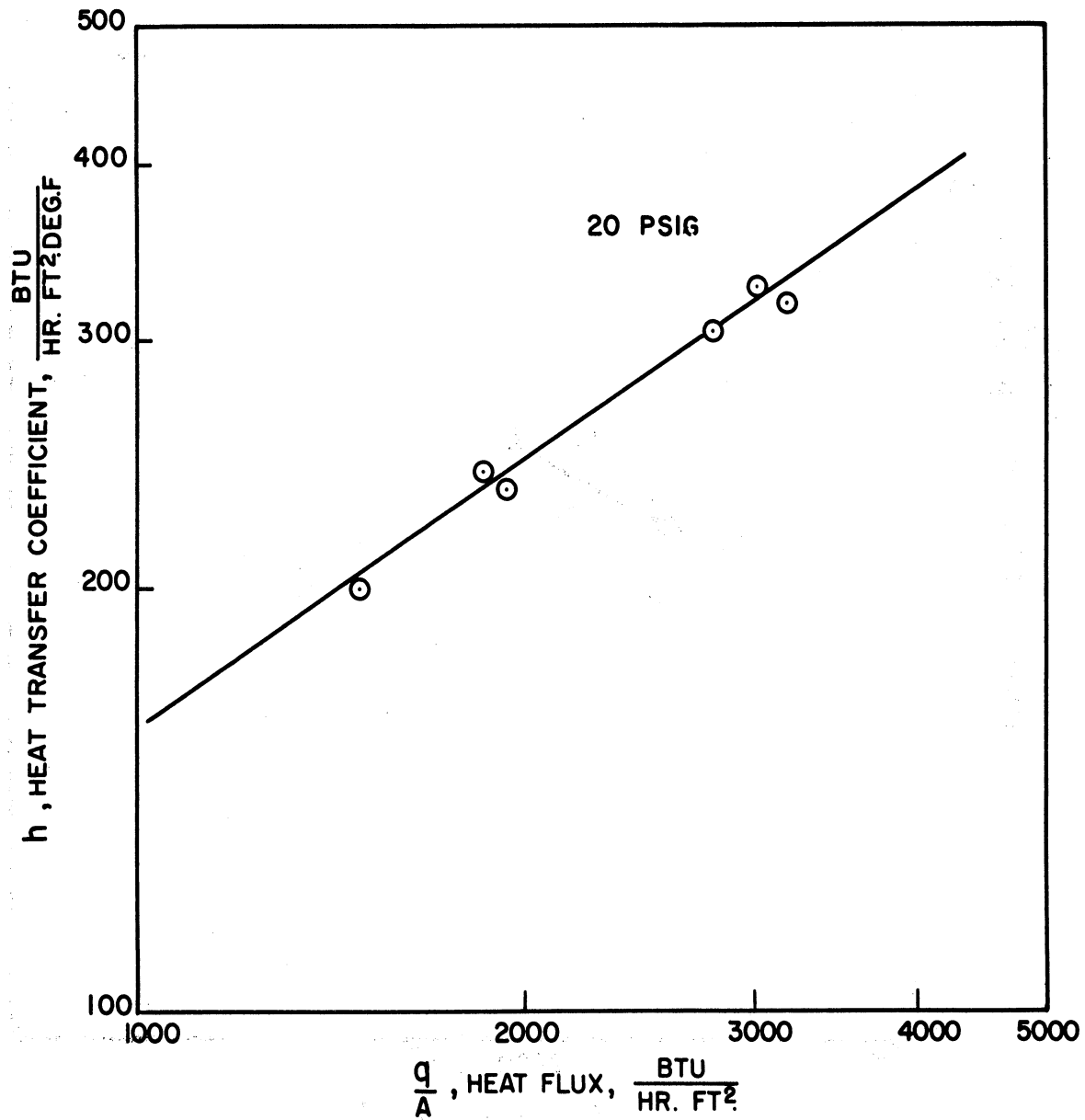


Figure 44. Boiling Heat Transfer Coefficient vs. Heat Flux, 20psig.

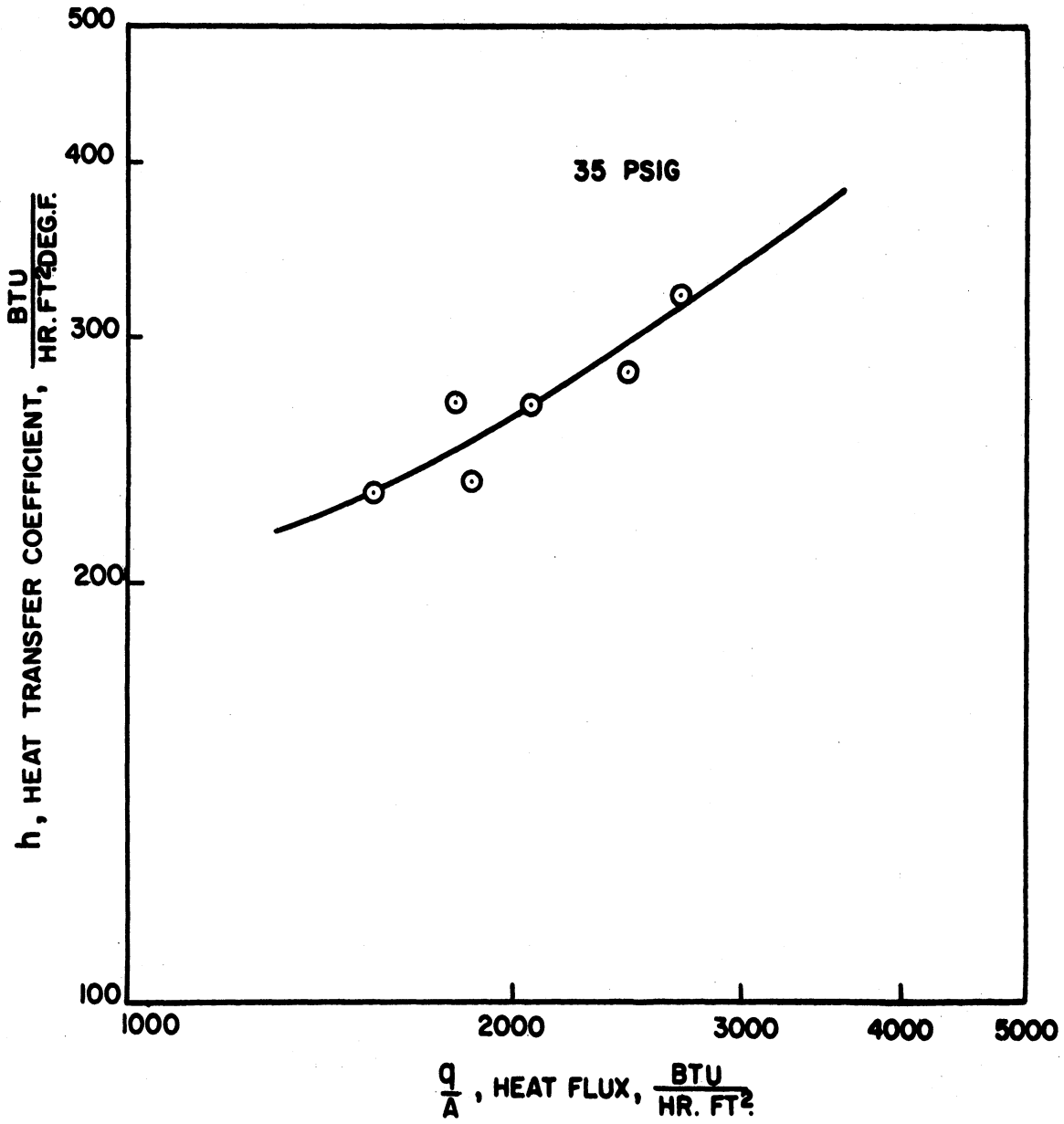


Figure 45. Boiling Heat Transfer Coefficient vs. Heat Flux, 35 psig.

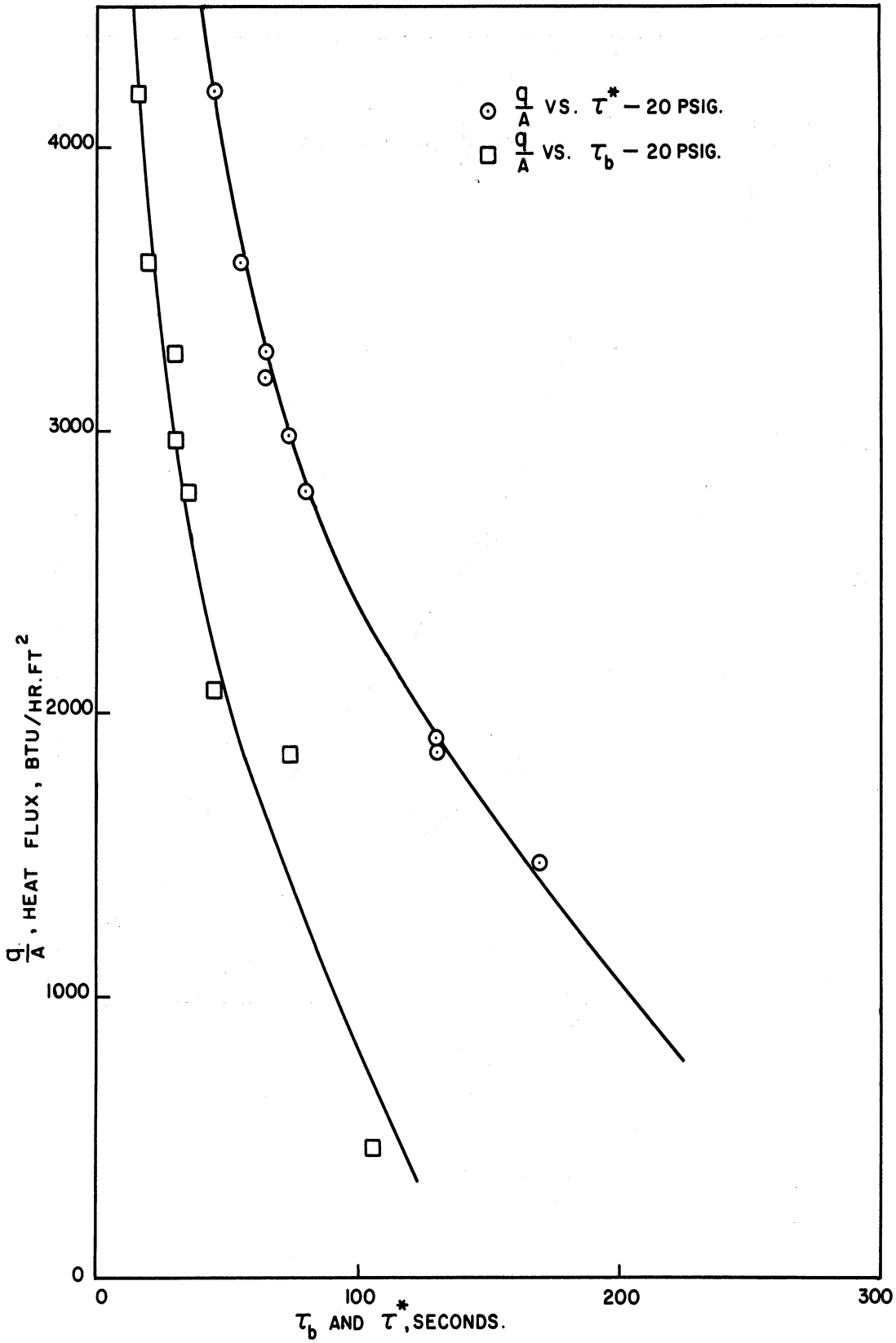


Figure 46. Heat Flux vs. τ_b and τ^* , 20 psig.

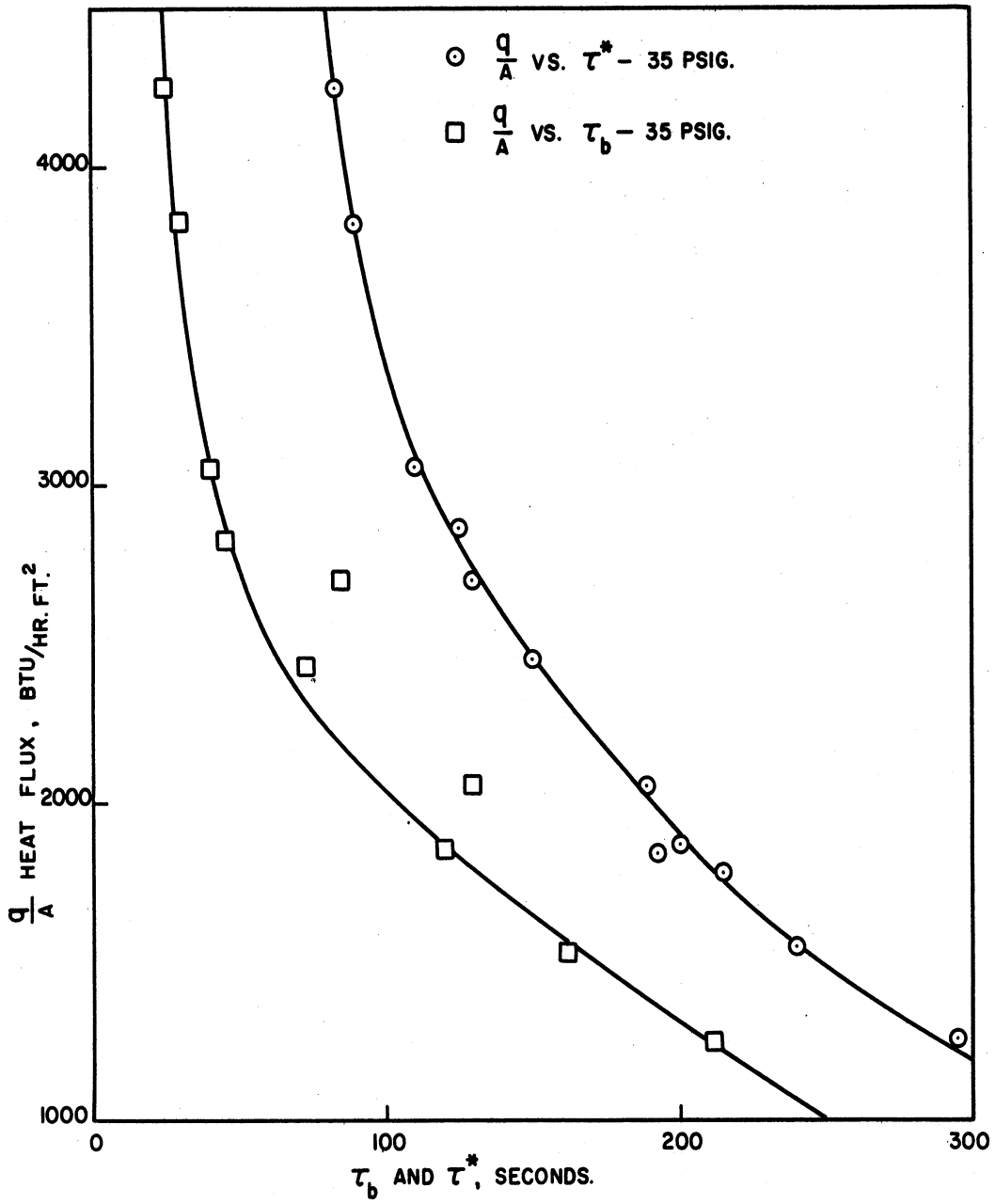


Figure 47. Heat Flux vs. τ_b and τ^* , 35 psig.

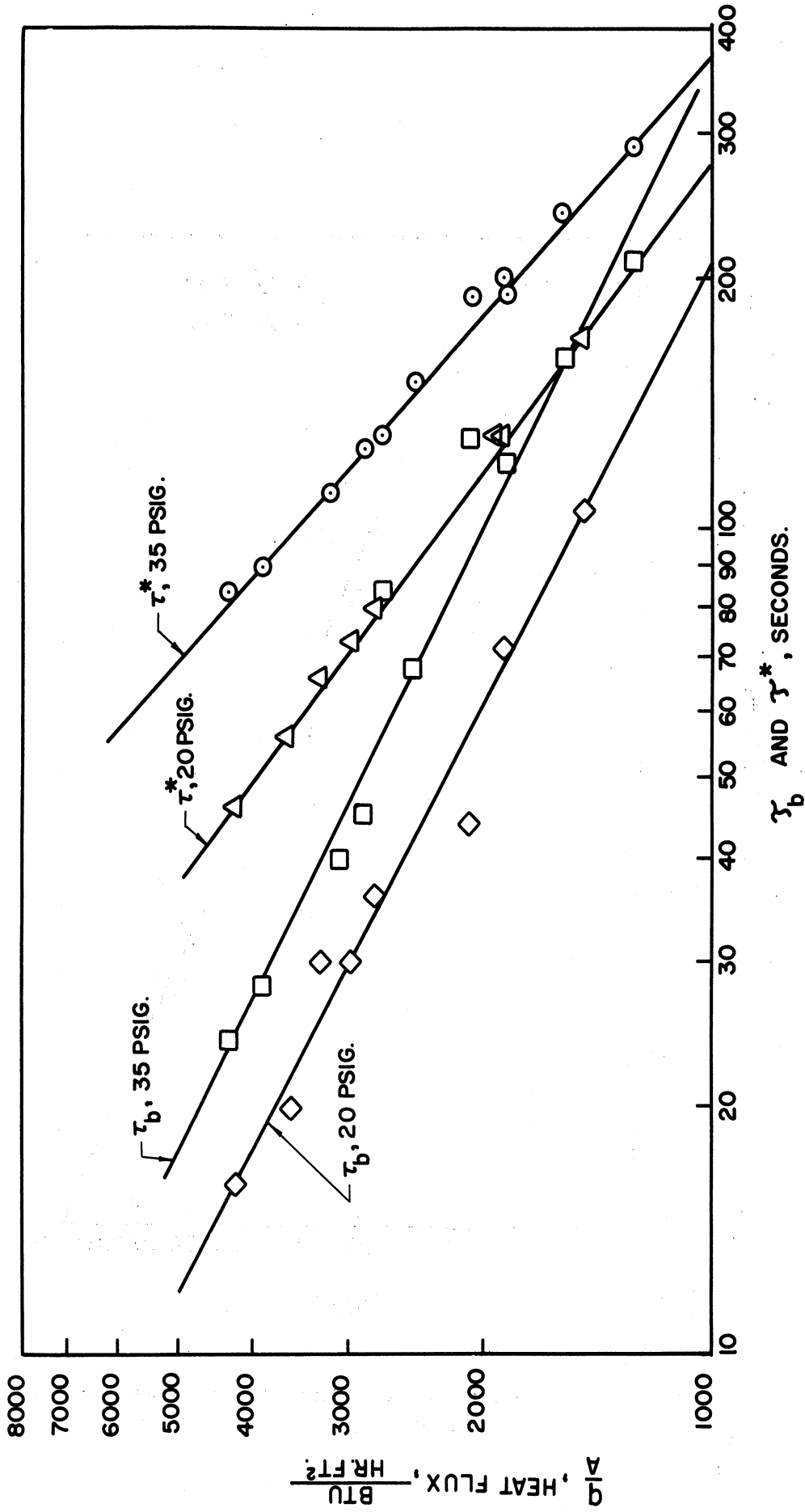


Figure 48. Heat Flux vs. τ_b and τ_b^* .

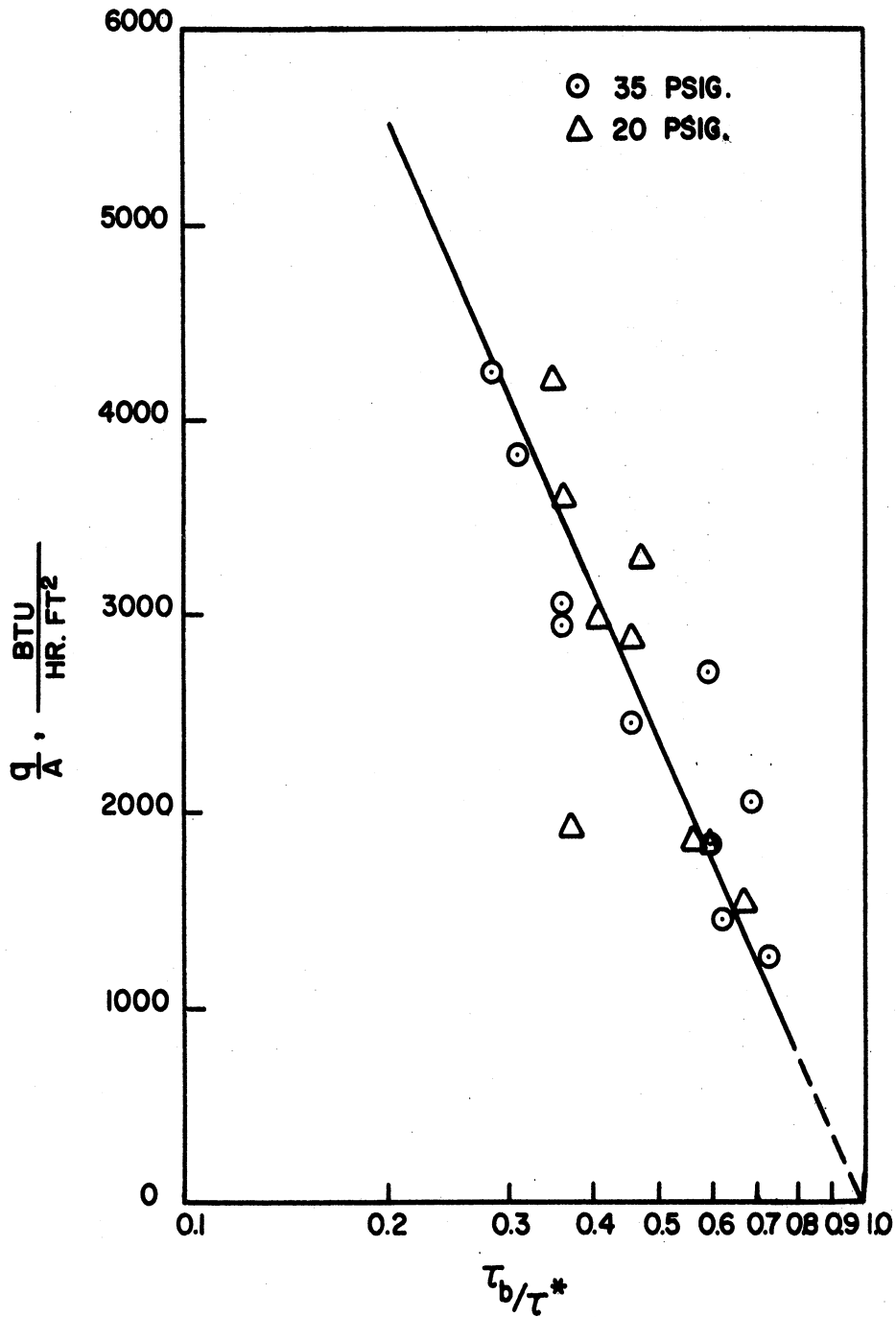


Figure 49. Heat Flux vs. Dimensionless Time For First Net Boiloff.

CHAPTER IV

ANALYSIS AND INTERPRETATION OF EXPERIMENTAL RESULTS

A. Steady State Boiling of a Saturated Liquid

Figures 39 - 41 show the trend characteristic of nucleate boiling. It is well established that the slope of curves in this regime of boiling, when plotted on log-log coordinates is quite high. McAdams⁽²⁰⁾ cites many examples of this phenomenon. The values of "n" obtained in this investigation ranged from 2.2 to 3.8. Banchemo, Barker, and Boll⁽¹⁾ found for liquid nitrogen the range of "n" was 2.5 to 5. Associated with the small temperature differences between the wall and saturated liquid are the high coefficients of heat transfer characteristic of nucleate boiling, (Figures 43 - 45).

That the temperature differences, for a given heat flux, decrease as the pressure at which boiling occurs increases, is shown in Figure 42. Similar results for the nucleate boiling of liquid oxygen are indicated in Reference 1, and for a variety of liquids in References 2 and 19.

It will be shown that the role of steady state boiling prior to pressurization is very important in understanding the events which follow pressurization.

B. Pressurization Process

Upon pressurization of the boiling liquid nitrogen under test, boiling ceases almost immediately because the liquid is now subcooled by as much as 22°F. depending upon the magnitude of the new pressure.

The time required for collapse of a spherical bubble may be approximately calculated from hydrodynamical considerations (Reference 15) and is found to be considerably less than one second.

The time required to effect pressurization varied from approximately two to four seconds. That the time to reach the new pressure was not effected instantaneously after opening the solenoid valve between the test cylinder and the pressurization cylinder was due to the inertia of the pressurizing gas and also to the condensation of this gas on the liquid nitrogen surface. This condensation takes place at such a high rate that if the inlet gas flow were discontinued after reaching the final pressure, a sharp drop in cylinder pressure would result. This was demonstrated in preliminary experimental runs. Because condensation tends to cause a drop in pressure, and the wall temperature immediately after pressurization and for some time thereafter is insufficient to cause boiling, external gas flow into the cylinder must be continued even after the final pressure has been attained.

Regardless of the actual departure from a mathematical step pressurization, the body of the liquid is nevertheless subcooled throughout the time interval from pressurization until the final pressure is achieved. This is apparent from odd-numbered Figures 11 - 33, which indicate that the liquid temperatures rise much more slowly than does the pressure, taking four seconds as the maximum time required to reach the final pressure.

It is expected however, that the liquid nitrogen at the liquid-vapor interface is at the saturation temperature corresponding very closely to the instantaneous value of the pressure, because of the

condensation process occurring there.

C. Period from Start of Pressurization
to Steady State Boiling

Before pressurization is begun, the boiloff rate equals the rate of mass leaving the vapor space above the liquid in the cylinder. We shall consider this space, approximately constant, to be the control volume. The following may therefore be written:

$$w_b = w_o$$

$$\frac{dm}{d\tau}_{CV} = 0$$

$$\frac{dp}{d\tau}_{CV} = 0$$

During the pressurization process, there is as yet no boiling occurring anywhere in the system and the following may be written:

$$w_b = w_o = 0$$

$$w_i - w_c = \frac{dm}{d\tau}_{CV}$$

$$\frac{dp}{d\tau}_{CV} > 0$$

After the new pressure has been reached, gas must continue to enter the control volume from the pressurization cylinder in order that the pressure not fall below the prescribed test pressure. During the period after pressurization during which there is no boiling, or boiling is insufficient to maintain the pressure at its new value, the following equations are valid:

$$w_o = 0$$

$$w_b + w_i - w_c = 0 = \frac{dm}{d\tau}_{CV}$$

$$\frac{dp}{d\tau}_{CV} = 0$$

Soon boiling becomes vigorous enough to permit the pressurization valve to be closed:

$$\begin{aligned}w_i &= w_o = 0 \\w_b - w_c &= 0 = dm/d\tau)_{CV} \\dp/d\tau)_{CV} &= 0\end{aligned}$$

The above conditions exist for an infinitesimally short time. Immediately after this point is reached, the boiloff rate becomes greater than the condensation rate and the regulator opens as the pressure increases in the control volume. For the period following the closure of the pressurization valve, but before the outlet valve of the regulator has opened, the following may be written:

$$\begin{aligned}w_i &= w_o = 0 \\w_b - w_c &= dm/d\tau)_{CV} \\dp/d\tau)_{CV} &> 0\end{aligned}$$

Since the cylinder pressure was kept slightly lower than the pressure required to cause the regulator to open, the positive time derivative of pressure causes the regulator to open a very short time after the pressurization gas valve is closed. When the regulator opens:

$$\begin{aligned}w_b - w_c &= w_o \\w_i &= 0 \\dp/d\tau)_{CV} &= 0\end{aligned}$$

The time is recorded as the time for first net boiloff from the system.

When all the liquid attains the saturation temperature, bulk boiling is fully re-established. Therefore:

$$w_i = 0$$

$$w_b = w_o$$

$$dp/d\tau)_{cv} = 0$$

These are of course identical with the expressions for the period before pressurization is begun.

D. Wall and Liquid Temperature Transients Following Pressurization

In the following analysis of the wall and liquid temperature transients after pressurization, it will be assumed that the step pressurization results in a step change in the coefficient of heat transfer. This, on the basis of calculated results, is not the case. The heat transfer coefficient as it actually appears, and as it will be assumed for purposes of analysis are shown in the illustrations below:

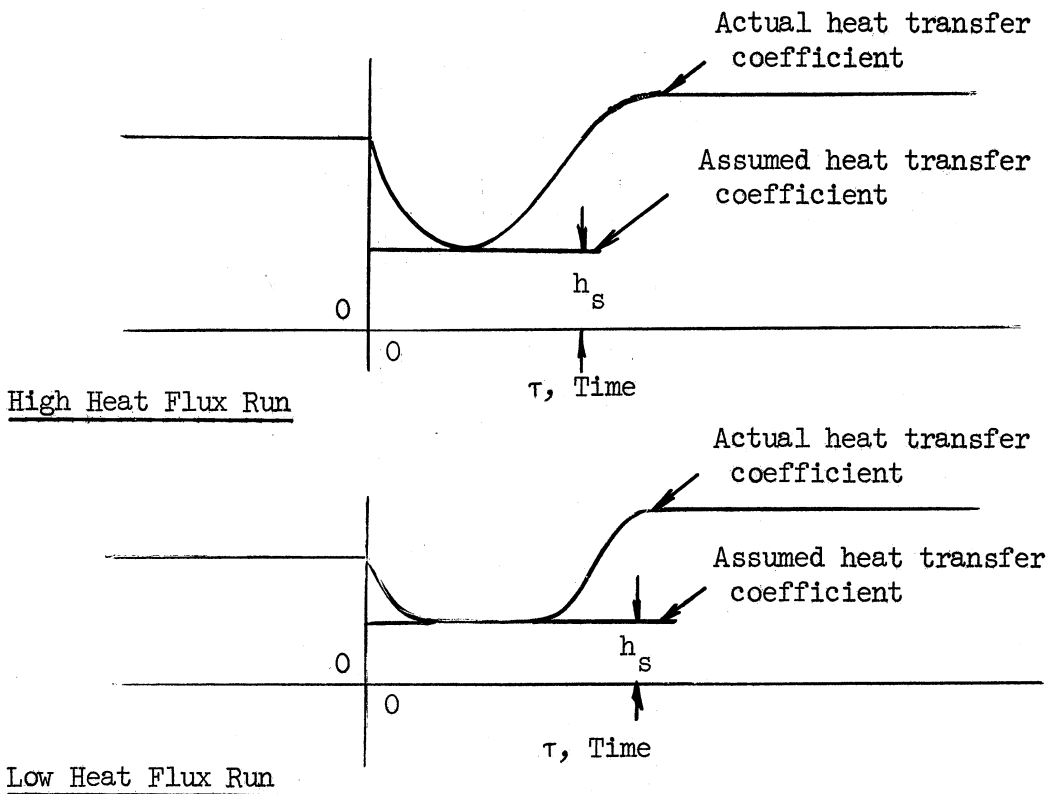


Figure 50. Comparison of Actual and Idealized Heat Transfer Coefficient.

The idealization does not cover the range of wall temperature beyond the point where bubbles begin to form. Furthermore while the actual data shows a longitudinal temperature gradient to exist at all times after pressurization in the liquid, this analysis will consider the liquid to have uniform temperature throughout its entire mass.

The drawings below pertain to the analysis:

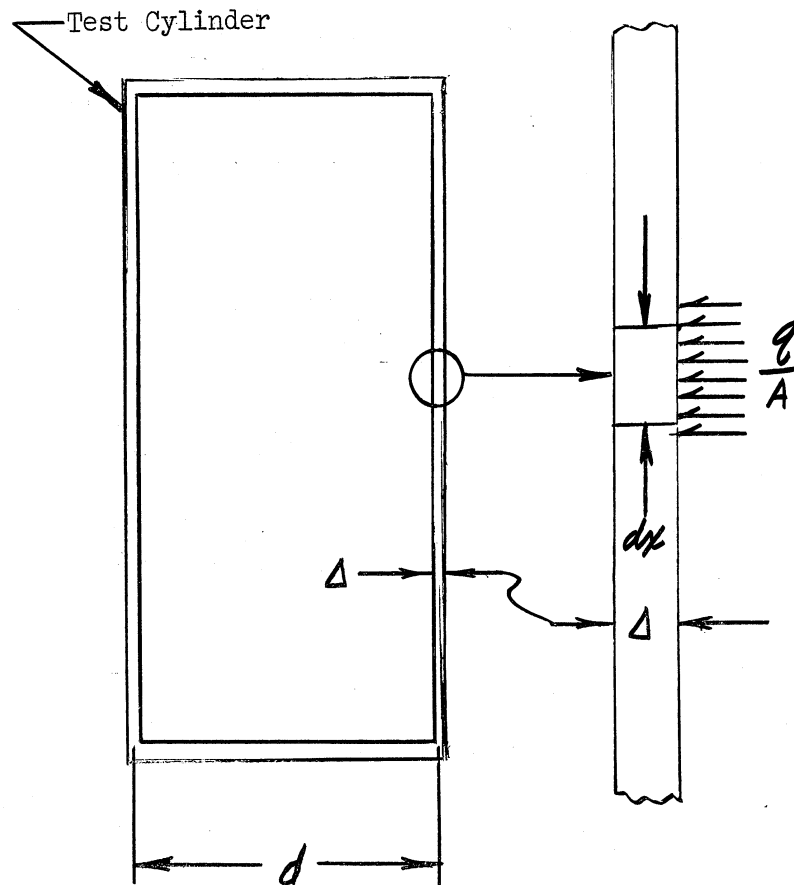


Figure 51. Sketch Defining Geometrical Quantities Used in Idealized Analysis.

Neglecting axial conduction, we may write for a differential element of the cylinder wall:

$$\pi d \left(\frac{q}{A} \right) dx = \rho_w \pi d \Delta dx C_{pw} \frac{dt_w}{dT} + h_s (t_w - t_L) \pi d \cdot dx \quad (5)$$

$$\left(\frac{q}{A} \right) = \rho_w \Delta C_{pw} \frac{dt_w}{dT} + h_s (t_w - t_L) \quad (5a)$$

Equations (5) and (5a) represent the energy storage and transfer for an elemental volume of the cylinder wall.

Now, considering the energy transfer and storage of the liquid:

$$\pi d h_s (t_w - t_L) dx = \rho_L \frac{\pi}{4} d^2 dx C_{pL} \frac{dt_L}{dT} \quad (6)$$

$$h_s (t_w - t_L) = \rho_L \frac{d}{4} C_{pL} \frac{dt_L}{dT} \quad (6a)$$

Rewriting Equation (5a), we have:

$$\frac{dt_w}{dT} = \frac{\left(\frac{q}{A} \right)}{\rho_w \Delta C_{pw}} - \frac{h_s (t_w - t_L)}{\rho_w \Delta C_{pw}} \quad (5b)$$

Similarly for Equation (6a):

$$\frac{dt_L}{dT} = \frac{4 h_s (t_w - t_L)}{\rho_L d C_{pL}} \quad (6b)$$

In order to simplify the equations, the following are defined:

$$B \equiv \frac{\frac{q}{A}}{\rho_w \Delta C_{pw}} \quad (7)$$

$$D \equiv \frac{h_s}{\rho_w \Delta C_{pw}} \quad (8)$$

$$E \equiv \frac{4 h_s}{\rho_L d C_{pL}} \quad (9)$$

Therefore, equations (5b) and (6b) take the form:

$$\frac{dt_w}{d\tau} = B - D(t_w - t_L) = B - Dt_w + Dt_L \quad (5c)$$

$$\frac{dt_L}{d\tau} = E(t_w - t_L) = Et_w - Et_L \quad (6c)$$

From Equation (5c):

$$t_L = \frac{1}{D} \frac{dt_w}{d\tau} - \frac{B}{D} + t_w \quad (5d)$$

Differentiating t_L above, with respect to time:

$$\frac{dt_L}{d\tau} = \frac{1}{D} \frac{d^2 t_w}{d\tau^2} + \frac{dt_w}{d\tau} \quad (10)$$

Substituting Equations (5d) and (10) into Equation (6c) yields:

$$\frac{d^2 t_w}{d\tau^2} + (D+E) \frac{dt_w}{d\tau} = EB \quad (11)$$

Defining:

$$\alpha \equiv D+E \quad (12)$$

and

$$\beta \equiv EB \quad (13)$$

we obtain:

$$\frac{d^2 t_w}{d\tau^2} + \alpha \frac{dt_w}{d\tau} = \beta \quad (11a)$$

Integrating Equation (11a) with respect to τ :

$$\frac{dt_w}{d\tau} + \alpha t_w = \beta\tau + C_1 \quad (14)$$

The solution of Equation (14) is:

$$t_w = e^{-\int \alpha d\tau} \int (\beta\tau + C_1) e^{\int \alpha d\tau} d\tau + C_2 e^{-\int \alpha d\tau} \quad (15)$$

$$t_w = \frac{\beta}{\alpha^2} (\alpha\tau - 1) + \frac{C_1}{\alpha} + C_2 e^{-\alpha\tau} \quad (16)$$

The boundary conditions are:

$$\tau = 0, t_w = t_{w0} \quad (17)$$

$$\tau = 0, t_w - t_L = \Delta T_0 \quad (18)$$

Applying the first condition, Equation (17):

$$t_{w0} = -\frac{\beta}{\alpha^2} + \frac{C_1}{\alpha} + C_2 \quad (19)$$

Differentiating Equation (16):

$$\frac{dt_w}{d\tau} = \frac{\beta}{\alpha} - \alpha C_2 e^{-\alpha\tau} \quad (20)$$

Applying the second condition, Equation (18):

$$\left. \frac{dt_w}{d\tau} \right|_{\tau=0} = \frac{\beta}{\alpha} - \alpha C_2 \quad (21)$$

Substituting (21) into (5c):

$$\left. \frac{dt_w}{d\tau} \right|_{\tau=0} = \frac{\beta}{\alpha} - \alpha C_2 = B - D\Delta T_0 \quad (22)$$

$$C_2 = \frac{\beta}{\alpha^2} + \frac{D}{\alpha} \Delta T_0 - \frac{B}{\alpha} \quad (22a)$$

Substituting (22a) into (19) yields:

$$C_1 = \alpha t_{w0} - D\Delta T_0 + B \quad (23)$$

Therefore the equation for the wall temperature transient is as follows:

$$t_w - t_{w0} = \Theta_w = \frac{B}{\alpha^2} (\alpha^2 \tau - 1) - \frac{D}{\alpha} \Delta T_0 + \frac{B}{\alpha} + \left(\frac{B}{\alpha^2} + \frac{D}{\alpha} \Delta T_0 - \frac{B}{\alpha} \right) e^{-\alpha^2 \tau} \quad (24)$$

The temperature transient of the liquid may be obtained from Equation

$$(5d): \quad t_L = \frac{1}{D} \frac{dt_w}{d\tau} - \frac{B}{D} + t_w$$

$$\frac{dt_w}{d\tau} = \frac{B}{\alpha} - \alpha^2 \tau e^{-\alpha^2 \tau} \quad (20)$$

Therefore:

$$t_L = \frac{1}{D} \left(\frac{B}{\alpha} - \alpha^2 \tau e^{-\alpha^2 \tau} \right) - \frac{B}{D} + t_w \quad (25)$$

In applying the equations for the wall and liquid transients, an average coefficient of heat transfer is employed. It is observed from the data that the minimum value of the heat transfer coefficient is roughly .4 of the coefficient for nucleate boiling. Since in a practical application the minimum which actually does exist is not known before testing, this criterion will be used to obtain h_s .

Figure 52 shows typical wall and liquid temperature transients for the conditions indicated. A comparison of the idealized process and the actual data is given in Figures 53 and 54. The liquid temperature curve for the actual process represents the average for the three longitudinal locations beneath the liquid-vapor interface.

Both the idealized curves and the data show that the wall transient is steep to begin with and then falls off. The liquid temperature transients show the opposite trends. Since the energy input per unit time is a constant for a given area, and since the wall transient is steepest at the beginning, it is expected that the liquid

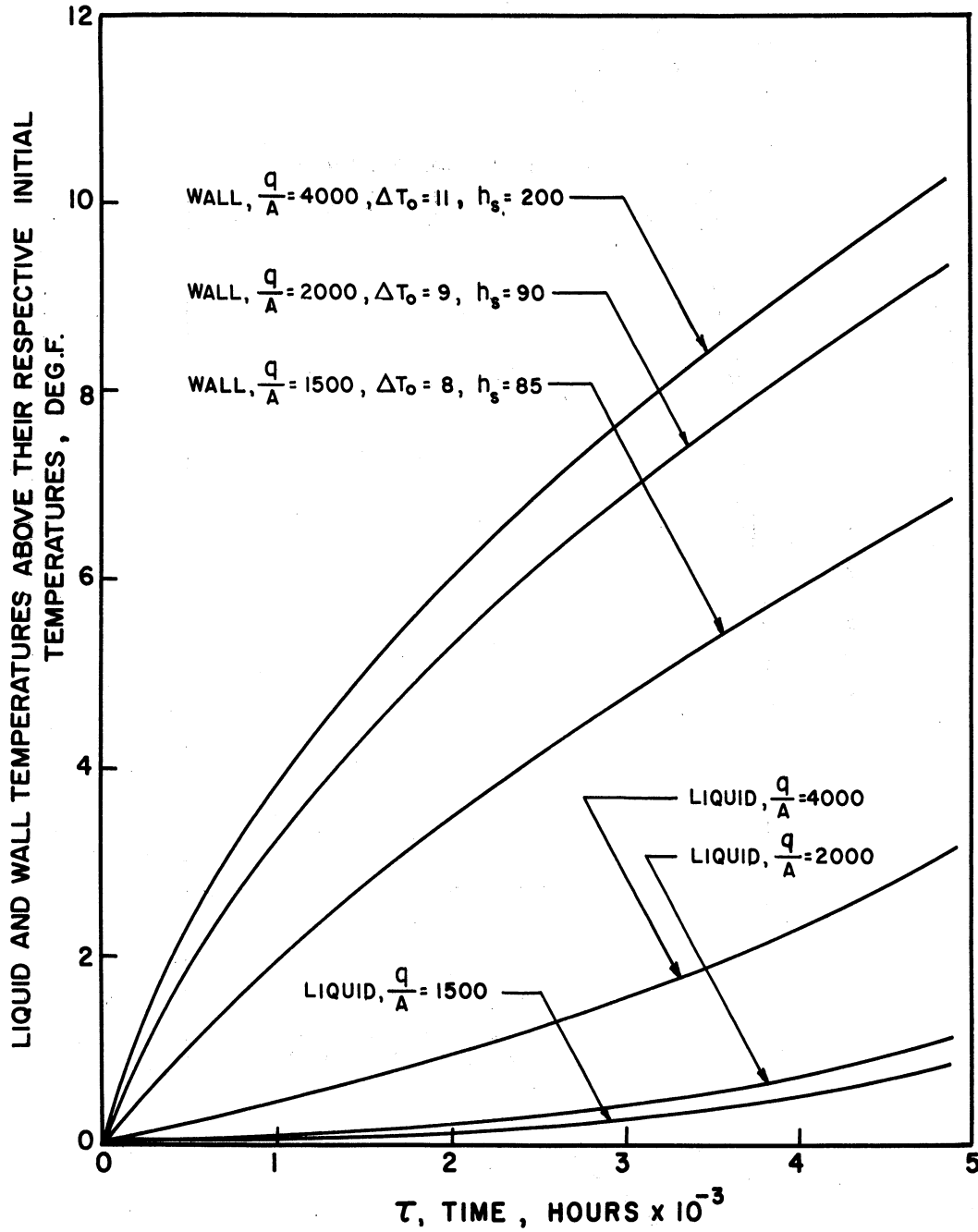


Figure 52. Wall and Liquid Transients - Idealized Analysis.

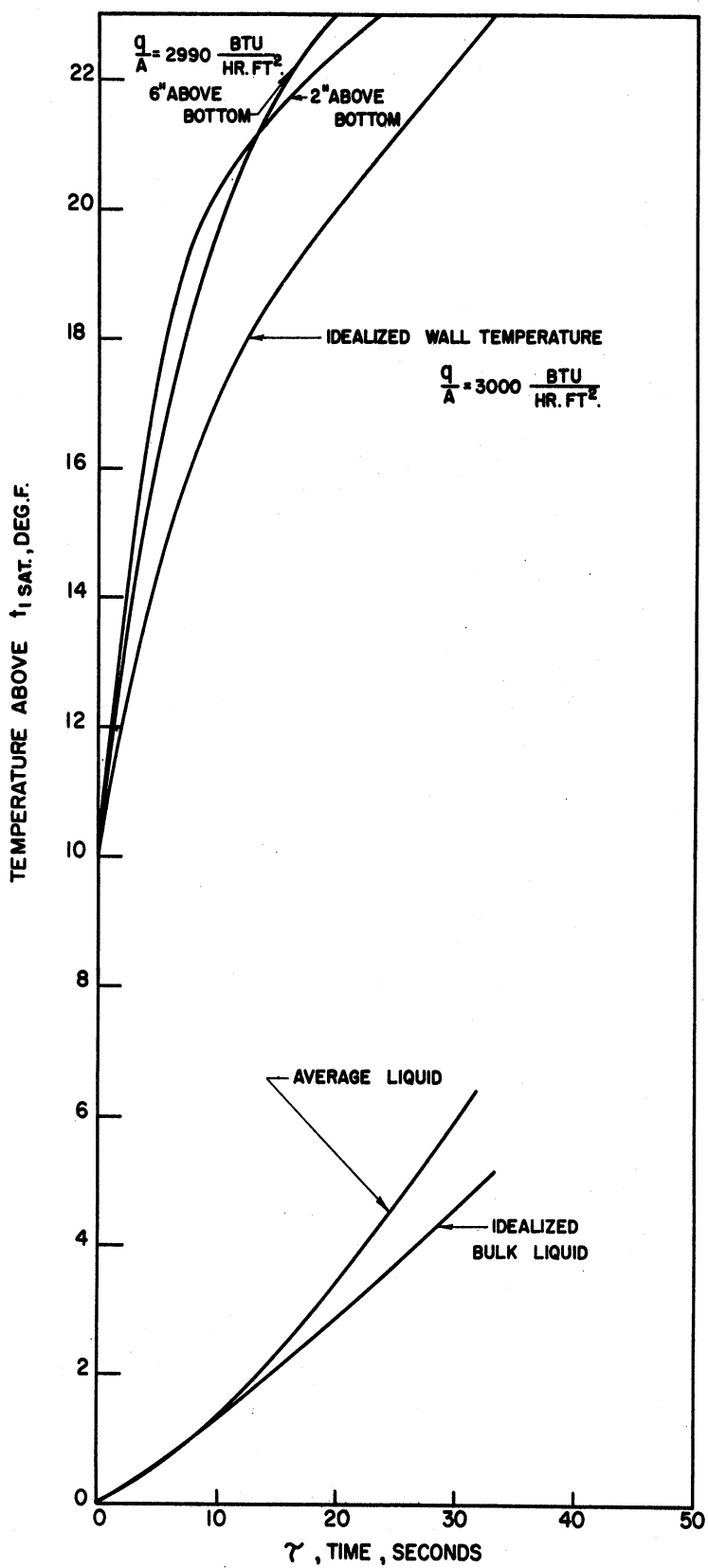


Figure 53. Comparison of Idealized Theory with Run R8-700-20.

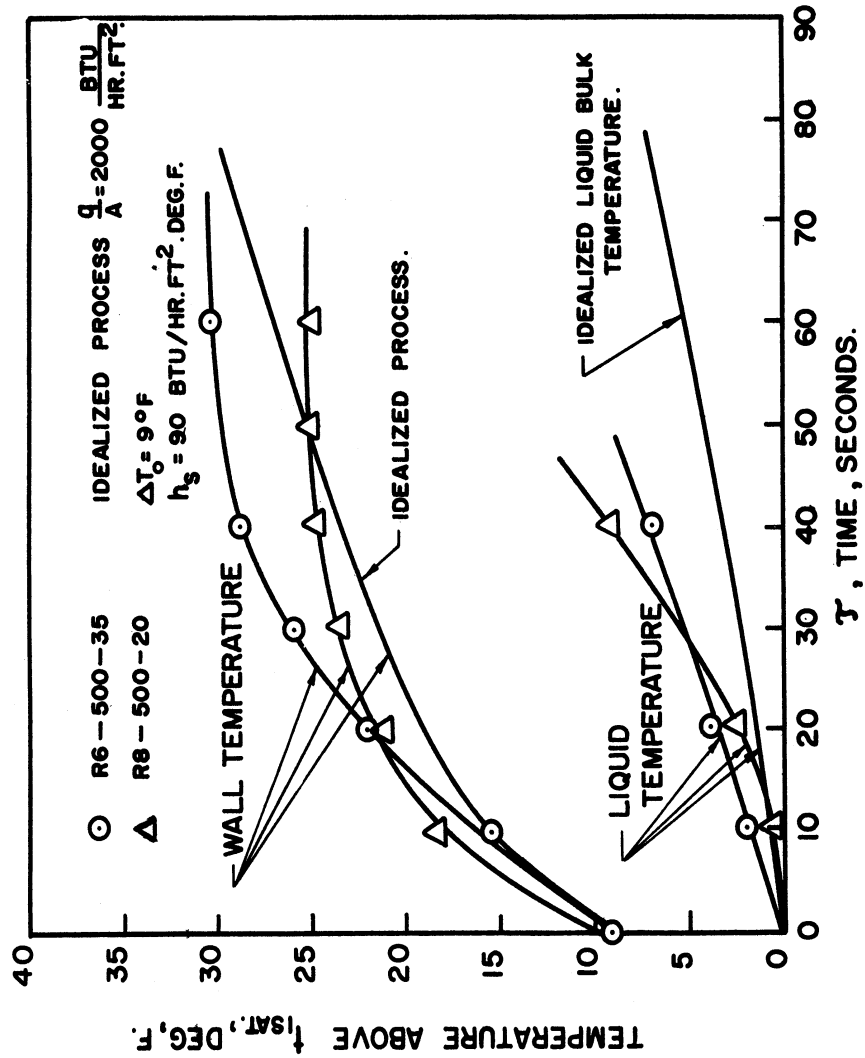


Figure 54. Comparison of Idealized Wall and Liquid Transients with Data.

temperatures after pressurization show tendencies opposite to that of the wall.

This analysis, as has been mentioned, does not take into account the boiling which begins to take place at the walls, especially near the top of the liquid.

It is this boiling which causes the liquid temperature transient to level off as "layer" after "layer" of the liquid is brought to the boiling temperature corresponding to the new pressure. As this occurs, the heat transfer coefficient goes to a value associated with boiling, and an equilibrium is established between wall and liquid temperatures.

E. Time Variation of the Heat Transfer Coefficient

The transient behavior of the heat transfer coefficient is characterized by a rapid rate of decrease following pressurization, a minimum point or dwell period depending upon the longitudinal location and flux, and finally a rapid increase until steady boiling is re-established.

During steady boiling, the coefficient at a given distance above the bottom of the test cylinder remains constant with time. Upon pressurization, the bubbles collapse, and the agitation associated with bubble formation and escape ceases causing the fluid motion to decelerate.

Whereas the entire problem here under study may be classed as a transient free convection, for purposes of clarity we shall use the term "free convection" to describe only that component of fluid motion due to temperature differences between the wall and the liquid.

Neglecting momentarily the effect of free convection after pressurization and cessation of boiling, the diminution of the coefficient can be attributed entirely to the relationship of inertia forces to viscous forces existing instantaneously in the liquid. Actually, the temperature difference between the wall and the liquid increases for some time after pressurization thus tending to increase the free convection effects.

The Reynolds number is the modulus generally used to express the relationship of inertia to viscous forces. The following Reynolds number is defined:

$$\begin{aligned} \text{Re} &\equiv \text{Inertia forces/Viscous forces} \\ &= \frac{\rho L U L}{\mu_f} = \frac{U L}{\nu_f} = \frac{L^2}{\gamma \nu_f} \end{aligned} \quad (26)$$

The following expression for the decay of the heat transfer coefficient due to viscous deceleration of the liquid nitrogen is thus postulated:

$$\frac{\Delta h}{\Delta h_0} = e^{-\frac{C_2}{\text{Re}}} = e^{-\frac{C_2 \nu_f \gamma}{L^2}} \quad (27)$$

To prove the validity of the above statement, it is necessary to isolate the effect of viscous deceleration from other effects which are occurring simultaneously.

After pressurization the forces acting to influence the heat transfer coefficient may be classed as follows:

(1) Viscous forces tending to decelerate the fluid and hence decrease the coefficient.

(2) Free convection tending to increase the coefficient during the period in which the wall-liquid temperature difference is increasing.

(3) Bubble formation tending to increase the coefficient.

Focusing our attention on the low heat flux runs (below approximately 2000 BTU/hr.ft²) in order to examine the system least affected by bubble formation, it is noted that the coefficient reaches a minimum value and remains in the region of the minimum for some time before increasing again. This may be seen in Figures 12, 16 and 18. This is particularly true for the liquid near the cylinder bottom where the fluid is in its lowest state of agitation. It will be assumed that in the period after pressurization up to this minimum only the first two influences cited above play a role in the performance of the heat transfer coefficient. That is to say, no bubbles have formed in this period of time.

The following reasons are listed as substantiation of this assumption:

(1) When pressurization occurs, the rate of decrease of the heat transfer coefficient is very rapid because the primary cause of fluid motion, bubble formation, growth and departure, no longer exists. If cessation of bubble formation can cause such a rapid decrease, it is reasonable to assume that a rapid rise in the coefficient is due to the re-initiation of bubble formation. The formation of bubbles causes violent agitation of the liquid and therefore an

increase in the heat transfer coefficient. This is true whether they form in a liquid whose bulk temperature corresponds to a subcooled state, (in which case they condense), or in a saturated liquid. Since there is a dwell period before this rise, it is assumed that no bubbles have formed.

(2) In order for nucleate boiling to take place, a certain number of degrees of wall superheat are necessary. From the curves of wall temperature versus time shown in Figures 11, 15, and 17, for example, it is apparent that for a certain period there exists a wall superheat in excess of that required for boiling. This wall superheat is indicative of a superheated liquid existing at the wall at essentially the same temperature. It is postulated that during the period in which the excess superheat begins to become evident until some time before the maximum in wall temperature is reached, no bubbles whatsoever have formed.

If bubbles began to form at the time when the excess begins to manifest itself, the wall temperature would remain constant, and the excess superheat would disappear. Keenan⁽¹⁴⁾ states that if a change to a more stable state is to occur, it must be initiated by the formation of a minute amount of the more stable phase within the mass in metastable equilibrium. Since a metastable state is one which can exist despite infinitesimal disturbances, a small enough bubble will not cause the highly superheated liquid to evaporate. Instead, the bubble will condense. This explains why the heat transfer coefficient is observed to increase before the maximum wall temperature is reached. The excess superheat is increasing despite the formation

of bubbles near the maximum in wall temperature. If the maximum wall temperature represented the time of first fracture of the liquid, the coefficient would start to rise at that time. After the wall temperature reaches its stable value, the liquid temperature at that longitudinal location goes to saturation, indicating that boiling there is fully re-established.

The experimental work of Rosenthal and Miller⁽²³⁾ on transient boiling provides some information as to the time of first bubble formation in a different but related system. Their apparatus permitted heat to be generated exponentially in platinum and aluminum ribbons which were immersed in water whose bulk temperature was varied from 90°F to a value near the boiling point. The time for the power transient varied from 5 to 75 milliseconds. They observed that the rapidly increasing ribbon temperature passed the saturation value for water, exceeded it by an amount which they termed the "temperature overshoot", decreased, and then levelled off. At the point of maximum ribbon temperature, motion pictures showed an "almost explosive" formation of bubbles.

Since the period of power generation was so short, the fact that no bubbles formed before the ribbon temperature peak is not surprising.

In a similar experiment, Cole⁽³⁾ observed also that the ribbon temperature peaked and then levelled off.

(3) That boiling is non-existent at the time of minimum heat transfer coefficient is further supported by the fact that first net boiloff occurs some time after this minimum, usually thirty or more

seconds later.

It will be assumed, on the basis of the foregoing, that up until the time of the minimum heat transfer coefficient, the only driving force present to tend to increase the coefficient is the temperature difference between the wall and the liquid. Furthermore, it will be presumed that at the minimum, viscous deceleration is essentially complete, and the heat transfer coefficient is due entirely to the buoyant forces associated with free convection. During the period in which the minimum heat transfer coefficient is observed, a coefficient based upon turbulent free convection from a vertical surface can be calculated. The calculated coefficient also does not change during this period. The viscous deceleration tends to decrease the coefficient however, so that if it were not negligible in the period of dwell, the net effect would be a decrease in the coefficient. The contribution due to residual motion imparted to the fluid by the previous boiling process is therefore presumed zero at the time the coefficient goes to a minimum value.

It now remains for us to subtract out the effect of free convection from the total heat transfer coefficient during the period from pressurization to dwell. In calculating the free convection effect, two assumptions will be made:

(1) The same parameters governing free convection heat transfer from vertical flat surfaces or outside of vertical tubes apply for free convection inside of vertical cylinders.

(2) It is valid to treat the transient free convection process as though a quasi-steady state exists at each time for which a coefficient

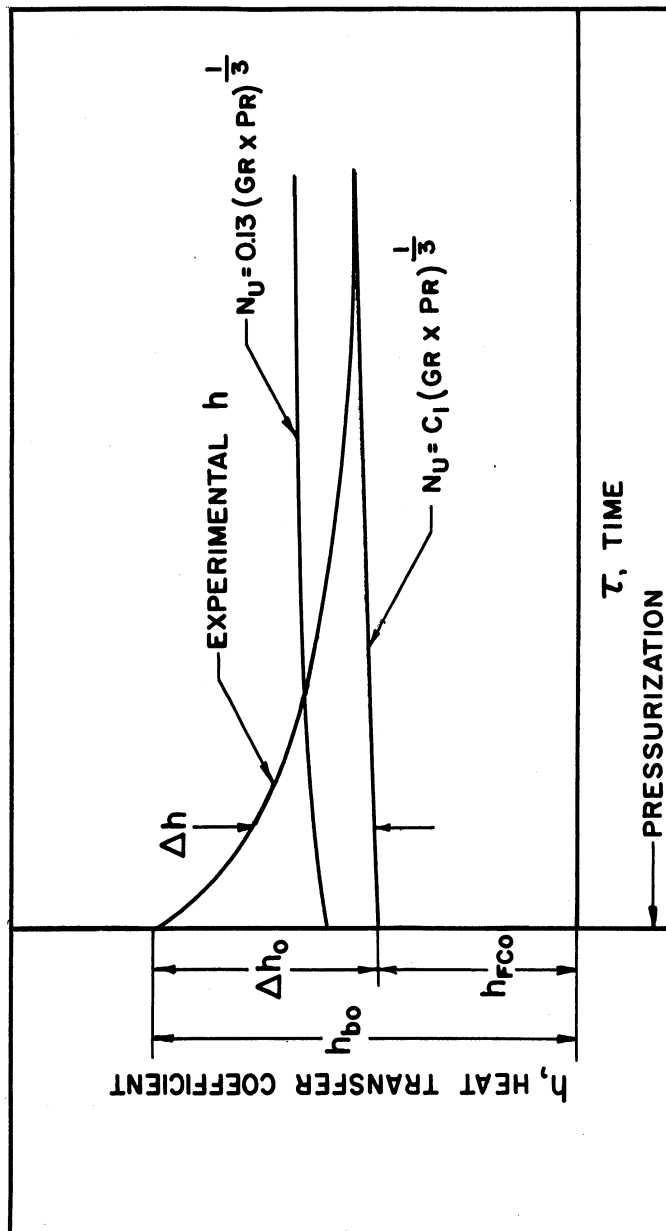


Figure 55. Curves Showing Definition of Δh and Δh_0 .

is thus calculated.

The correlation used for turbulent free convection from vertical surfaces, sometimes called the Jakob⁽¹³⁾ correlation is as follows:

$$\text{Nu} = 0.13 (\text{Gr} \cdot \text{Pr})^{1/3} \quad (28)$$

If now, the heat transfer coefficient for turbulent free convection is calculated as a function of time and drawn on the same graph as the experimentally obtained heat transfer coefficient, a similar result to that shown in Figure 55 is observed.

As is seen from Figure 55, the correlation used gives values which are too high for convection inside of vertical tubes. Since it has been assumed however, that the basic convection phenomenon is governed by the same parameters as in the case of vertical surfaces, only the coefficient 0.13 in the correlation used need be changed to make the calculated heat transfer coefficient valid.

The ratio of the experimentally determined heat transfer coefficient to the value calculated from the correlation for vertical surfaces, evaluated at the minimum of the test curve tells us by what amount the constant in the Jakob⁽¹³⁾ correlation is too high. This information is then used to compute the appropriate constant. When this value is used, a new free convection curve is drawn, as in Figure 55, and the fraction $\Delta h / \Delta h_0$ calculated. Table V shows that as the distance above the bottom of the cylinder increases, the heat transfer coefficient more closely equals the value calculated for vertical surfaces. This is a reasonable result since the reason there is any difference to begin with is attributable to the stagnant zone which

necessarily exists at the bottom. As the elevation increases, the influence of the closed end becomes less and less evident.

Several workers have also observed this decreased coefficient. Hartnett and Welsh⁽⁹⁾ provide data from which it may be deduced that the coefficient 0.13 is replaced by a value equal to 0.06 in the turbulent free convection correlation. Their work related to a constant heat flux vertical tube with an L/d ratio of 10.5. They studied a steady state convection process however, since a means of abstracting the heat supplied through the walls was provided. This latter point is common to the references which will be cited with regards free convection inside of vertical tubes and spaces.

Martin and Cohen⁽¹⁹⁾ in their work concerning heat transfer by free convection in an open thermosiphon tube of L/d equal to approximately 24, found that the heat transfer rates were well below those predicted for both laminar and turbulent boundary layer flow. The distribution of local heat transfer rates in their constant temperature tube was not at all constant with distance from the bottom. They found that the highest heat transfer occurred at the top (where the coefficient is largest), falling off toward the bottom. They state that while the general condition is one of turbulence, laminar flow may occur near the closed end.

The results of Martin⁽¹⁸⁾ are similar to those cited above.

Eckert and Diaguila⁽⁴⁾ state that for a tube of L/d approximately equal to 7, the Nusselt numbers in the turbulent range average 35 percent below the known relations for vertical flat plates. They worked with a constant wall temperature apparatus.

Siegel and Norris⁽²⁶⁾, in their tests of free convection in a partially enclosed space between two heated vertical plates at essentially uniform flux found that when the space between the plates was opened sufficiently at the bottom, the results were consistent with the Jakob correlation. With the bottom closed however, the coefficient was lower than the value associated with free convection from vertical surfaces as calculated from this correlation.

For the low heat flux runs, values of $\Delta h/\Delta h_0$ are tabulated in Table VI for several times after pressurization. These times occur before the minimum is reached in heat transfer coefficient. It was necessary to interpolate in order to arrive at these results, but the consistency shown yields some fairly conclusive information. These data are plotted in Cartesian coordinates (Figure 56) and semi-logarithmic coordinates (Figure 57). Since the latter plot is a straight line, the validity of Equation (27) is supported. Such a straight line is indicative of a first order effect.

The attenuation of the coefficient of heat transfer due to viscous deceleration is therefore expressed in terms of the empirically determined value of the constant, C_2 .

$$C_2 = 0.892 \times 10^5$$

We may write, therefore:

$$\frac{\Delta h}{\Delta h_0} = e^{-0.892 \times 10^5 \frac{\sqrt{L}}{L^2}} \quad (27a)$$

or:

$$\Delta h = \Delta h_0 e^{-0.892 \times 10^5 \frac{\sqrt{L}}{L^2}} \quad (27b)$$

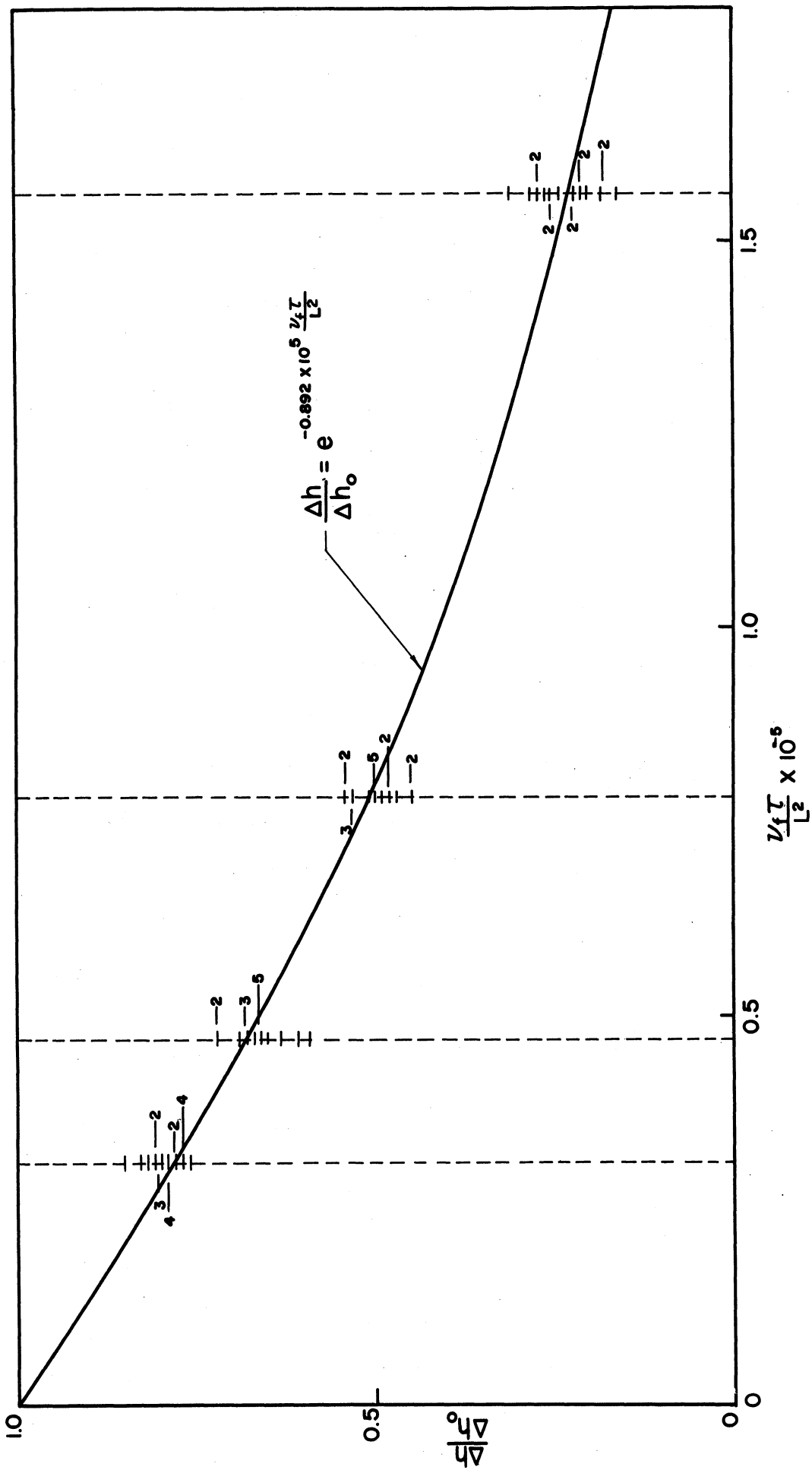


Figure 56. Viscous Attenuation of the Heat Transfer Coefficient.

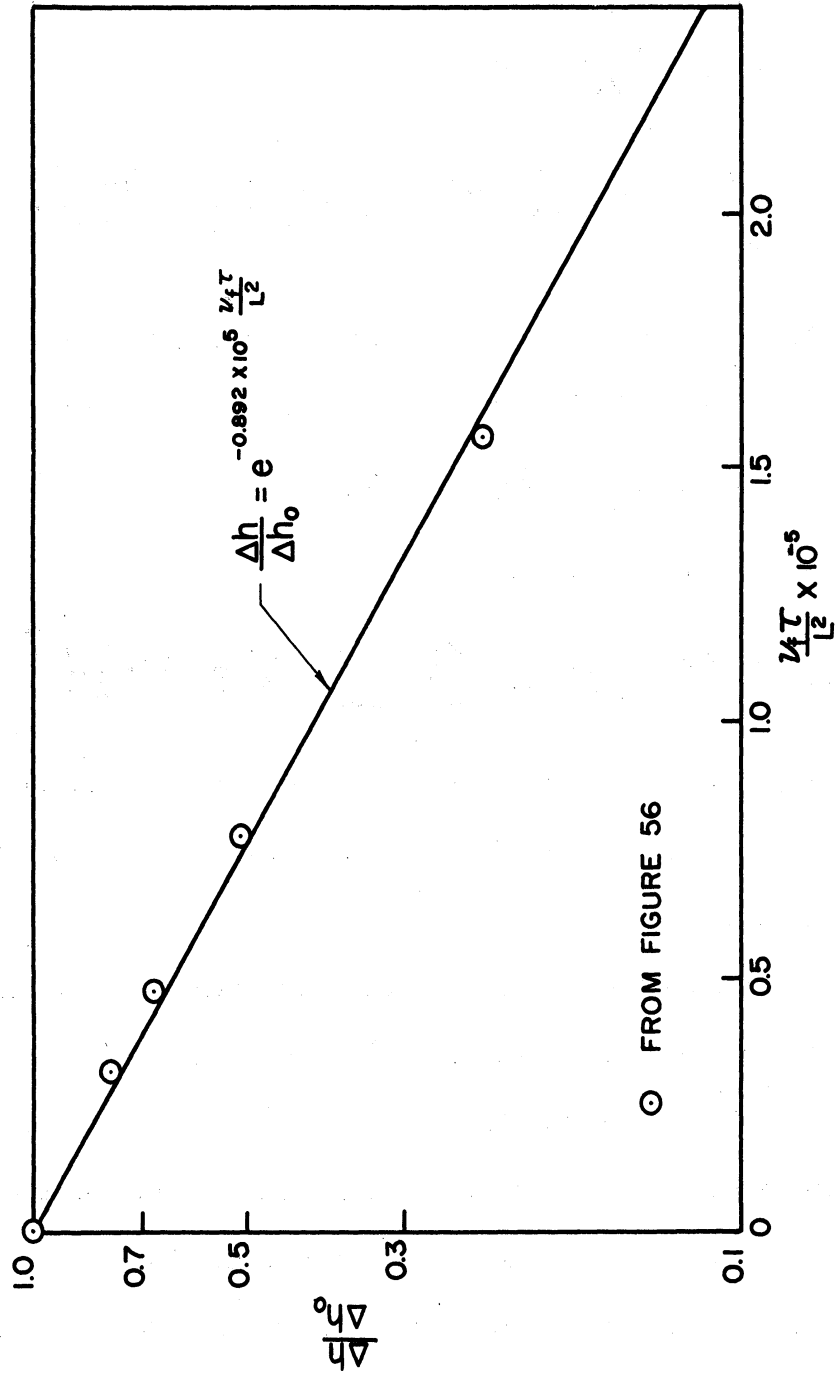


Figure 57. Viscous Attenuation of the Heat Transfer Coefficient.

The coefficient of heat transfer following pressurization up to the time of first bubble formation is expressed as the sum of two terms. The first relates to the free convection contribution, the second to the viscous diminution of the initial turbulence:

$$h = h_{FC} + \Delta h \quad (29)$$

$$\frac{hL}{K_L} = C_1 (Gr \cdot Pr)^{\frac{1}{3}} + \frac{\Delta h_0 L}{K_L} e^{-\frac{.892 \times 10^5 \sqrt{Gr}}{L^2}} \quad (30)$$

The appropriate value of C_1 may be calculated from the information supplied in Table V for the longitudinal location of interest.

$$\text{Since } \Delta h_0 = h_{b0} - h_{FC0} \quad (31)$$

Equation (30) may be stated as follows:

$$\frac{hL}{K_L} = C_1 (Gr \cdot Pr)^{\frac{1}{3}} + \frac{(h_{b0} - h_{FC0})L}{K_L} e^{-\frac{.892 \times 10^5 \sqrt{Gr}}{L^2}} \quad (32)$$

h_{b0} may be obtained from test data. h_{FC0} is calculated on the basis of the temperature difference between the wall and the liquid at time zero.

The instantaneous value of the heat transfer coefficient cannot be calculated from Equation (32) however, until the wall and liquid transients are known. This is because the Grashof number is dependent upon the wall-liquid temperature difference, and the fluid properties depend (to a much lesser degree) on it also.

The wall transient may however be estimated using the results of the idealized analysis described on pages 63-72. These wall transients, together with the dimensionless liquid transients

shown in Figure 38 may be used to calculate the free convection contribution to the total heat transfer coefficient transient. The procedure outlined yields an estimate of the variation with time of the heat transfer coefficient following pressurization.

F. Longitudinal Liquid Temperature Gradients

As has already been mentioned, the central liquid thermocouples and those midway between the centerline and the cylinder wall, at a given time, measure substantially the same temperature. This has been observed for both the boiling and non-boiling periods of a run.

Mair⁽¹⁷⁾ in tests with non-boiling liquid oxygen subjected to climatic heating at a flux of 1160 BTU/hr. ft² found that the temperature remained substantially constant in going from the centerline to a radius of 34 inches in a 35 inch radius cylinder approximately 160 inches in length.

A similar result was obtained by Harrje⁽⁸⁾ for boiling and non-boiling liquid oxygen at a flux of approximately 5500, this for a cylinder four feet high and one foot in diameter.

During the period in which the liquid nitrogen is being heated to its new saturation temperature following pressurization, buoyancy forces cause it to move upward at the wall. Continuity dictates that the liquid, once it has moved into the region of the liquid-vapor interface must change its direction and move downward through the central portion of the test cylinder. The liquid immediately in contact with the walls must have zero velocity. It is reasonable then to assume that the upward velocity near the wall attains a maximum value before

it again goes through a zero of velocity at some distance from the wall. This is the description characteristic of the velocity profile associated with a laminar or turbulent boundary layer in free convection.

Since the previous condition of the liquid was vigorous nucleate boiling, the liquid travelling downward in the central portion as well as that flowing upward at the walls must be in turbulent flow. Focusing on the central region, the literature concerning turbulent flow through pipes may be used to good advantage to give an indication of the velocity and temperature profiles which may be expected. The Martinelli analogy (Reference 20) for flow through uniformly heated pipes indicates for a Reynolds number of 10,000 and a Prandtl number of unity, that the velocity at a radial location midway between the centerline and the wall is 90% of its maximum value at the centerline. For a Prandtl number of unity, the temperature and velocity profiles are identical. For the liquid nitrogen system under study, the Prandtl number is approximately 1.5 and the Reynolds number immediately after pressurization may be as high as 50,000 as computed from velocities discussed later. The higher Prandtl and Reynolds numbers cause the theoretical velocity profiles to become even flatter than indicated above.

McAdams⁽²⁰⁾ in citing the work of Seban and Shimazaki⁽²⁴⁾, Koo, and Isakoff and Drew, shows that the temperature distribution in upward moving fluids flowing in vertical heated pipes is similar to those discussed above. The Reynolds number was in the neighborhood of 40,000.

It is not surprising therefore that the temperature profile as indicated by the two thermocouples at each longitudinal level appears to be flat. Furthermore, we would expect the velocity profile of the central region of the test cylinder to be similarly flat. On the basis of the foregoing, Figure 58 illustrates what is judged to be reasonable temperature and velocity profiles in the cylinder for the period following pressurization.

This description relates then to an almost constant velocity core moving downward, and a peaked velocity shell moving upward. Since we expect the thickness of the shell or turbulent boundary layer to be very small relative to the diameter of the central core, the laws of continuity dictate that the upward velocity mean or maximum be much larger than the downward velocity mean or maximum.

Assuming that there is no mass or energy interchange between the upward and downward moving streams, the energy input through the walls serves to heat the upward moving shell only. The temperature of a differential element of liquid in moving down the core to return to the narrow annular channel would not change until it in fact re-entered the channel to be heated at constant flux by the walls. The simplified analysis which follows will serve to indicate the expected trends for the liquid temperature gradient in the core as a function of heat flux.

For the shell travelling upward at the cylinder wall the following assumptions are made:

- (1) The shell or boundary layer thickness is constant with height above the bottom of the cylinder.

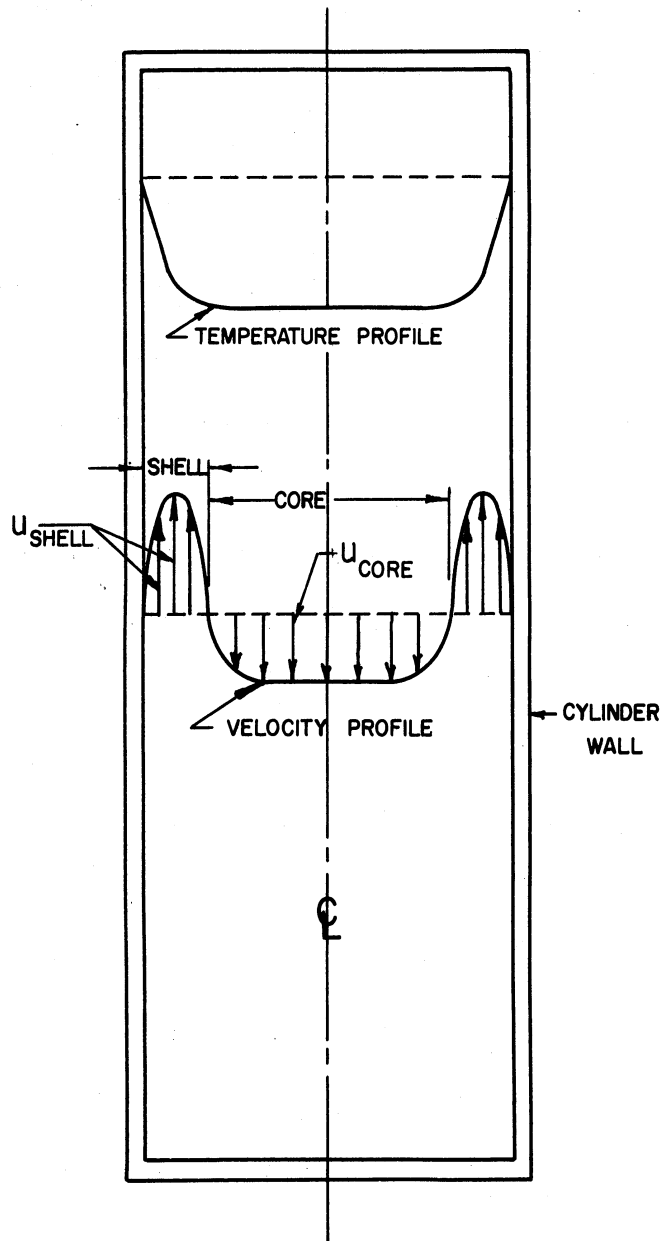


Figure 58. Liquid Velocity and Temperature Profiles.

(2) The shell velocity remains constant at the value specified by boundary layer thickness and continuity.

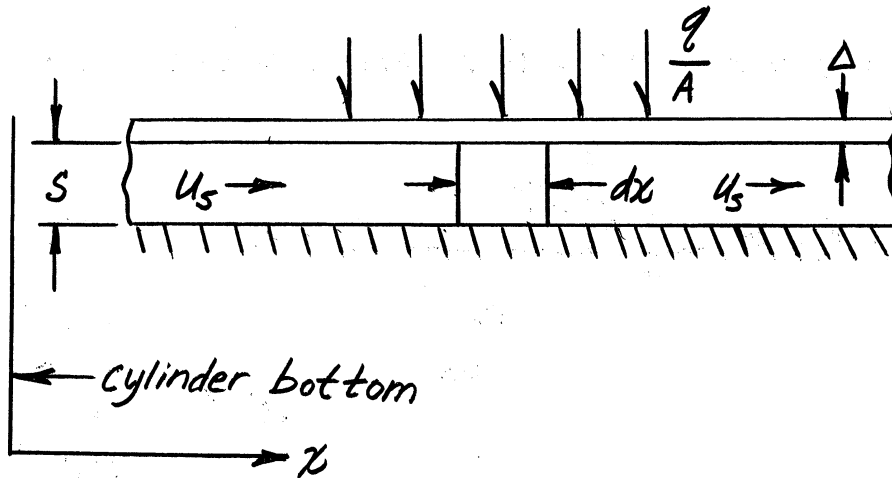


Figure 59. Sketch Depicting Quantities Used in Shell Temperature Analysis.

The differential equation for an elemental volume of liquid moving upward through the shell at constant velocity u_s is as follows:

$$k_L A_s \frac{d^2 t_L}{dx^2} - \rho_L u_s A_s C_{pL} \frac{dt_L}{dx} = -\left(\frac{q}{A}\right) \quad (33)$$

Neglecting axial conduction:

$$\rho_L u_s A_s C_{pL} \frac{dt_L}{dx} = \left(\frac{q}{A}\right) \quad (34)$$

The solution of Equation (34) is:

$$t_L = \frac{\left(\frac{q}{A}\right) x}{\rho_L u_s A_s C_{pL}} + C_3 \quad (35)$$

At $x=0, t_L = t_{LS}$, therefore: (36)

$$t_3 = t_{LS} \quad (37)$$

The temperature variation in the shell is therefore given by:

$$t_L - t_{LS} = \frac{\left(\frac{q}{A}\right)x}{P U_S A_S C_{PL}} \quad (38)$$

From continuity we may state that:

$$U_S A_S = U_C A_C \quad (39)$$

Therefore:

$$t_L - t_{LS} = \frac{\left(\frac{q}{A}\right)x}{P U_C A_C C_{PL}} \quad (40)$$

Based on the arbitrary choice of average core velocity (30 ft/hr) and for heat fluxes of 1500 and 3000 BTU/hr. ft², Equation (40) was used to calculate the temperature distribution in the shell at several different times after pressurization. These distributions are shown in Figures 60 and 62. These may be compared with Figures 64, 65, and 66, which show the actual distribution of temperature for various times after pressurization in the core, (since the distribution of temperature in the shell is seen at a later time in the core according to the idealization). The actual temperature distributions do not depart severely from straight lines. Their slopes however are not constant. Also, they are directed toward the origin. This means that the shell and core velocities are different for different longitudinal locations. This is expected since the closed end causes a stagnant region at the bottom. On the basis of the calculated longitudinal temperature distributions, the temperature transients for three different

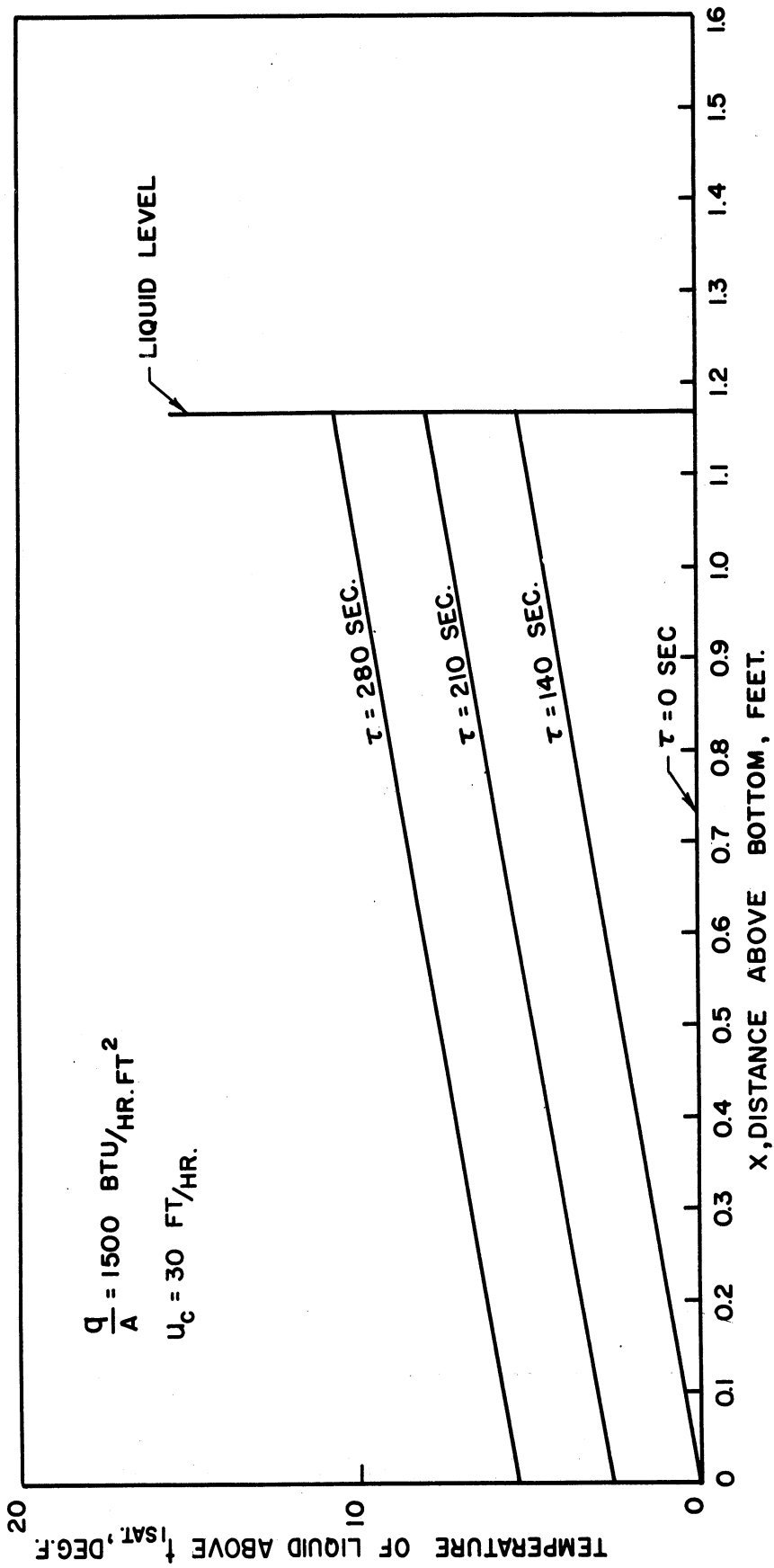


Figure 60. Liquid Temperature vs. Longitudinal Location (Idealization).
 $q/A = 1500 \text{ BTU/hr.ft}^2$.

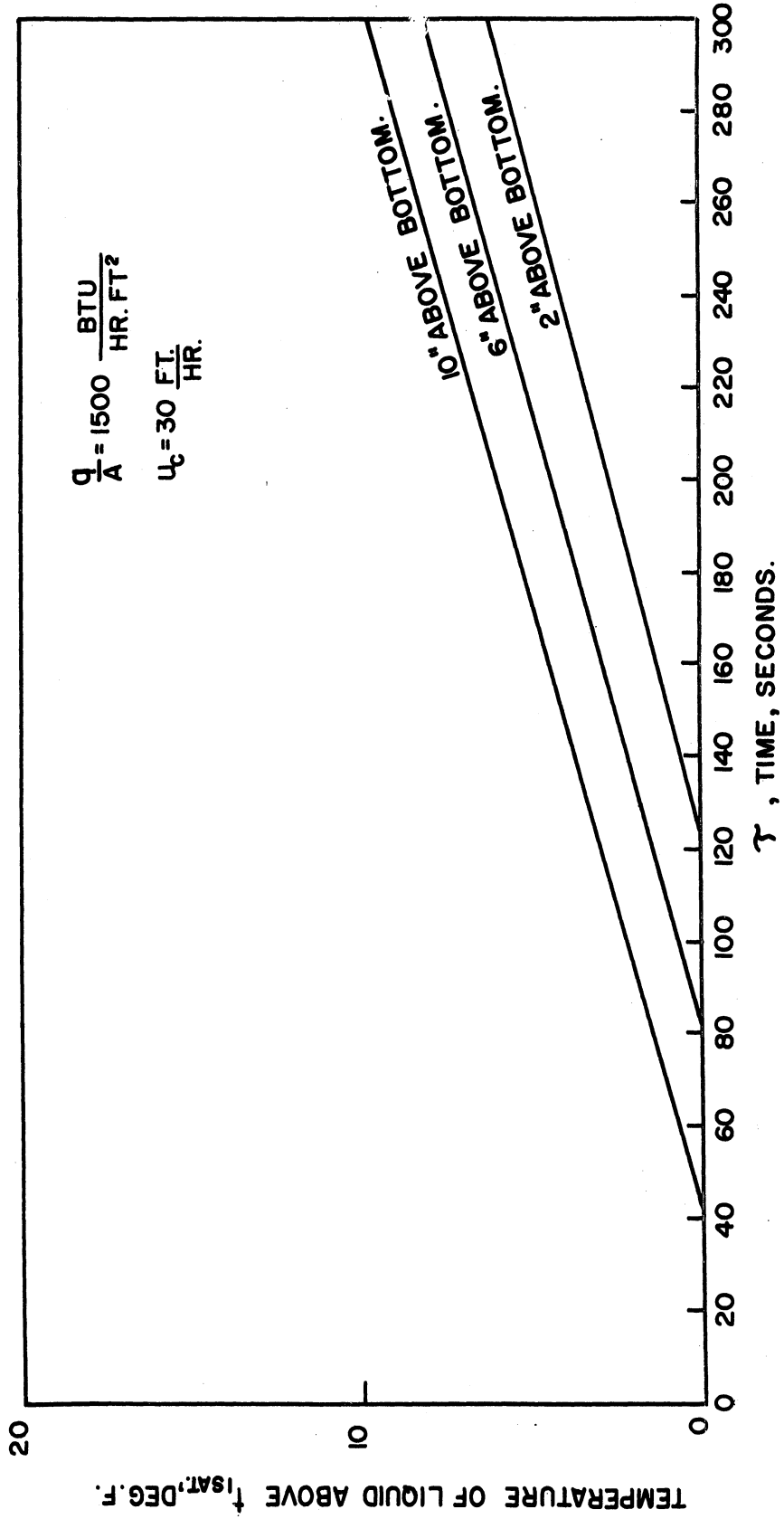


Figure 61. Liquid Temperature vs. Time (Idealization).
 $q/A = 1500 \text{ BTU/hr.ft}^2$.

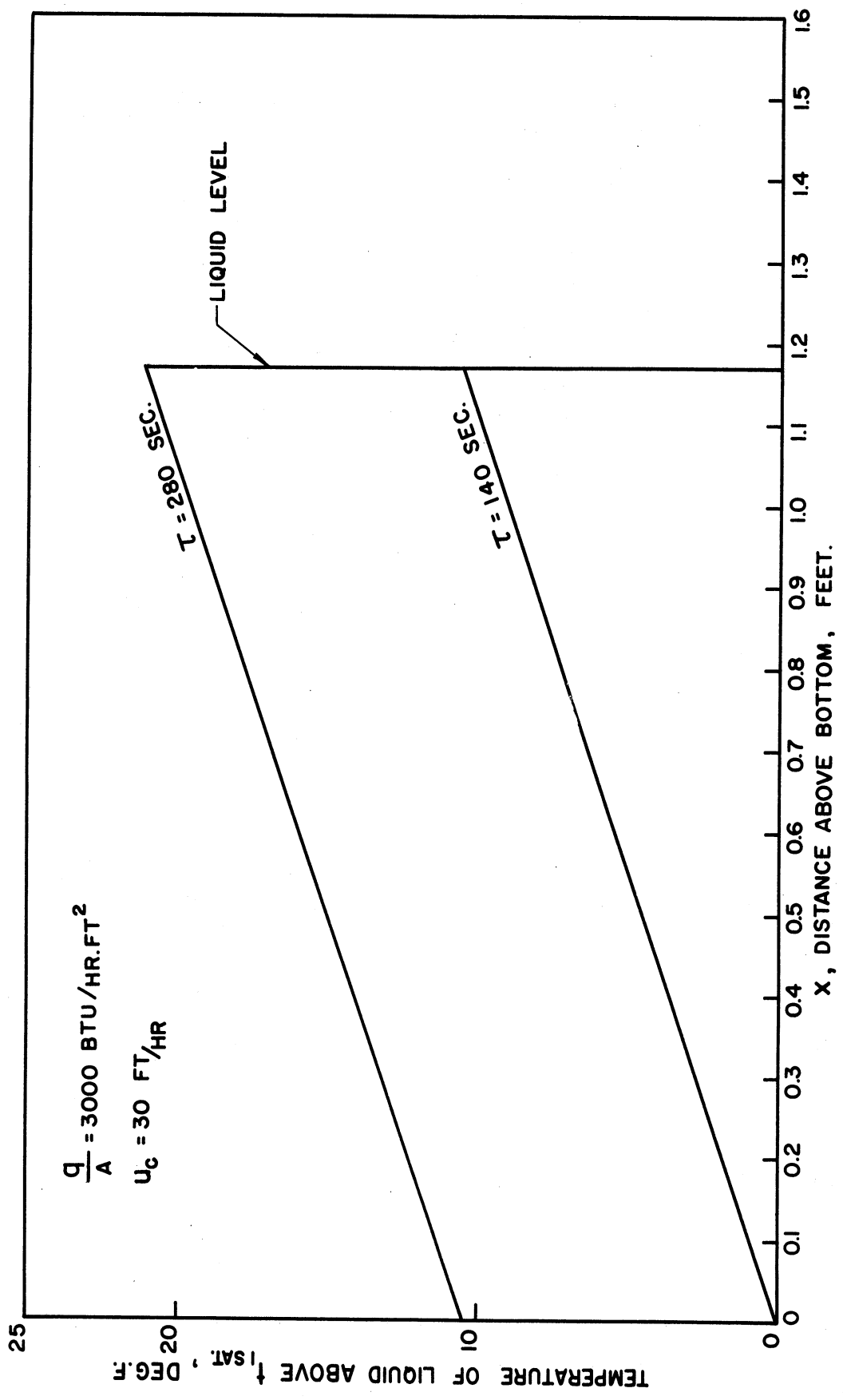


Figure 62. Liquid Temperature vs. Longitudinal Location (Idealization). q/A = 3000 BTU/hr.ft².

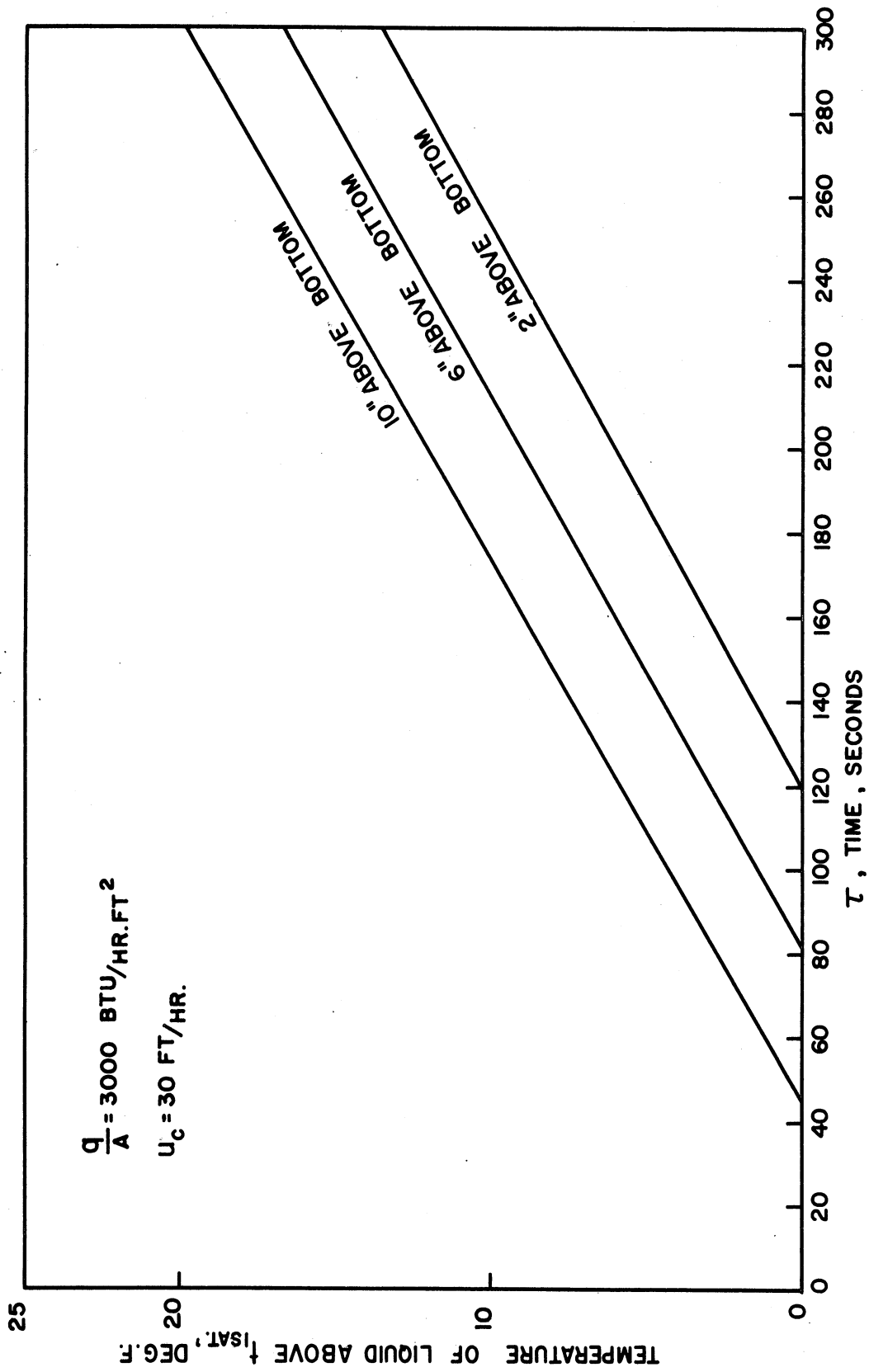


Figure 63. Liquid Temperature vs. Time (Idealization).
 $q/A = 3000 \text{ BTU/hr.ft}^2$.

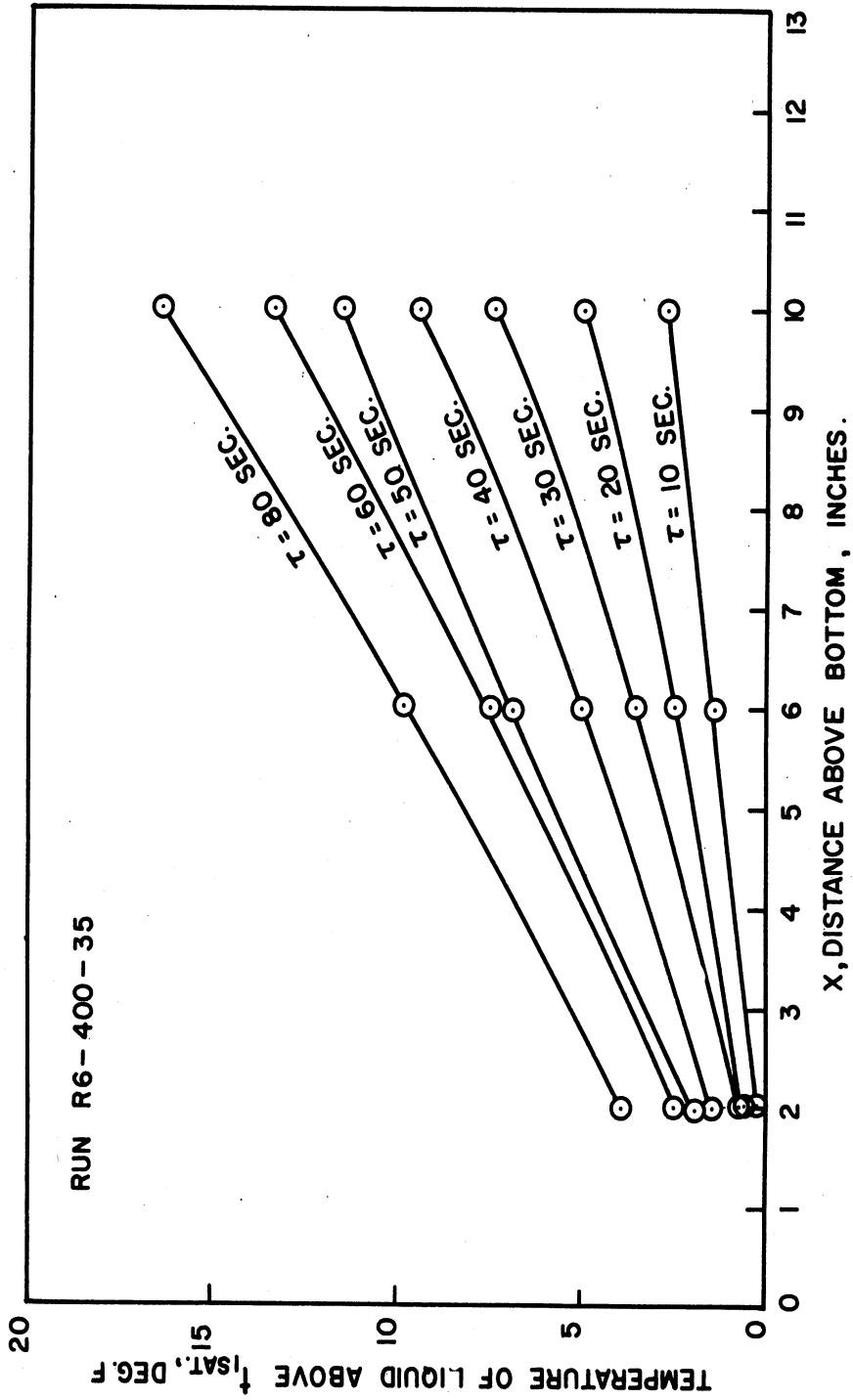


Figure 64. Liquid Temperature vs. Longitudinal Location, Run R6-400-35.

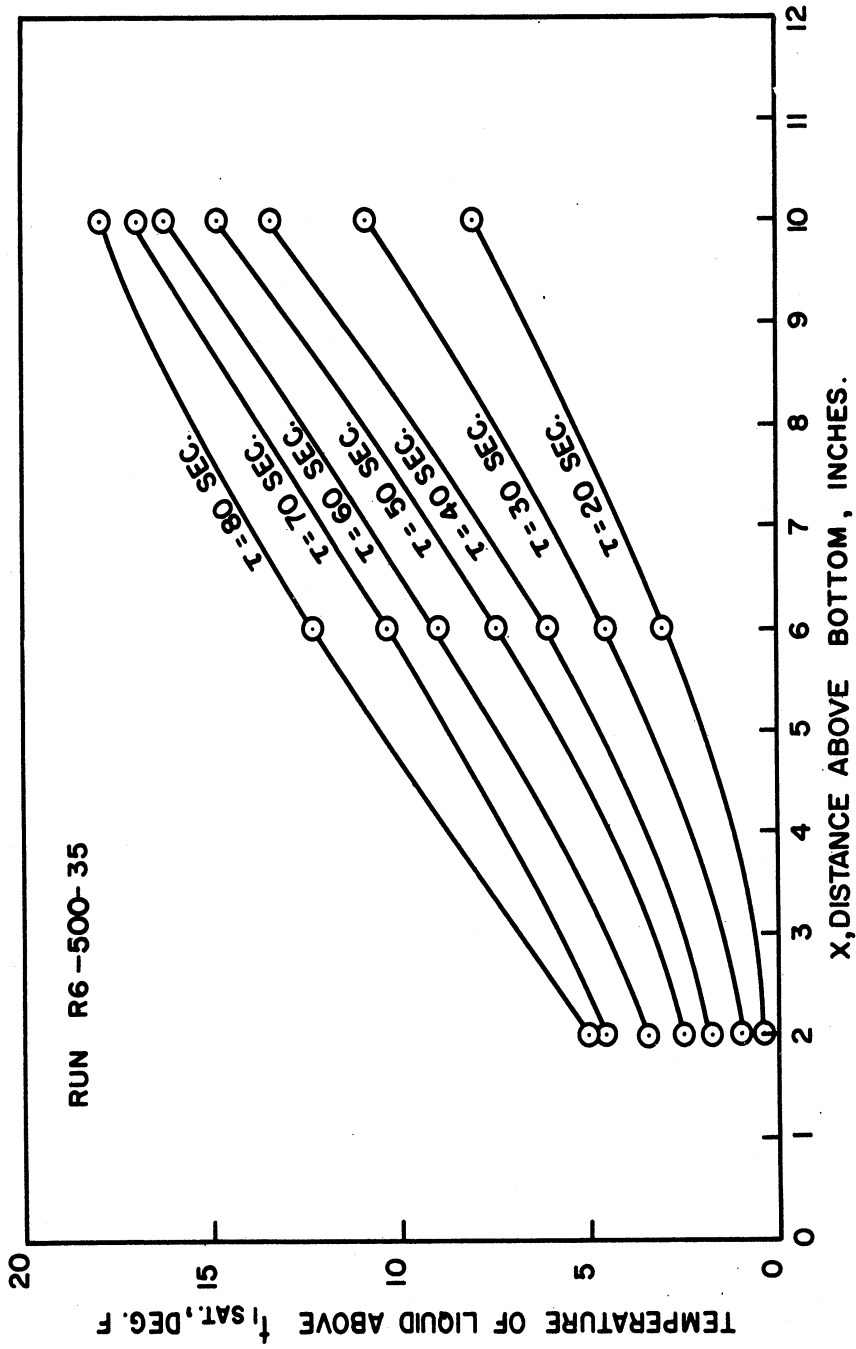


Figure 65. Liquid Temperature vs. Longitudinal Location, Run R6-500-35.

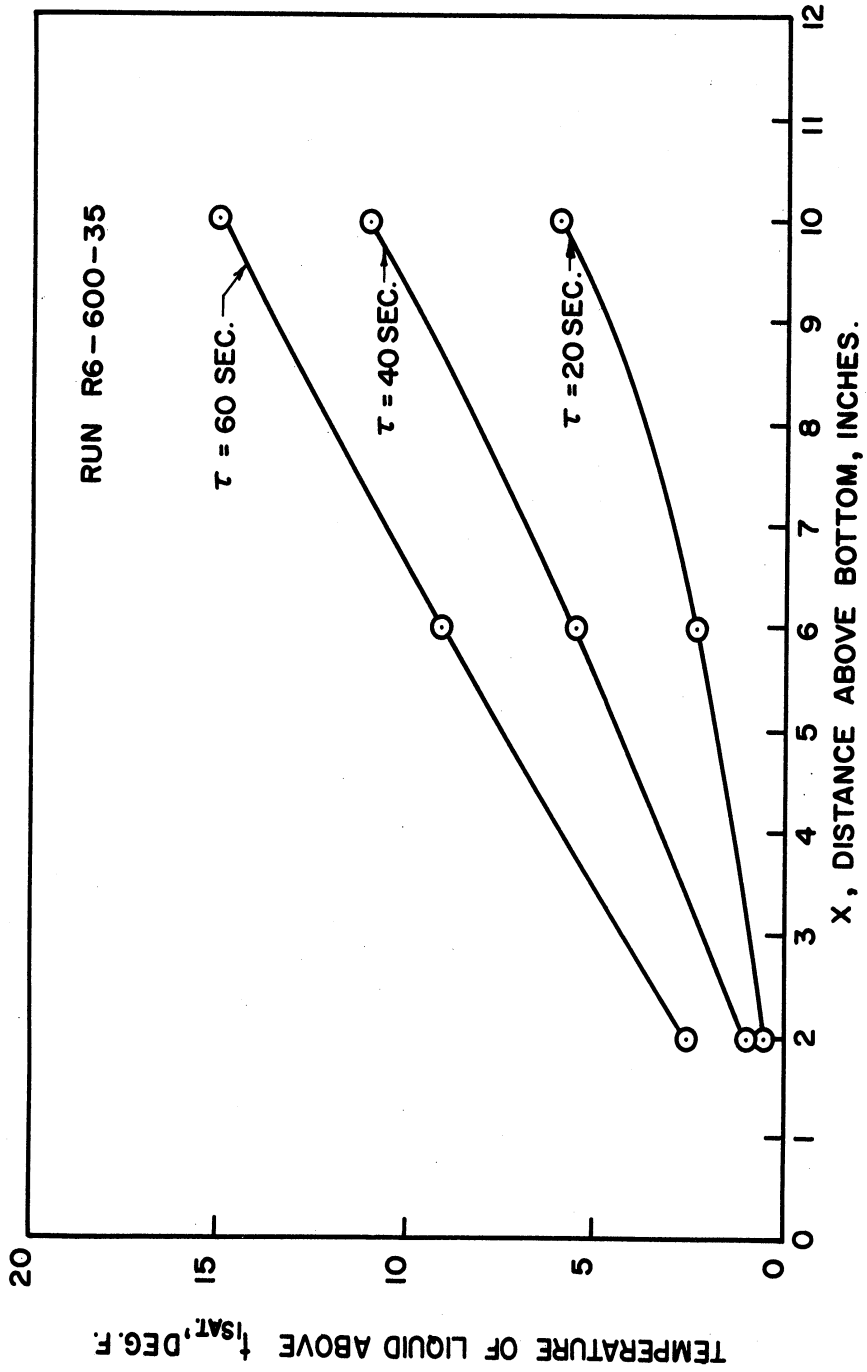


Figure 66. Liquid Temperature vs. Longitudinal Location, Run R6-600-35.

longitudinal locations were calculated and the results plotted in Figures 61 and 63. These may be compared with the actual test results shown in Figures 11, etc. Since the thermocouples in the core do not instantaneously record temperature changes occurring in the shell because of the time necessary for a fluid particle in the shell to travel to a particular location in the core, the liquid temperature transients are shifted by an appropriate amount as shown in Figures 61 and 63. The actual liquid temperature transients indicate that the liquid at the 2 inch location takes the longest time to show a change. The actual data indicates that while the general picture of the fluid flow is correct, there is some mass diffusion from the shell to the core which decreases the time necessary for temperature changes in the shell to manifest themselves in the core.

Figures 64, 65, and 66 provide a simple means of estimating the fluid velocities in the core. The basic assumption made in this calculation is that the rate at which a temperature is observed to move through the core is identical with the downward component of the fluid velocity. Three types of information are thus made available.

(1) The velocity with which a fluid element moves downward as a function of elevation above the cylinder bottom.

(2) The instantaneous longitudinal velocity profile.

(3) The velocity history at a given longitudinal location.

Item (1) above is obtained by noting, for a constant liquid temperature the distance travelled in moving from one constant time line to the next. The average velocity during the time interval is computed by dividing the distance travelled by the elapsed time.

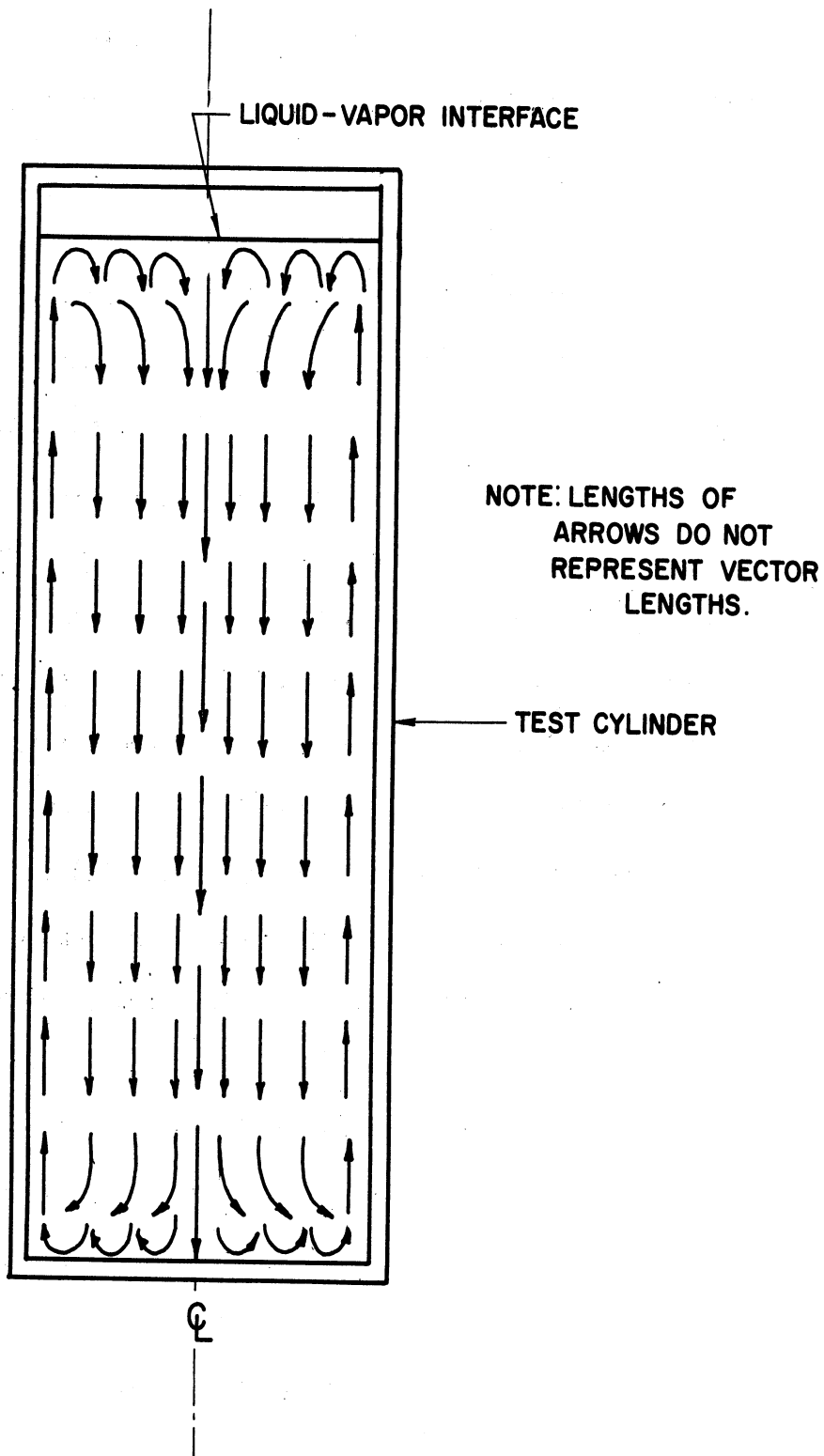


Figure 67. Convection Pattern in Liquid.

Since the temperature of a particle is assumed to remain constant in the core, focusing our attention on a specific temperature is identical with following a particular differential element of the liquid.

Results of such a calculation are shown in Figure 68. It is noted that as the "temperature" comes closer to the bottom of the cylinder, there is manifest a decrease in the downward component of velocity, which must go to zero at the bottom. The data is insufficient to compute the velocities for the region near zero time (corresponding to the liquid surface). The downward component at the liquid-vapor interface in the core must also be zero, and apparently the acquisition of downward velocity takes place in a very small longitudinal region as judged from the figure cited. Figure 71 indicates the steps taken in computation of item (1).

The instantaneous velocity profile (2) is obtained by measuring the distance travelled in going from one constant time line to the next. This differs from the procedure outlined to obtain (1) in that a constant temperature line is not followed. Instead various decreasing temperatures are traced in going from large to small longitudinal distances above the bottom. Always however, the time interval is between the same two constant time lines as is shown in Figure 72. The time at which the velocity is computed is taken to be the average value between the two constant time lines in question.

Figure 69 shows the results of this calculation. Note that once again the velocity approaches zero for zero distance from the

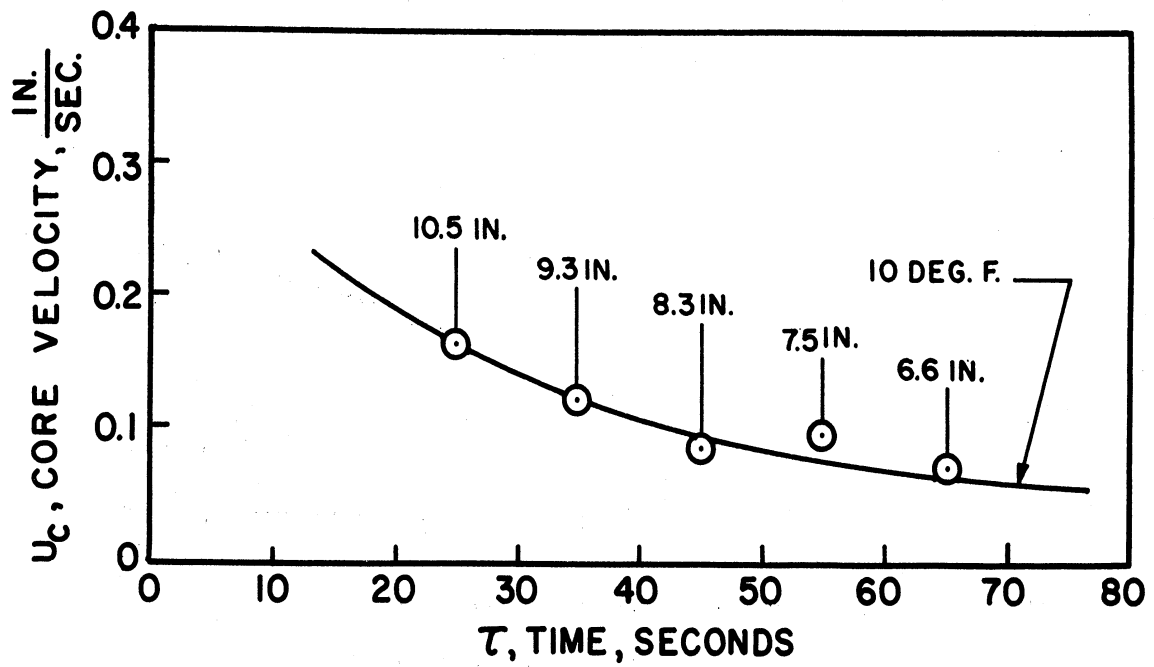


Figure 68. Core Velocity vs. Time, Run R6-500-35.

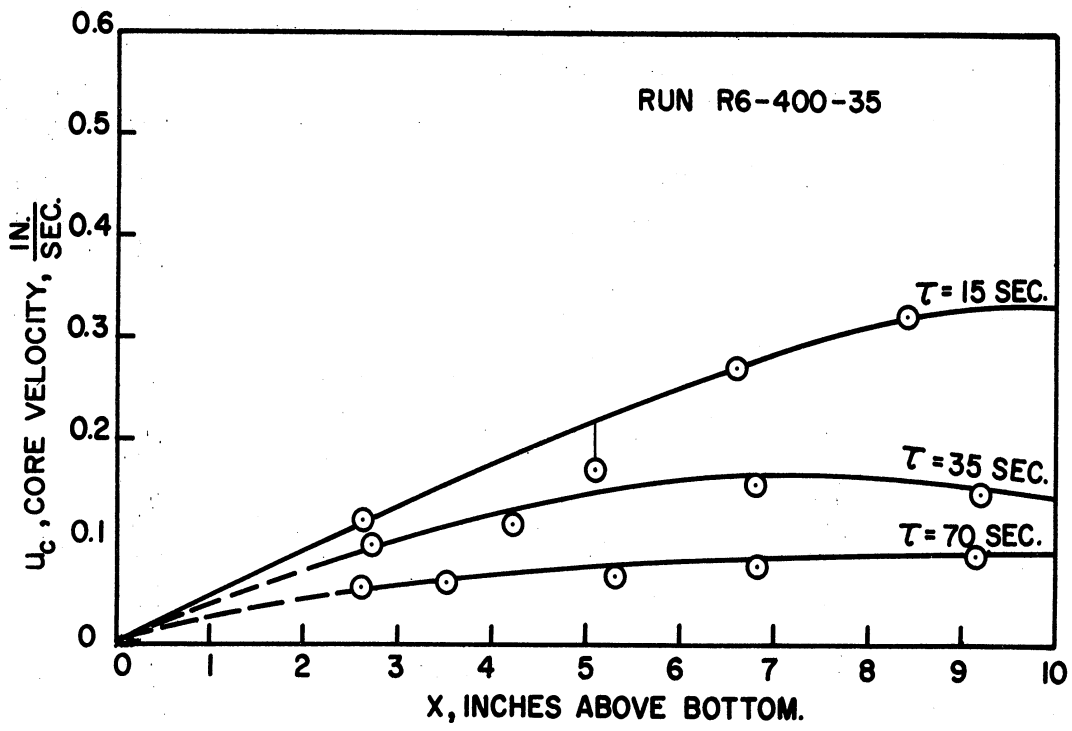


Figure 69. Core Velocities vs. Longitudinal Location
Run R6-400-35.

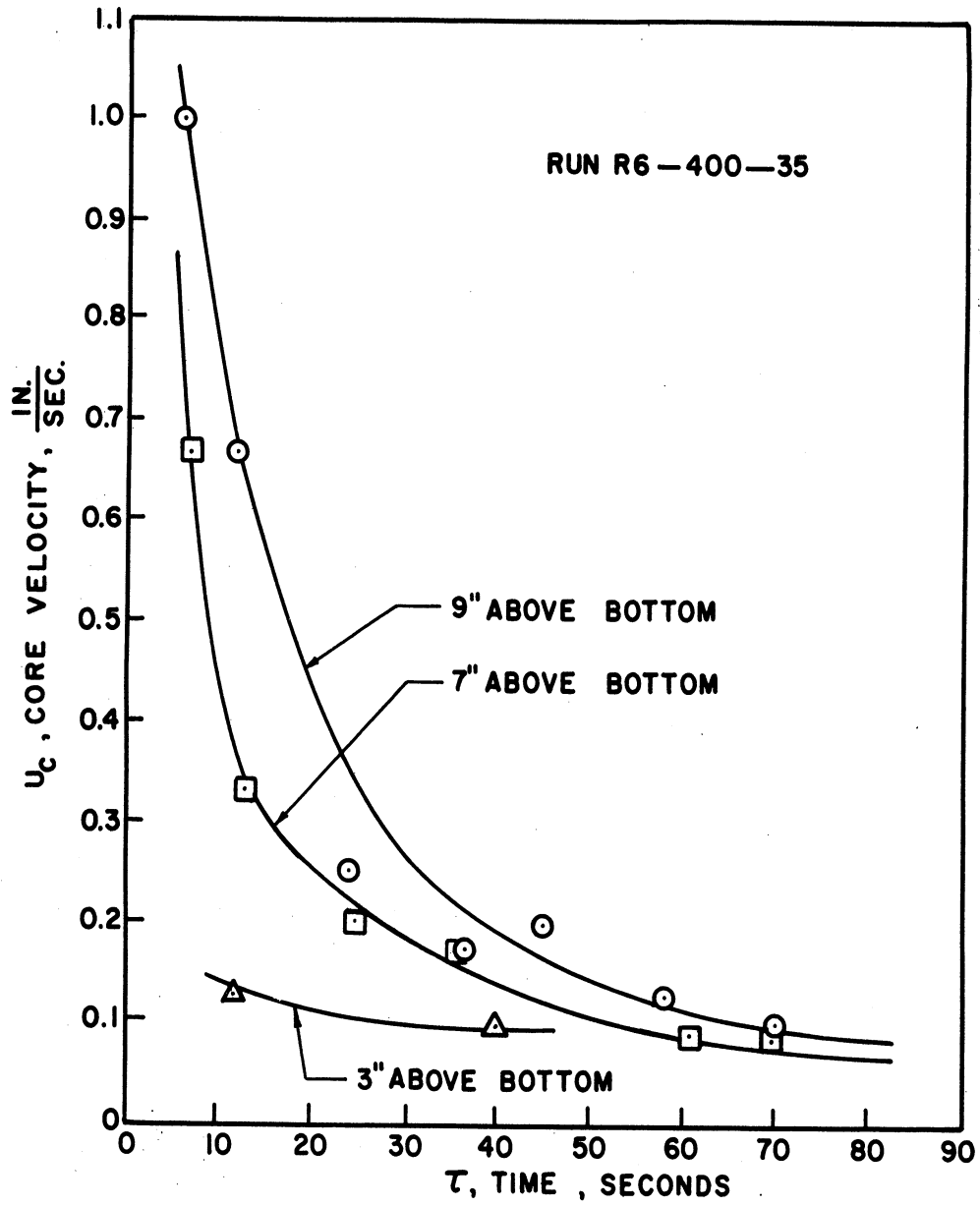


Figure 70. Core Velocities vs. Time, Run R6-400-35.

bottom. Toward the top of the liquid the velocity should diminish to zero. That this does occur is indicated by the 35 second line. However, the indication is that the velocity decreases over a rather short longitudinal distance. The liquid surface is at approximately 14 inches from the bottom.

Figure 69 tells us also that as the time after pressurization increases, the fluid velocities in the core diminish. This supports the idea that a viscous deceleration is taking place in the liquid. This will be further reinforced by the results of the next calculation.

The velocity history at a given longitudinal location is obtained by drawing two lines perpendicular to the abscissa as shown in Figure 73. The midpoint between these lines represents the longitudinal location whose temperature or velocity history is being calculated. For different temperatures of the liquid, the amount of time elapsed is estimated by drawing approximate constant time lines so that an intersection is effected between the two vertical lines and these time lines.

It is apparent from Figure 70, which shows the results of calculation (3), that there is considerable deceleration of the fluid after pressurization. This further supports the viscous deceleration theory to explain the nature of the decrease in the heat transfer coefficient postulated earlier. Since the fluid at the higher portions of the core has a higher downward component of velocity, it is these areas in which the most severe deceleration is seen.

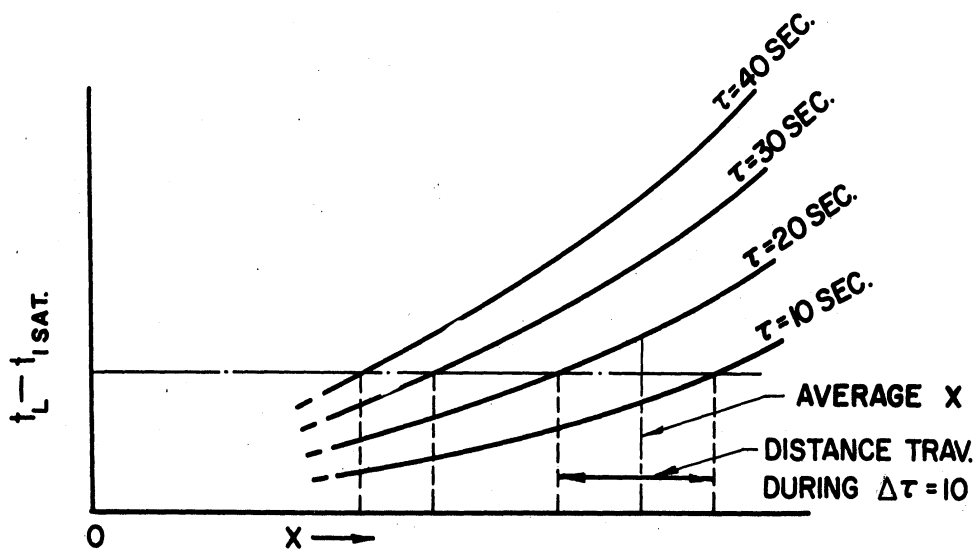


Figure 71

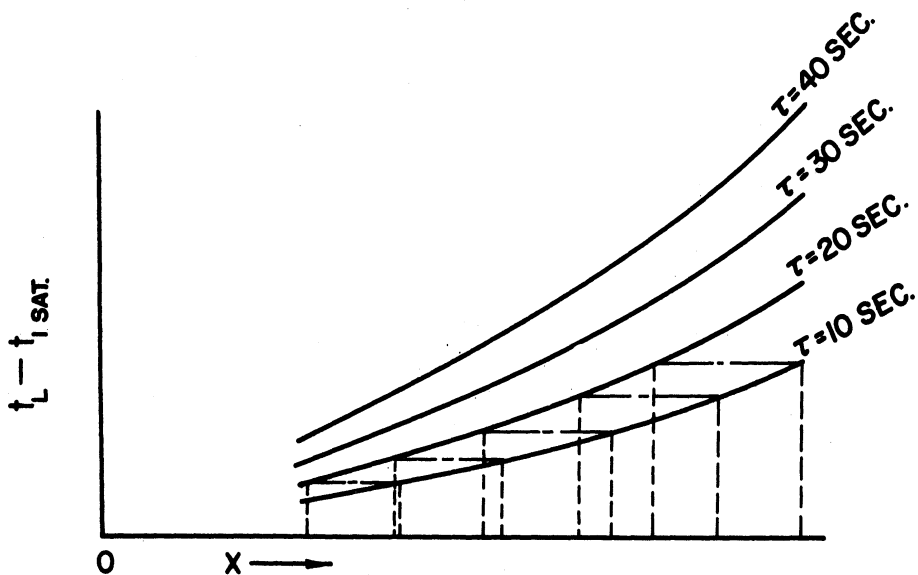


Figure 72

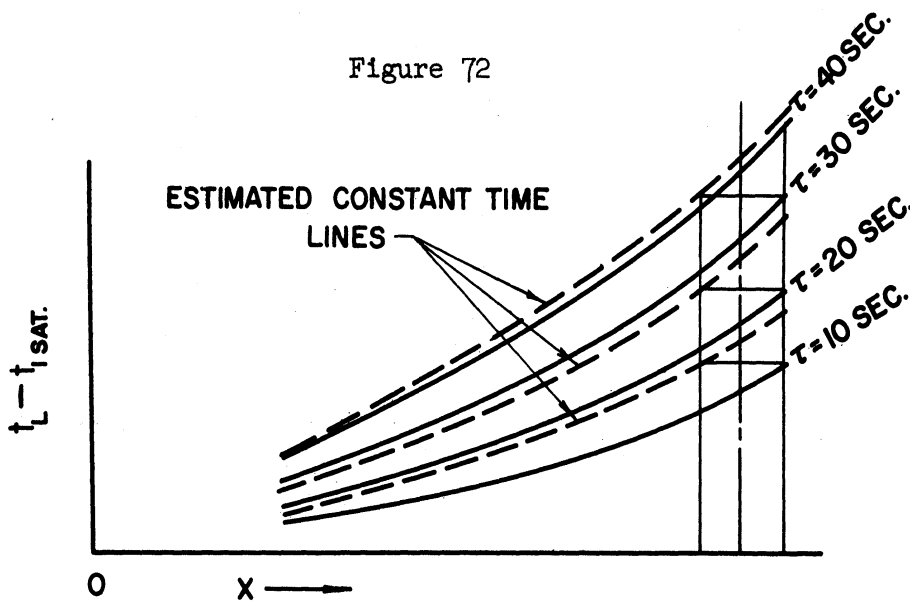


Figure 73

Curves Illustrating Core Velocity Determination Techniques.

Since the tendency for the liquid toward the bottom of the test cylinder is to decelerate in the downward direction, it must be acquiring a radial component of velocity. This means that the net mass diffusion taking place toward the bottom is from the core to the shell, and the assumption that the temperature velocity is identical with the fluid velocity is good in this region. This is because mass diffusion away from the core does not contribute toward changing the core temperature.

At the top of the cylinder, the reverse is true however. The velocity of the shell must go to zero at the top, and in so doing it must acquire a radial (inward) component of velocity. This means that there will be mass diffusion from the warmer shell to the core, and the computed velocities will not be as meaningful.

On the basis of the foregoing, the flow pattern shown in Figure 67 is presumed to be valid for the liquid contained in the test cylinder.

G. Turbulent Boundary Layer Considerations

In order to estimate the thickness of the shell, turbulent boundary layer theory will be implemented. Eckert and Jackson⁽⁵⁾, for an assumed velocity profile,

$$u_s = 1.54 u_{s,max} \left(\frac{y}{\delta} \right)^{\frac{1}{7}} \left(1 - \frac{y}{\delta} \right), \quad (41)$$

have derived the following expression relating the displacement thickness, δ^* , to the commonly used free convection Moduli:

$$\frac{\delta^*}{x} = 2.04 (Gr \cdot Pr)^{-0.167} Pr^{-0.35} \quad (42)$$

The displacement thickness, δ^* , is the thickness the boundary layer would have if the velocity within it were constant and equal to the maximum velocity, $u_{s,max}$, and the volume flow were equal to its true value.

$$\delta^* = \int_0^{\delta} \frac{u_s}{u_{s,max}} dy \quad (43)$$

$$\delta^* = 0.628 \delta \quad (44)$$

Therefore, δ^* corresponds to the shell thickness discussed previously, since they are both based on equal volumetric flow.

The authors cited give the following expression for the maximum Reynolds number, based on x :

$$Re_{x,max} = \frac{u_{s,max} \cdot x}{\nu_f} = 0.377 (Gr \cdot Pr)^{0.500-0.65} Pr \quad (45)$$

Therefore, on the basis of observed temperature differences between wall and fluid, and the known properties of liquid nitrogen, a shell thickness and velocity may be computed. The results of this calculation are shown in Table VII.

It is of interest to compare the ratio of core area to shell area (as computed from boundary layer displacement thickness) to the ratio of shell velocity ($u_{s,max}$) to core velocity as computed from temperature data as previously outlined. These ratios should at least have

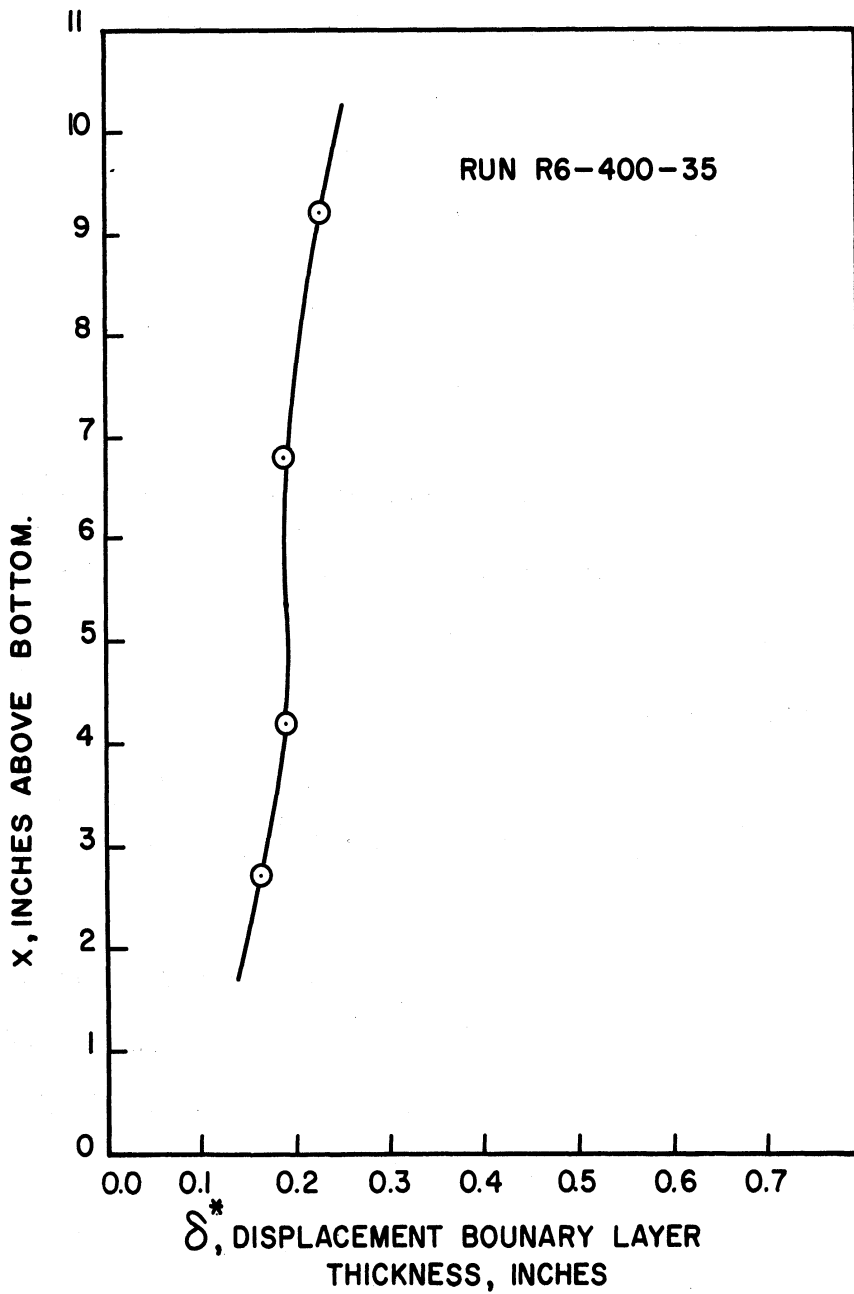


Figure 74. Longitudinal Location vs. Displacement Boundary Layer Thickness, Run R6-400-35.

the same order of magnitude. It should be noted however, that small errors in δ^* , will result in large disparities in the ratios. The comparison of the two ratios is given in Table VII and shows reasonably good agreement.

H. Time for First Net Boiloff

Figures 46, 47 and 48 show that the time for first net boiloff decreases as the final pressure is reduced, which is the expected result since for the lower pressure, there is a correspondingly lower saturation temperature. However, the curves show that as the flux is increased, the times for first net boiloff begin to approach one another. This is reasonable since for infinite flux, we would expect the time to be zero regardless of the value of the final pressure, except if it too is infinite. For runs in which the regulator opened prematurely due to a surge in the inlet gas pressure, the values of τ_0 have been disregarded.

Figure 49, the plot of heat flux versus the dimensionless first boiloff time on semi-logarithmic coordinates, shows that as the flux decreases toward zero the time for first net boiloff and the time for the liquid to reach the saturation temperature (assuming no boiling to occur) approach one another. The higher the heat flux, the faster does the wall achieve a temperature capable of initiating bubble formation, as shown by the curves in Figure 52. As the flux is diminished however, a point is reached where the wall takes as long to reach this value as the liquid takes to go to saturation. In addition, for the low heat flux runs, there is more time for the lower temperature portions of the liquid to mix with the warmer parts thus tending to reduce the time of first boiling. Thus at extremely low flux runs the liquid temperature will be relatively

uniform, and the time for first net boiloff will more approximately equal the time for the liquid to reach the saturation temperature. Because, as is shown in Figure 52, the time for the wall to reach a particular value of temperature is not linear with heat flux, but instead shows an exponential behavior, the curves of heat flux versus time for first boiloff shown in Figure 48 would not be expected to be linear. Of course other phases of the phenomenon include condensation rates of the gaseous pressurizing nitrogen so that the total process is more complicated than can be explained merely on the basis of wall temperature.

I. Dimensionless Temperature vs. Dimensionless Time

According to the convection patterns shown in Figure 67 and the associated discussion, the test results should show the liquid at the 10 inch level going to saturation before that at the 6 inch level, and that at the 6 inch level going to saturation before the liquid 2 inches above the bottom. Figures 11, etc. show that this actually does occur. Furthermore, the bottommost liquid thermocouple should begin to indicate a temperature rise later than the thermocouple above it, and so on. This too is borne out by the experimental data. The dimensionless curves for the liquid transients shown in Figure 38 indicate the same phenomena in more generalized terms. There is considerable scatter apparent in Figure 35. It was found that this could not be reduced by isolating the effects of heat flux or pressure. Since the curves shown in Figures 36 and 37 show considerably less scatter, an effect due to distance above the bottom was sought. The product, Gr. Pr., of 10^9 is generally used as an approximate line of demarcation between the regimes of turbulent and

laminar convection, numbers above 10^9 corresponding to turbulence. Table VII shows a typical variation of Grashof-Prandtl product with elevation. It is noted that in the region of $x = 2$ in. the transition from laminar to turbulent convection is taking place. Thus, the scatter shown in Figure 35 is probably due to flow instability associated with this transition.

J. Summary

It has been shown that upon pressurization of the boiling liquid, boiling ceases and the wall and liquid undergo transients in temperature which depend upon the longitudinal location in question, the heat flux, and the level of pressurization.

The wall and bulk liquid transients may be estimated from an analysis which assumes that the step pressurization results in a step change in the heat transfer coefficient. The range of application of these results extends to the time bubbles begin to form.

The actual variation in the heat transfer coefficient, up until the time of first bubble formation, was shown to be influenced by the viscous deceleration of the initial turbulence due to boiling, and the free convection effects due to the wall-liquid temperature difference.

Assuming that no energy or mass interchange occurs between the upward moving shell at the cylinder wall, and the downward moving core, core velocities were calculated. These further substantiated the viscous deceleration approach, and supported the anticipated velocity patterns in the test cylinder.

CHAPTER V

RECOMMENDATIONS FOR FURTHER WORK AND CONCLUDING REMARKS

Regarding the work herein described, there are many areas for extension, analysis, and refinement. The following are suggestions for additional research connected with the rapid pressurization of boiling systems:

- (1) It would be extremely useful, in order to provide some insight into the complicated convection patterns in the test cylinder throughout the experiment, to measure velocities at many locations.
- (2) A more complete picture of the thermal response of the liquid and wall could be gained by a more extensive thermocouple coverage. For example, thermocouples might be located at the cylinder bottom, corner, very close to the wall, and at the liquid-vapor interface.
- (3) An improved indication of the wall and liquid transients would be gained through the use of continuous rather than point temperature measuring and recording equipment. This is especially important at high heat fluxes where the transients are rapid.
- (4) The study should be extended to peak heat flux and beyond.
- (5) The range of pressures should be expanded.
- (6) Different fluids might be investigated, especially non-cryogenic liquids.
- (7) The effect of cylinder geometry needs study.
- (8) Pressurization by a non-condensable gas is of interest.

The research described concerns only one small phase of the problem of transient free convection and boiling. Vast areas of investigation exist in this virtually unexplored field. It would be advantageous in future work perhaps to isolate the single phase convection phenomenon both in experiment and analysis in order to provide a less complex starting point. For example, the heating of a non-boiling fluid contained in a closed ended cylinder subjected to constant wall heat flux or constant temperature, with no heat rejection provides an important study subject. Similarly, the horizontal or vertical plate and cylinder subjected to transient wall temperature represent an interesting area of study insofar as they produce convection transients in the fluid being heated.

APPENDIX

PART I

TABLE I

Pages 116 through 127

TEMPERATURE VS. TIME

Time, Sec.	Temp. above T_1 sat.	Inches from Bottom	Wall (w) or Liquid (l)	$\frac{\tau}{\tau^*}$	$\frac{\theta}{\theta^*}$
<u>Run R 5-300-20</u>					
0	6.6	10	w		
0	7.5	6	w		
0	9.2	2	w		
12	0.5	10	l	.09	.04
16	1.2	6	l	.12	.09
20	0.25	2	l	.16	.02
30	21.0	10	w		
35	22.2	6	w		
39	23.2	2	w		
52	11.8	10	l	.40	.85
56	5.6	6	l	.43	.40
60	2.2	2	l	.46	.16
70	21.5	10	w		
75	21.4	6	w		
79	24.0	2	w		
92	13.5	10	l	.71	.97
96	12.7	6	l	.74	.91
100	4.7	2	l	.77	.34
110	20.6	10	w		
115	21.5	6	w		
119	24.9	2	w		
132	14.0	10	l	1.02	1.00
136	13.6	6	l	1.05	.97
140	13.4	2	l	1.08	.96
150	20.6	10	w		
155	21.5	6	w		
159	22.9	2	w		

Temperatures repeat at later times

TEMPERATURE VS. TIME

Time, Sec.	Temp. above T_1 sat.	Inches from Bottom	Wall (w) or Liquid (l)	$\frac{\tau}{\tau^*}$	$\frac{\theta}{\theta^*}$
<u>Run R 5-700-20</u>					
0	8.8	10	w		
0	10.8	6	w		
0	13.8	2	w		
2	0.4	6	l	.03	.03
6	0.0	2	l	.09	.00
16	19.8	10	w		
22	22.9	6	w		
26	24.9	2	w		
38	11.2	10	l	.58	.93
42	9.0	6	l	.64	.75
46	2.0	2	l	.70	.17
56	20.8	10	w		
62	21.7	6	w		
66	23.5	2	w		
78	12.0	10	l	1.20	1.00
82	12.0	6	l	1.26	1.00
86	12.0	2	l	1.32	1.00

Temperatures repeat at later times

TEMPERATURE VS. TIME

Time, Sec.	Temp. above T_1 sat.	Inches from Bottom	Wall (w) or Liquid (l)	$\frac{\tau}{\tau^*}$	$\frac{\theta}{\theta^*}$
<u>Run R 6-400-35</u>					
0	6.4	10	w		
0	7.6	6	w		
0	11.8	2	w		
2	0.5	6	l	.01	.02
7	0.0	2	l	.03	.00
17	23.5	10	w		
23	23.5	6	w		
27	25.0	2	w		
38	9.8	10	l	.18	.45
42	5.5	6	l	.20	.25
46	1.8	2	l	.22	.08
57	28.8	10	w		
63	28.4	6	w		
67	26.2	2	w		
78	15.6	10	l	.37	.71
82	10.5	6	l	.39	.48
86	4.6	2	l	.40	.21
97	28.8	10	w		
103	29.2	6	w		
107	28.6	2	w		
118	20.8	10	l	.55	.95
122	17.9	6	l	.57	.81
126	8.7	2	l	.59	.40
137	27.5	10	w		
143	28.1	6	w		
147	30.8	2	w		
158	21.2	10	l	.74	.97
162	20.5	6	l	.76	.93
166	16.5	2	l	.78	.75
177	27.5	10	w		
183	28.2	6	w		
187	32.0	2	w		
198	22.0	10	l	.93	1.00
202	22.0	6	l	.95	1.00
206	22.0	2	l	.97	1.00
217	27.5	10	w		
223	28.2	6	w		
227	30.1	2	w		

Temperatures repeat at later times

TEMPERATURE VS. TIME

Time, Sec.	Temp. above T_1 sat.	Inches from Bottom	Wall (w) or Liquid (l)	$\frac{\tau}{\tau^*}$	$\frac{\theta}{\theta^*}$
<u>Run R 6-500-35</u>					
0	13.0	2	w		
0	9.2	6	w		
0	7.3	10	w		
2	8.4	10	w		
7	12.6	6	w		
11	19.9	2	w		
23	9.2	10	l	.12	.42
27	4.2	6	l	.14	.19
31	1.1	2	l	.16	.05
42	29.4	10	w		
47	30.0	6	w		
51	29.0	2	w		
63	16.4	10	l	.33	.75
67	10.2	6	l	.35	.46
71	4.4	2	l	.38	.20
82	27.5	10	w		
87	29.0	6	w		
91	30.3	2	w		
103	19.9	10	l	.55	.91
107	19.7	6	l	.57	.89
111	8.4	2	l	.59	.38
122	27.9	10	w		
127	29.2	6	w		
131	34.0	2	w		
143	22.0	10	l	.76	1.00
147	21.2	6	l	.78	.97
151	19.1	2	l	.80	.87
162	28.0	10	w		
167	29.2	6	w		
171	31.2	2	w		
183	22.0	10	l	.97	1.00
187	22.0	6	l	.99	1.00
191	22.0	2	l	1.01	1.00

Temperatures repeat at later times

TEMPERATURE VS. TIME

Time, Sec.	Temp. above T_1 sat.	Inches from Bottom	Wall (w) or Liquid (l)	$\frac{\tau}{\tau^*}$	$\frac{\theta}{\theta^*}$
<u>Run R 6-600-35</u>					
0	7.6	10	w		
0	9.4	6	w		
0	13.0	2	w		
32	27.9	10	w		
37	28.9	6	w		
41	30.5	2	w		
54	14.2	10	l	.41	.69
58	8.4	6	l	.44	.41
62	2.7	2	l	.47	.13
72	26.2	10	w		
77	27.0	6	w		
81	30.8	2	w		
94	18.4	10	l	.72	.90
98	18.0	6	l	.75	.88
102	7.8	2	l	.78	.38
112	27.7	10	w		
117	28.2	6	w		
121	31.2	2	w		
134	20.6	10	l	1.02	1.00
138	20.4	6	l	1.05	.99
142	19.1	2	l	1.08	.93
152	27.6	10	w		
157	28.2	6	w		
161	30.0	2	w		
174	20.6	10	l	1.33	1.00
178	20.6	6	l	1.36	1.00
182	20.6	2	l	1.39	1.00
192	27.6	10	w		
197	28.2	6	w		
201	30.0	2	w		

Temperatures repeat at later times

TEMPERATURE VS. TIME

Time, Sec.	Temp. above T_1 sat.	Inches from Bottom	Wall (w) or Liquid (l)	$\frac{\tau}{\tau^*}$	$\frac{\theta}{\theta^*}$
<u>Run R 7-300-3 5</u>					
0	6.3	10	w		
0	6.4	6	w		
0	8.3	2	w		
1	6.9	6	w		
5	12.3	2	w		
17	7.9	10	l	.07	.37
21	2.7	6	l	.09	.13
25	0.8	2	l	.11	.04
36	26.2	10	w		
41	22.0	6	w		
45	22.8	2	w		
57	12.2	10	l	.24	.57
62	7.3	6	l	.26	.34
65	2.2	2	l	.27	.10
76	29.6	10	w		
81	26.0	6	w		
85	24.6	2	w		
97	16.4	10	l	.41	.76
101	10.7	6	l	.43	.50
105	5.6	2	l	.44	.26
116	28.0	10	w		
121	29.0	6	w		
125	27.0	2	w		
137	21.0	10	l	.58	.98
141	14.8	6	l	.59	.69
145	9.0	2	l	.61	.42
156	27.5	10	w		
161	29.0	6	w		
165	29.4	2	w		
177	21.5	10	l	.74	1.00
181	21.0	6	l	.76	.98
185	12.2	2	l	.78	.57
196	27.2	10	w		
201	27.8	6	w		
205	32.2	2	w		
217	21.5	10	l	.91	1.00
221	21.5	6	l	.93	1.00
225	20.0	2	l	.94	.93

TEMPERATURE VS. TIME

Time, Sec.	Temp. above T_1 sat.	Inches from Bottom	Wall (w) or Liquid (l)	$\frac{\tau}{\tau^*}$	$\frac{\theta}{\theta^*}$
<u>Run R 7-300-3 5 Cont'd</u>					
236	27.2	10	w		
241	27.8	6	w		
245	30.4	2	w		
257	21.5	10	l	1.07	1.00
261	21.5	6	l	1.09	1.00
265	21.5	2	l	1.11	1.00
276	27.2	10	w		
281	27.8	6	w		
285	29.5	2	w		

Temperatures repeat at later times

TEMPERATURE VS. TIME

Time, Sec.	Temp. above T_1 sat.	Inches from Bottom	Wall (w) or Liquid (l)	$\frac{r}{r^*}$	$\frac{\theta}{\theta^*}$
<u>Run R 7-500-35</u>					
0	7.8	10	w		
0	9.0	6	w		
0	12.0	2	w		
11	19.7	10	w		
16	23.2	6	w		
20	26.6	2	w		
32	11.2	10	l	.16	.52
36	5.4	6	l	.18	.25
40	1.2	2	l	.20	.06
51	28.8	10	w		
56	30.0	6	w		
60	28.8	2	w		
72	19.6	10	l	.36	.91
76	12.1	6	l	.38	.56
80	5.6	2	l	.40	.26
91	26.8	10	w		
96	28.9	6	w		
100	30.5	2	w		
112	20.5	10	l	.56	.95
116	20.2	6	l	.58	.94
120	10.2	2	l	.60	.48
131	28.2	10	w		
136	28.8	6	w		
140	33.2	2	w		
152	21.5	10	l	.76	1.00
156	21.0	6	l	.78	.98
160	20.8	2	l	.80	.97
171	28.2	10	w		
176	28.8	6	w		
180	30.2	2	w		
192	21.5	10	l	.96	1.00
196	21.5	6	l	.98	1.00
200	21.5	2	l	1.00	1.00

Temperatures repeat at later times

TEMPERATURE VS. TIME

Time, Sec.	Temp. above T_1 sat.	Inches from Bottom	Wall (w) or Liquid (l)	$\frac{\tau}{\tau^*}$	$\frac{\theta}{\theta^*}$
<u>Run R 7-700-35</u>					
0	8.2	10	w		
0	9.4	6	w		
0	12.6	2	w		
10	30.0	10	w		
15	30.0	6	w		
19	32.0	2	w		
31	18.9	10	l	.21	.90
35	10.0	6	l	.23	.48
39	3.4	2	l	.26	.16
50	29.0	10	w		
55	30.3	6	w		
59	33.5	2	w		
71	20.8	10	l	.47	.99
75	19.6	6	l	.50	.94
79	13.6	2	l	.53	.65
90	29.0	10	w		
95	29.2	6	w		
99	32.5	2	w		
111	21.0	10	l	.74	1.00
115	21.0	6	l	.77	1.00
119	21.0	2	l	.80	1.00
130	29.0	10	w		
135	29.2	6	w		
139	30.8	2	w		
151	21.0	10	l		
155	21.0	6	l		
159	21.0	2	l		
170	29.0	10	w		
175	29.2	6	w		
179	30.8	2	w		

Temperatures repeat at later times

TEMPERATURE VS. TIME

Time, Sec.	Temp. above T ₁ sat.	Inches from Bottom	Wall (w) or Liquid (l)	$\frac{\tau}{\tau^*}$	$\frac{\theta}{\theta^*}$
<u>Run R 8-300-20</u>					
0	5.6	10	w		
0	6.3	6	w		
0	12.1	2	w		
5	1.1	10	l	.03	.08
9	0.5	6	l	.05	.04
13	0.5	2	l	.08	.04
24	20.6	10	w		
29	19.3	6	w		
33	20.0	2	w		
45	7.8	10	l	.27	.54
49	5.5	6	l	.29	.38
53	2.2	2	l	.31	.15
64	22.0	10	w		
69	22.6	6	w		
73	21.5	2	w		
85	13.6	10	l	.50	.95
89	9.0	6	l	.53	.63
93	4.8	2	l	.55	.33
104	20.2	10	w		
109	23.0	6	w		
113	23.3	2	w		
125	14.4	10	l	.74	1.00
129	13.1	6	l	.77	.91
133	10.8	2	l	.79	.75
144	20.6	10	w		
149	20.9	6	w		
153	25.6	2	w		
165	14.4	10	l	.98	1.00
169	14.4	6	l	1.00	1.00
173	14.4	2	l	1.02	1.00
184	20.6	10	w		
189	20.9	6	w		
193	25.6	2	w		

Temperatures repeat at later times

TEMPERATURE VS. TIME

Time, Sec.	Temp. above T_1 sat.	Inches from Bottom	Wall (w) or Liquid (l)	$\frac{\tau}{\tau^*}$	$\frac{\theta}{\theta^*}$
<u>Run R 8-500-20</u>					
0	8.3	10	w		
0	8.5	6	w		
0	12.0	2	w		
3	0.3	6	l	.02	.02
7	0.0	2	l	.05	.00
17	20.9	10	w		
22	23.6	6	w		
26	25.0	2	w		
38	11.8	10	l	.30	.82
42	6.2	6	l	.32	.43
46	1.6	2	l	.35	.11
57	24.8	10	w		
62	23.0	6	w		
66	26.6	2	w		
78	13.6	10	l	.60	.94
82	13.1	6	l	.63	.91
86	12.3	2	l	.66	.85
97	22.5	10	w		
102	22.0	6	w		
106	26.0	2	w		
118	14.5	10	l	.91	1.00
122	14.5	6	l	.94	1.00
126	14.5	2	l	.97	1.00
137	22.5	10	w		
142	22.0	6	w		
146	26.1	2	w		
158	14.5	10	l		
162	14.5	6	l		
166	14.5	2	l		
177	22.5	10	w		
182	21.5	6	w		
186	24.0	2	w		

Temperatures repeat at later times

TEMPERATURE VS. TIME

Time, Sec.	Temp. above T_1 sat.	Inches from Bottom	Wall (w) or Liquid (l)	$\frac{\tau}{\tau^*}$	$\frac{\theta}{\theta^*}$
<u>Run R 8-600-20</u>					
0	7.8	10	w		
0	7.4	6	w		
0	12.5	2	w		
5	0.5	10	l	.06	.04
9	0.25	6	l	.11	.02
13	0.00	2	l	.16	.00
23	22.2	10	w		
28	24.0	6	w		
32	26.3	2	w		
46	11.2	10	l	.56	.89
49	10.7	6	l	.61	.85
53	2.2	2	l	.67	.18
63	21.0	10	w		
68	21.4	6	w		
72	25.0	2	w		
85	12.6	10	l	1.07	1.00
89	12.6	6	l	1.12	1.00
93	12.6	2	l	1.17	1.00
103	21.0	10	w		
108	21.0	6	w		
112	23.5	2	w		

Temperatures repeat at later times

<u>Run R 8-700-20</u>					
0	7.8	10	w		
0	9.2	6	w		
0	13.0	2	w		
1	8.6	10	w		
6	16.3	6	w		
10	22.2	2	w		
22	7.2	10	l	.30	.58
26	5.8	6	l	.35	.46
30	1.2	2	l	.41	.10
41	22.0	10	w		
46	22.3	6	w		
50	26.0	2	w		
62	12.5	10	l	.85	1.00
66	12.5	6	l	.90	1.00
70	12.5	2	l	.96	1.00
81	21.4	10	w		
86	20.5	6	w		
90	22.8	2	w		

Temperatures repeat at later times

TABLE II

Pages 129 through 137

HEAT TRANSFER COEFFICIENT VS. TIME

Time, Sec.	Temperature above T_1 sat. ($^{\circ}\text{F}$)			Heat transfer coefficient		
	2"	6"	10"	2"	6"	10"
<u>Run R 5-300-20, $q/A = 1860$ h, BTU/hr. ft² $^{\circ}\text{F}$</u>						
0	9.2	7.5	6.6	202	248	282
10	16.6	14.8	13.4	112	126	139
20	20.0	18.2	16.0	93.0	102	116
30	21.6	19.6	16.0	86.0	105	116
40	22.3	19.1	11.8	83.5	97.5	158
50	22.3	18.4	10.2	83.5	101	183
60	22.0	17.0	10.0	84.5	110	186
70	21.7	15.0	9.0	85.5	124	206
80	21.4	12.3	8.0	87.0	151	232
90	20.8	10.0	7.6	89.5	186	244
100	20.0	8.8	6.8	93.0	212	274
110	18.8	8.0	6.6	99.0	233	282
120	17.0	7.6	6.6	109.5	244	282
130	13.4	7.5	6.6	139	248	282
140	11.2	7.5	6.6	166	248	282
150	10.0	7.5	6.6	186	248	282
160	9.0	7.5	6.6	207	248	282
170	8.9	7.5	6.6	209	248	282

Temperatures repeat at later times.

<u>Run R 5-700-20, $q/A = 3180$ h, BTU/hr. ft² $^{\circ}\text{F}$</u>						
0	13.8	10.8	8.8	230	294	362
10	23.0	20.6	19.0	138	154	167
20	25.5	21.0	14.0	125	151	228
30	24.4	17.6	11.0	130	181	289
40	23.4	14.0	9.4	136	227	339
50	21.2	12.5	8.8	150	254	362
60	17.6	11.6	8.8	181	274	362
70	14.0	10.6	8.8	227	300	362
80	12.1	9.7	8.8	263	328	362
90	11.5	9.7	8.8	276	328	362

Temperatures repeat at later times.

HEAT TRANSFER COEFFICIENT VS. TIME

Time, Sec.	Temperature above T_1 sat. ($^{\circ}\text{F}$)			Heat transfer coefficient		
	2"	6"	10"	2"	6"	10"
Run R 6-400-35, $q/A = 1780$ h, BTU/hr. ft ² $^{\circ}\text{F}$						
0	11.8	7.6	6.4	151	234	278
10	19.3	16.8	15.2	92.3	106	117
20	22.8	20.0	19.2	78.0	89.0	93.0
30	24.4	21.8	19.0	73.0	81.5	93.6
40	24.4	22.2	18.0	73.0	80.0	99.0
50	24.4	22.2	17.2	73.0	80.0	103
60	23.8	21.2	15.8	74.9	80.5	112
70	23.2	20.0	14.4	76.6	89.0	123
80	22.6	19.0	13.0	78.9	93.6	137
90	22.2	17.6	11.4	80.1	101	156
100	22.0	15.4	9.8	81.0	115	182
110	22.0	13.2	8.6	81.0	135	207
120	21.6	11.2	7.4	82.4	159	241
130	21.2	10.0	6.8	84.0	178	262
140	20.0	8.8	6.4	89.0	202	278
150	18.0	8.2	6.2	99.0	217	288
160	16.2	7.8	6.0	110	228	296
170	14.4	7.4	5.7	124	241	312
180	13.0	6.8	5.5	137	262	324
190	12.0	6.4	5.5	148	278	324
200	10.6	6.2	5.5	168	287	324
210	9.0	6.2	5.5	198	287	324
220	8.5	6.2	5.5	210	287	324
230	8.1	6.2	5.5	220	287	324

Temperatures repeat at later times.

HEAT TRANSFER COEFFICIENT VS. TIME

Time, Sec.	Temperature above T ₁ sat. (°F)			Heat transfer coefficient		
	2"	6"	10"	2"	6"	10"
<u>Run R 6-500-35, q/A = 2040 h, BTU/hr. ft² °F</u>						
0	13.0	9.2	7.3	157	222	279
10	19.6	14.0	11.4	96.0	146	179
20	22.6	19.6	13.2	90.0	104	154
30	25.4	20.8	15.0	80.5	98.0	136
40	26.6	22.6	15.6	76.6	90.5	131
50	27.2	23.0	14.8	75.0	88.5	138
60	26.4	21.8	13.0	77.4	93.5	157
70	25.8	19.6	11.0	79.0	104	185
80	25.0	16.8	9.6	81.5	121	212
90	24.2	13.8	8.8	84.1	148	232
100	23.6	10.6	8.0	86.5	192	255
110	23.8	9.4	7.4	85.6	217	276
120	23.0	9.0	6.7	88.6	226	305
130	20.2	8.4	6.3	101	243	324
140	17.0	8.2	6.0	120	248	340
150	14.2	7.8	6.0	144	262	340
160	11.5	7.4	6.0	177	276	340
170	10.0	7.2	6.0	204	283	340
180	9.4	7.2	6.0	217	283	340
190	9.2	7.2	6.0	222	283	340

Temperatures repeat at later times.

HEAT TRANSFER COEFFICIENT VS. TIME

Time, Sec.	Temperature above T_1 sat. ($^{\circ}\text{F}$)			Heat transfer coefficient		
	2"	6"	10"	2"	6"	10"
<u>Run R 6-600-35, $q/A = 2700$ h, BTU/hr. ft^2 $^{\circ}\text{F}$</u>						
0	13.0	9.4	7.6	208	284	356
10	19.8	21.2	20.6	136	127	131
20	24.8	24.8	22.4	109	109	120
30	27.4	25.2	20.0	98.5	107	135
40	29.0	23.8	16.6	93.0	103	163
50	29.0	21.2	13.8	93.0	127	195
60	28.4	18.6	11.4	95.0	145	235
70	27.6	16.0	9.6	98.0	168	282
80	26.2	13.6	8.8	103	198	307
90	25.0	11.6	8.0	108	232	338
100	23.6	9.0	8.0	114	300	338
110	21.6	8.6	7.6	125	314	356
120	17.4	7.6	7.1	155	356	380
130	13.8	7.6	7.1	196	356	380
140	12.6	7.6	7.1	214	356	380
150	10.7	7.6	7.1	252	356	380
160	10.0	7.6	7.1	270	356	380
170	9.6	7.6	7.1	281	356	380
180	9.4	7.6	7.1	287	356	380

Temperatures repeat at later times.

HEAT TRANSFER COEFFICIENT VS. TIME

Time, Sec.	Temperature above T_1 sat. ($^{\circ}$ F)			Heat transfer coefficient		
	2"	6"	10"	2"	6"	10"
<u>Run R 7-300-35, $q/A = 1555$ h, BTU/hr. ft² $^{\circ}$F</u>						
0	8.3	6.4	6.3	187	243	246
10	13.6	12.6	9.0	114	123	173
20	17.0	13.6	12.0	91.5	114	130
30	19.2	19.2	15.6	81.0	99.5	105
40	20.7	17.0	16.4	75.0	91.5	94.8
50	21.6	18.2	16.6	72.0	85.5	93.6
60	22.1	18.4	16.7	70.3	84.5	93.0
70	22.2	18.0	16.0	70.0	86.5	97.0
80	22.0	17.6	14.8	70.6	88.2	105
90	21.4	17.4	13.2	72.5	89.3	118
100	21.0	17.0	11.8	74.0	91.4	132
110	20.4	16.8	10.0	76.0	92.5	155
120	19.8	16.3	8.6	78.5	95.5	181
130	19.6	15.7	7.4	79.5	99.0	210
140	19.2	14.6	6.2	81.0	106	250
150	18.8	12.8	6.0	82.5	121	259
160	18.8	10.8	5.7	82.5	144	272
170	19.2	9.0	5.7	81.0	173	272
180	19.2	7.7	5.7	81.0	202	272
190	19.0	7.2	5.7	82.0	216	272
200	17.8	6.6	5.7	87.5	235	272
210	15.4	6.3	5.7	101	246	272
220	13.0	6.3	5.7	119	246	272
230	12.5	6.3	5.7	124	246	272
240	10.0	6.3	5.7	155	246	272
250	9.0	6.3	5.7	173	246	272
260	8.4	6.3	5.7	185	246	272
270	8.2	6.3	5.7	190	246	272
280	8.0	6.3	5.7	195	246	272

Temperatures repeat at later times.

HEAT TRANSFER COEFFICIENT VS. TIME

Time, Sec.	Temperature above T_1 sat. ($^{\circ}\text{F}$)			Heat transfer coefficient		
	2"	6"	10"	2"	6"	10"
<u>Run R 7-500-35, $q/A = 1860$ h, BTU/hr. ft² $^{\circ}\text{F}$</u>						
0	12.0	9.0	7.8	155	206	238
10	22.0	18.0	15.4	84.5	103	121
20	25.8	21.2	15.8	72.1	87.5	118
30	26.6	22.0	15.2	70.0	84.5	122
40	26.6	22.4	14.6	70.0	83.0	127
50	26.3	21.8	13.5	70.6	85.4	138
60	25.4	20.8	12.2	73.1	89.4	153
70	24.4	19.0	9.8	76.1	98.0	190
80	23.8	16.6	8.0	79.5	112	232
90	23.4	13.8	6.8	79.5	135	274
100	22.8	12.6	6.8	81.5	148	274
110	22.4	9.6	6.8	83.5	194	274
120	21.4	8.4	6.7	87.0	222	278
130	19.6	8.0	6.7	94.7	232	278
140	16.6	7.6	6.7	112	245	278
150	13.6	7.3	6.7	137	255	278
160	11.0	7.3	6.7	169	255	278
170	9.4	7.3	6.7	198	255	278
180	9.0	7.3	6.7	207	255	278
190	8.7	7.3	6.7	214	255	278

Temperatures repeat at later times.

<u>Run R 7-700-35, $q/A = 2450$ h, BTU/hr. ft² $^{\circ}\text{F}$</u>						
0	12.6	9.4	8.2	194	261	299
10	28.4	27.2	23.0	86.2	90	107
20	31.2	25.6	15.4	78.5	95.7	159
30	30.9	22.6	10.8	79.1	108	227
40	29.2	19.2	9.6	84.0	128	256
50	27.4	16.0	9.0	89.5	153	272
60	25.2	13.2	8.4	97.1	186	292
70	22.6	11.0	8.2	108	222	299
80	19.8	9.6	8.0	124	255	306
90	17.0	8.7	8.0	144	282	306
100	14.0	8.2	8.0	175	299	306
110	12.6	8.2	8.0	194	299	306
120	10.3	8.2	8.0	238	299	306
130	9.8	8.2	8.0	250	299	306

Temperatures repeat at later times.

HEAT TRANSFER COEFFICIENT VS. TIME

Time Sec.	Temperature above T_1 sat. ($^{\circ}$ F)			Heat transfer coefficient		
	2"	6"	10"	2"	6"	10"
Run R 8-300-20, $q/A = 1470$ h, BTU/hr. ft ² $^{\circ}$ F						
0	12.1	6.3	5.6	121	234	262
10	15.2	12.8	16.0	96.5	115	92.0
20	17.4	15.8	17.2	84.5	93.0	86.0
30	18.6	17.4	16.6	79.0	84.5	88.5
40	19.0	17.0	15.0	77.5	86.5	98.0
50	18.8	16.2	13.6	78.0	91.0	108
60	18.6	15.6	11.6	79.0	94.0	127
70	18.4	14.8	9.7	80.0	99.0	152
80	18.0	14.7	8.2	81.5	100	179
90	17.6	14.2	7.2	83.5	103	204
100	17.0	13.2	6.2	86.5	111	237
110	16.0	12.0	5.6	92.0	122	262
120	14.6	10.2	5.4	101.0	144	272
130	13.4	8.8	5.6	110	167	262
140	13.0	7.6	5.8	113	193	254
150	12.2	6.6	6.2	120	223	237
160	11.3	6.5	6.2	130	226	237
170	11.6	6.5	6.2	127	226	237
180	11.6	6.5	6.2	127	226	237
190	11.2	6.5	6.2	131	226	237
200	10.7	6.5	6.2	137	226	237
210	10.4	6.5	6.2	141	226	237
220	10.0	6.5	6.2	147	226	237
230	9.8	6.5	6.2	150	226	237
240	9.4	6.5	6.2	156	226	237

Temperatures repeat at later times.

HEAT TRANSFER COEFFICIENT VS. TIME

Time Sec.	Temperature above T_1 sat. (°F)			Heat transfer coefficient		
	2"	6"	10"	2"	6"	10"
<u>Run R 8-500-20, $q/A = 1925$ h, BTU/hr. ft² °F</u>						
0	12.0	8.5	8.3	161	226	232
10	23.0	20.4	17.0	83.8	94.5	113
20	25.0	21.8	17.0	77.0	88.5	113
30	24.7	20.8	13.4	78.0	92.5	144
40	24.7	17.8	12.0	78.0	108	160
50	24.2	15.2	12.0	79.5	127	160
60	22.6	12.8	12.0	85.0	151	160
70	19.8	11.0	11.3	97.5	175	171
80	15.8	9.6	10.2	122	200	189
90	14.0	8.8	9.0	137	218	214
100	13.0	7.8	8.0	148	247	241
110	12.0	7.0	8.0	161	273	241
120	11.4	7.0	8.0	169	273	241
130	11.4	7.0	8.0	169	273	241
140	11.4	7.0	8.0	169	273	241
150	11.4	7.0	8.0	169	273	241
160	10.8	7.0	8.0	178	273	241
170	10.0	7.0	8.0	193	273	241
180	9.6	7.0	8.0	201	273	241
190	9.5	7.0	8.0	202	273	241

Temperatures repeat at later times.

HEAT TRANSFER COEFFICIENT VS. TIME

Time, Sec.	Temperature above T_1 sat. ($^{\circ}\text{F}$)			Heat transfer coefficient		
	2"	6"	10"	2"	6"	10"
<u>Run R 8-600-20, $q/A = 2790$ h, BTU/hr. ft² $^{\circ}\text{F}$</u>						
0	12.5	7.4	7.8	223	378	358
10	22.0	17.4	14.0	127	160	199
20	26.4	21.8	17.0	106	128	164
30	26.0	20.0	13.2	107	140	211
40	24.9	14.6	10.8	112	191	258
50	24.0	12.0	9.8	116	232	285
60	22.2	10.8	9.0	126	258	310
70	19.6	9.6	8.4	142	290	332
80	12.0	8.8	8.4	232	317	332
90	11.8	8.5	8.4	242	332	332
100	11.5	8.4	8.4	249	332	332
110	11.2	8.4	8.4	249	332	332
120	11.0	8.4	8.4	254	332	332

Temperatures repeat at later times.

<u>Run R 8-700-20, $q/A = 2990$ h, BTU/hr/ft² $^{\circ}\text{F}$</u>						
0	13.0	9.2	7.8	230	325	383
10	22.0	17.6	14.0	136	170	214
20	23.6	17.8	17.6	132	168	170
30	24.0	15.8	13.4	125	189	222
40	22.4	13.0	10.6	133	230	282
50	18.8	12.2	9.6	159	245	312
60	14.6	10.0	9.4	204	299	318
70	12.0	9.4	8.9	249	318	336
80	11.0	8.6	8.9	272	348	336
90	10.3	8.0	8.9	290	374	336

Temperatures repeat at later times.

TABLE III

DATA USED FOR CALCULATING τ^* AND TABULATED VALUES OF τ^*

Run No.	$T_{2\text{sat}} - T_{1\text{sat}}$ °F	w_L , lb _m	$\frac{q}{A}$, $\frac{\text{BTU}}{\text{hr. ft}^2}$	q , $\frac{\text{BTU}}{\text{hr.}}$	τ^* , Hr.	τ^* , Sec.
R2-300-35	22.0	25.5	1252	3520	.0814	293
R2-500-35	21.0	25.6	1830	5120	.0533	192
R2-700-35	20.0	24.8	3060	8350	.0304	110
R5-300-20	14.0	26.2	1860	5210	.0359	129
R5-700-20	12.0	25.9	3180	8760	.0181	65
R6-400-35	22.0	27.7	1780	5250	.0593	214
R6-500-35	22.0	26.7	2040	5720	.0525	189
R6-600-35	21.6	26.7	2700	7420	.0396	143
R7-300-35	21.5	26.3	1555	4360	.0664	239
R7-500-35	21.5	26.2	1860	5130	.0556	200
R7-700-35	21.0	26.0	2450	6680	.0416	150
R8-300-20	14.4	25.8	1470	4050	.0470	169
R8-500-20	14.5	28.7	1925	5660	.0336	121
R8-600-20	12.6	26.6	2790	7720	.0219	79
R8-700-20	12.5	25.4	2990	8050	.0202	73
R9-800-35	21.5	25.4	2830	7940	.0350	126
R9-900-35	21.0	26.4	3830	11,150	.0252	91
R9-1000-35	21.5	25.5	4260	12,000	.0232	84
R10-800-20	12.7	26.3	3280	9400	.0182	66
R10-900-20	12.0	23.6	3600	9300	.0155	56
R10-1000-20	11.5	23.1	4200	10,700	.0127	46

TABLE IV

TABULATED VALUES OF τ_b AND τ_b/τ^*

Run No.	$\frac{q}{A}, \frac{\text{BTU}}{\text{hr. ft}^2}$	$\tau_b, \text{Sec.}$	τ_b/τ^*
R2-300-35	1252	212	.73
R2-700-35	3060	40	.36
R5-300-20	1860	72	.56
R6-500-35	2040	128	.69
R6-600-35	2700	84	.59
R7-300-35	1555	160	.67
R7-500-35	1860	120	.60
R7-700-35	2450	68	.45
R8-300-20	1470	104	.62
R8-500-20	1925	44	.37
R8-600-20	2790	36	.46
R8-700-20	2990	30	.41
R9-800-35	2830	45	.36
R9-900-35	3830	28	.31
R9-1000-35	4260	24	.29
R10-800-20	3280	31	.47
R10-900-20	3600	20	.36
R10-1000-20	4200	16	.35

TABLE V

COMPARISON OF MINIMUM HEAT TRANSFER COEFFICIENTS
WITH VALUES COMPUTED USING CORRELATION FOR
VERTICAL SURFACES IN TURBULENT FLOW

Run No.	$\frac{h_{min.}}{h_{fc}}$		
	X = 2 in.	X = 6 in.	X = 10 in.
R5-300-20	0.55	0.67	0.85
R6-400-35	0.48	0.53	0.62
R6-500-35	0.48	0.58	0.97
R7-300-35	0.47	0.60	0.68
R7-500-35	0.44	0.55	0.88
R8-300-20	0.54	0.61	0.64
Mean	0.49	0.59	0.77

TABLE VI

$\Delta h/\Delta h_0$ FOR LOW HEAT FLUX RUNS

Run No.	$\Delta h/\Delta h_0, X = 2 \text{ in.}$	$\Delta h/\Delta h_0, X = 6 \text{ in.}$	$\Delta h/\Delta h_0, X = 10 \text{ in.}$
<u>$\tau = 2 \text{ Seconds}$</u>			
R7-500-35	0.83	0.77	0.81
R5-300-20	0.79	0.76	0.78
R6-400-35	0.82	0.80	0.79
R8-500-20	0.79	0.80	0.81
R6-500-35	0.73	0.78	0.77
R8-300-20	0.77	0.77	0.80
<u>$\tau = 3 \text{ Seconds}$</u>			
R7-500-35	0.67	0.63	0.67
R5-300-20	0.67	0.65	0.67
R6-400-35	0.73	0.67	0.65
R8-500-20	0.69	0.69	0.69
R6-500-35	0.73	0.78	0.68
R8-300-20	0.66	0.61	0.59
<u>$\tau = 5 \text{ Seconds}$</u>			
R7-500-35	0.50	0.48	0.50
R5-300-20	0.51	0.49	0.45
R6-400-35	0.54	0.50	0.48
R8-500-20	0.50	0.53	0.50
R6-500-35	0.54	0.61	0.53
R8-300-20	0.53	0.47	0.45
<u>$\tau = 10 \text{ Seconds}$</u>			
R7-500-35	0.25	0.21	0.25
R5-300-20	0.28	0.24	0.18
R6-400-35	0.27	0.22	0.20
R8-500-20	0.22	0.26	0.16
R6-500-35	0.27	0.39	0.33
R8-300-20	0.31	0.21	0.18

TABLE VII

TURBULENT BOUNDARY LAYER RESULTS FOR RUN R6-400-35, $\tau = 35$ Sec.

x in.	x ft.	ΔT °F	u_c , in/sec.	u_c , ft/hr.	Gr·Pr	δ^*/x	δ^* , in.	$Re_{x,max}$	$u_{s,max}$, ft/hr.	$\frac{u_{s,max}}{u_c}$	$\frac{Ac}{A\delta^*}$
9.2	.77	7.5	0.15	45	1.3×10^{11}	.025	0.23	10.5×10^4	1040	23.1	8.8
6.8	.57	5.0	0.16	48	3.5×10^{10}	.027	0.19	5.5×10^4	740	15.4	10.9
4.2	.35	2.8	0.13	39	4.0×10^9	.044	0.19	1.8×10^4	390	10.0	10.9
2.7	.23	1.5	0.10	30	0.6×10^9	.061	0.17	0.7×10^4	230	7.7	12.4

APPENDIX

PART II

IDEALIZED WALL AND LIQUID TRANSIENT
ANALYSIS: FLUX INCREASING LINEARLY WITH TIME

If now the heat flux is assumed to increase linearly with time after pressurization:

$$\left(\frac{q}{A}\right) = \left(\frac{q}{A}\right)_0 + \lambda \tau \quad (46)$$

So that the differential equations become:

$$\left(\frac{q}{A}\right)_0 + \lambda \tau = \rho_w \Delta C_{pw} \frac{dt_w}{d\tau} + h_s (t_w - t_L) \quad (47)$$

$$h_s (t_w - t_L) = \rho_L \frac{d}{4} C_{pL} \frac{dt_L}{d\tau} \quad (6a)$$

$$\frac{dt_w}{d\tau} = \frac{\left(\frac{q}{A}\right)_0}{\rho_w \Delta C_{pw}} + \frac{\lambda \tau}{\rho_w \Delta C_{pw}} - \frac{h_s (t_w - t_L)}{\rho_w \Delta C_{pw}} \quad (48)$$

Defining:

$$B_\lambda \equiv \frac{\left(\frac{q}{A}\right)_0}{\rho_w \Delta C_{pw}} \quad (49)$$

$$F \equiv \frac{\lambda}{\rho_w \Delta C_{pw}} \quad (50)$$

$$\frac{dt_w}{d\tau} = B_\lambda + F\tau - D(t_w - t_L) \quad (51)$$

As in the constant flux case:

$$\frac{dt_L}{d\tau} = E(t_w - t_L) \quad (6c)$$

Defining:

$$G \equiv EB_\lambda + F \quad (52)$$

We obtain:

$$\frac{d^2 t_w}{d\tau^2} + \alpha \frac{dt_w}{d\tau} - \lambda \tau = G \quad (53)$$

Applying boundary conditions as before, the solution of Equation

(53) is as follows:

$$\begin{aligned} t_w - t_{w0} = \Theta_w = & \frac{B_\lambda}{\alpha} - \frac{D}{\alpha} \Delta T_0 + \frac{\lambda}{\alpha^3} \\ & - \frac{G}{\alpha^2} + \left(\frac{G}{\alpha} - \frac{\lambda}{\alpha^2} \right) \tau + \left(\frac{\lambda}{2\alpha} \right) \tau^2 \\ & + \left(\frac{G}{\alpha^2} - \frac{\lambda}{\alpha^3} - \frac{B_\lambda}{\alpha} + \frac{D}{\alpha} \Delta T_0 \right) e^{-\alpha \tau} \end{aligned} \quad (54)$$

BIBLIOGRAPHY

1. Banchemo, J.T., Barker, G.E., and Boll, R.H., "Heat Transfer Characteristics of Boiling Oxygen, Flourine, and Hydrazine", Engineering Research Institute Final Report for Project M834, pp. 91, 96, 97, University of Michigan, 1951.
2. Cichelli, M.T., and Bonilla, C.F., "Heat Transfer to Liquid Boiling Under Pressure", Trans. AIChE, 41, pp. 755-787, 1945.
3. Cole, Robert, "Investigation of Transient Pool Boiling Due to Sudden Large Power Surge", NACA, Tech. Note 3885, 1956.
4. Eckert, E.R.G., and Diaguila, A.J., "Experimental Investigation of Free Convection Heat Transfer in Vertical Tube at Large Grashof Numbers", NACA, Report 1211, 1955.
5. Eckert, E.R.G., and Jackson, T.W., "Analytical Investigation of Flow and Heat Transfer in Coolant Passages of Free-Convection Liquid-Cooled Turbines", NACA, Res. Memo. E50D25, 1950.
6. Giaouque, W.F., and Clayton, J.O., "The Heat Capacity and Entropy of Nitrogen", Journal ACS, 55, pp. 4875-4888, 1933.
7. Hammann, G., "Thermal Conductivity of Liquid Oxygen, Nitrogen, and their Mixtures", Ann. Physik, 32, pp. 593-607, 1938.
8. Harrje, D.T., "A Study of Liquid-Oxygen Boiloff", Jet Propulsion Laboratory Memorandum No. 20-138, California Institute of Technology, 1956.
9. Hartnett, J.P., and Welsh, W.E., "Experimental Studies of Free Convection Heat Transfer in a Vertical Tube with Uniform Wall Heat Flux", Trans. ASME, 79, pp. 551-556, 1957.
10. Illingworth, C.R., "Unsteady Laminar Flow of Gas Near an Infinite Flat Plate", Proc. Camb. Phil. Soc., 46, Part 4, pp. 603-613, 1950.
11. Institute of Gas Technology, "Thermodynamic Properties of Nitrogen", Res. Bull. No. 18, p. 21, Chicago, 1952.
12. International Critical Tables, 1, pp. 20, 102, 103, 5, pp. 85, 88, McGraw-Hill Book Company, New York, 1929.
13. Jakob, M., Heat Transfer, I, pp. 529-530, John Wiley and Sons, New York, 1955.
14. Keenan, J.H., Thermodynamics, pp. 418, 425, 429, 433, John Wiley and Sons, New York, 1947.

15. Lamb, H., Hydrodynamics, Sixth Edition, p. 122, Dover Publications, New York, 1945.
16. Lighthill, M.J., "Theoretical Considerations of Free Convection in Tubes", Qrtly. J. of Mec. and App. Math., 6, Part 4, pp. 398-439, 1953.
17. Mair, C.E., "Preliminary Investigation of Thermal Conditions Inside Large Liquid Oxygen Container Exposed to Climatic Heating", Army Ballistic Missile Agency, Tech. Note No. G-024, 1956.
18. Martin, B.W., "Free Convection in an Open Thermosyphon, with Special Reference to Turbulent Flow", Proc. Royal Soc. of London, 230, Series A, pp. 502-530, 1955.
19. Martin, B.W., and Cohen, H., "Heat Transfer by Free Convection in an Open Thermosyphon Tube", Brit. J. of App. Phys., 5, pp. 91-95, 1954.
20. McAdams, W.H., Heat Transmission, Third Edition, pp. 172-173, 208, 210, 214, Ch. 14, McGraw-Hill Book Company, New York, 1954.
21. National Bureau of Standards Report 3569, Tech. Memo. No. 36.
22. Ostrach, S., "An Analysis of Laminar Free-Convection Flow and Heat Transfer about a Flat Plate Parallel to the Direction of the Generating Body Force", NACA, Report 1111, 1953.
23. Rosenthal, M.W., and Miller, R.L., "An Experimental Study of Transient Boiling", Oak Ridge National Laboratory, Paper No. 2294, 1957.
24. Seban, R.A., and Shimazaki, T.T., "Heat Transfer to a Fluid Flowing Turbulently in a Smooth Pipe with Walls at Constant Temperature", Trans. ASME, 73, pp. 803-809, 1951.
25. Siegel, R., "Transient Free Convection from a Vertical Flat Plate", ASME, Paper No. 57-SA-8, 1957.
26. Siegel, R., and Norris, R.H., "Tests of Free Convection in a Partially Enclosed Space between Two Heated Vertical Plates", Trans. ASME, 79, pp. 663-670, 1957.
27. Sparrow, E.M., and Gregg, J.L., "Laminar Free Convection from a Vertical Plate with Uniform Surface Heat Flux", Trans. ASME, 78, pp. 435-440, 1956.
28. Sparrow, E.M., and Gregg, J.L., "Similar Solutions for Free Convection from a Nonisothermal Vertical Plate", ASME, Paper No. 57-SA-3, 1957.
29. Technical Data Book, M.W. Kellogg Company, Curve G-602.301, New York, 1942.

UNIVERSITY OF MICHIGAN



3 9015 02826 7832